Locating Structural Damage in Real Time Using Contrast Maximization

by

Vikas Juneja

Dissertation submitted to the Faculty of the

Virginia Polytechnic Institute and State University

in partial fulfillment of the requirements for the degree of

DOCTOR OF PHILOSOPHY

in

Engineering Science and Mechanics

APPROVED

_____   _____

Raphael T. Haftka, Co-Chairman   Harley H. Cudney, Co-Chairman

_____   _____

Robert A. Heller   Daniel J. Inman

_____

Scott L. Hendricks

April, 1996

Blacksburg, VA

Locating Structural Damage in Real Time Using Contrast Maximization

by

Vikas Juneja

Raphael T. Haftka & Harley H. Cudney, Chairs

Engineering Science and Mechanics

(ABSTRACT)

A technique to identify structural damage in real time using limited instrumentation is presented, Contrast maximization is used to find the excitation forces that maximize the difference in the response of the damaged structure and the analytical response of the undamaged structure. The optimal excitations are then matched against a database of optimal excitations to locate the damage. To increase the reliability of the approach when modeling and measurement errors are present, the contrast maximization approach is then combined with an approach based on changes in frequency signature to develop the average angle technique. A damage detectability measure is defined which, for a given level and location of damage and a given amount of modeling and measurement errors, compares the magnitude of the damage to the magnitude of errors in a single number. The success of the average angle technique in damage detection is quantitatively defined by a success factor.

The technique is first tested analytically on a 132 degree of freedom truss. The structure can be either equipped with active members or collocated shakers/sensors. The technique has a high success rate in damage detection. The technique is then tested numerically on a 36 degree of freedom truss equipped with 3 collocated shakers/sensors. To simulate experimental conditions, an extensive study is carried out in the presence of numerical noise. It is seen that the success factor in the presence of noise depends upon the success factor in the absence of noise and the damage detectability measure. The members are classified into three groups based on the success factor in the presence of noise. A mathematical relationship between the damage detectability measure and the success factors with and without noise is developed using linear regression. Using the results of numerical simulations in the presence of noise and this mathematical relationship, we find members where we expect to locate damage experimentally, for a given amount of damage and given amount of noise.

A similar truss is built and the FEM model of the structure is corrected using experimental data. The average angle technique is applied to locate damage in a member when the member has a low level of damage (25%). The damage detectability measure indicated that the measurement errors are large compared to the damage and it is difficult to detect damage in most detectable locations. The steps taken to rectify that are described and after each step we show the improvement in damage detectability. The average angle technique is used to locate damage in 5 members. The experimental results indicate that the technique can robustly identify the damaged member with limited instrumentation.

Acknowledgements

Table of Contents

List of Figures

List of Tables

Chapter 1
Introduction

1.1 *Damage Identification*

Most structures are damaged at some phase of their operational life. The damage may be due to creep, fatigue, impact, crack growth, delaminations or some other reason. For proper functioning of the system, the damage should be located and repaired if possible. Damage detection problems are comprised of locating the damage and estimating its magnitude. The focus of this study will be on damage detection in space trusses. Due to constraints on the weight of the structure, truss structures are being used for space applications. Localized damage can propagate and have a catastrophic effect on the structure. This type of failure is termed as progressive phenomenon (*e.g.* Malla and Nalluri[1]). A periodic health monitoring of the structure is required to assess the integrity of the structure. Due to advent of computers and advances in signal processing equipment, vibration analysis techniques have been shown to be useful for damage detection. The methods used for damage detection can be broadly classified into 2 groups: methods which use some system identification methods to get an finite element model (FEM) model of the damaged structure and the methods which bypass this step. Some of the earlier work in this area is discussed next.

1.1.1 Damage Identification Methods

In 1963, Housner and Brady[2] derived equations for the natural periods of vibration of buildings and proposed that by comparing the measured natural periods before and after an earthquake, the degree of deformation of the building can be estimated. Vandiver[3] computed changes in natural frequencies to detect damage in structural members of an oil platform. Adams *et al.*[4] used sensitivity analysis to detect damage in a plate. Yao[5] in 1979 wrote a review paper on damage assessment and reliability evaluation of existing structures. Structural identification methods, pattern recognition algorithms and fuzzy sets were few of the methods which were being used at that time to study structural damage. In 1985, Adams and Cawley[6] wrote an overview about vibration analysis techniques in nondestructive testing. According to the paper, damage in a structure decreases the natural

frequency and increases the damping. Damage affects each mode, natural frequencies and mode shapes differently, depending upon the magnitude and location of damage.

Many of the current methods for damage detection of truss structures use some system identification technique to construct a model of the damaged truss. Smith and Hendricks[7], Lindner *et al.*[8], Baruch[9] and others have extended the system identification methods to damage detection by constructing a model of the damaged structure. By comparing the model of the damaged structure to the model of the undamaged structure, the damage is located. Chen and Garba[10] measured the mode shapes and eigenvalues and used them in conjunction with the undamaged mass and stiffness matrices to compute the residual forces. The residual forces were also expressed in terms of unknown stiffness parameters of the new structure. This resulted in a number of algebraic equations with the new member stiffness as the unknown parameters.

The above methods for damage identification refine the FEM model of the undamaged structure by some optimization scheme. A number of researchers[11-19] have proposed damage detection algorithms which bypass structural identification. The FEM model of the undamaged structure is not updated, and they rely directly on the measured data to identify the damage. The measured data may include the natural frequencies[3], mode shapes[11,12] or mode shape curvature[13,14]. The measured data of the damaged structure is then compared to the measurements of the undamaged structure to identify the damage.

Rickles and Kosmatka[11] used residual modal force vectors to locate the damage and then conducted a weighted sensitivity analysis to assess the extent of mass and stiffness variations. The damaged members are the ones that are located at the degrees of freedom that have large magnitudes in the residual force vector. The extent of damage was estimated iteratively by constructing a sensitivity matrix that relates the change in structural parameters to changes in natural frequencies and mode shapes. The rate of convergence depended upon the number and quality of modal vectors.

The Modal assurance Criterion (MAC) and Coordinate Modal Assurance Criterion (COMAC) has been used by many researchers to find the correlation between the mode shapes before and after damage and use this to locate the damage. MAC is applied to check if damage has occurred in the structure by computing the correlation between the

experimental mode shapes of the structure at two different stages. To locate the damage, COMAC is applied to the mode shapes of the undamaged and the damaged structure. It is expected that the damage occurs at the node where a large change in the mode shapes of certain modes is observed. Lin[12] generated the receptance matrix which consisted of contributions from measured mode shapes of the damaged structure and the analytical mode shapes of the undamaged structure. The receptance matrix thus generated is multiplied by the analytical stiffness matrix and deviations of the resulting matrix from the unity matrix revealed the degrees of freedom which are affected by damage.

Pandey *et al.*[13] used the changes in the curvature of mode shapes to detect damage in a beam. Numerical study showed that the changes in the curvature of mode shapes were localized in the region of damage unlike the displacement component of the mode shapes. Pabst and Hagedorn[14] mathematically showed that a crack in a beam has its largest influence if it occurs at a location where the curvature of its mode shape has its maximum.

Recently, a number of researchers have used *neural network approaches* for damage identification. Barga *et al.*[15] used the time history of acoustic emission waveforms to train the neural network and classify two kinds of damage- crack and fretting. Tsou *et al.*[16] used modal parameters for structural damage identification. Povich *et al.*[17] used frequency response functions (FRF's) to train and identify the damage. The FRF's presented the advantages that the modal parameter identification process is not required and the characteristics of the FRF's can be incorporated into the damage identification process. Rhim and Lee[18] used transfer functions instead of FRF's to locate the damage. The transfer function was used because it represents complete and compact information about a dynamic system from given input-output data. The method can be used with limited number of sensors. Sensmeier *et al.*[19] used contrast maximization excitation vectors in conjunction with neural networks to locate the damage in a composite beam. **Contrast maximization** (a.k.a. anti-optimization[20]) determines excitations that maximize the difference between the response of the damaged and undamaged structures.

1.1.2 Damage Detection with Limited Number of Measurements

Due to constraints on the instruments and weight of space structures, the number of sensors and actuators available for damage detection is limited. For large space structures,

the percentage of degrees of freedom that can be equipped with sensors rarely exceeds 10%. This means that mode shapes cannot be fully measured. In order to overcome this difficulty, either the measured degrees of freedom are expanded using the technique developed by Berman and Nagy[21] or the number of degrees of freedom of the FEM model is reduced by some model reduction technique, like the Guyan reduction technique[22]. Kim and Bartkowicz[23] discussed a hybrid model reduction/ eigenvector expansion technique in which the measured degrees of freedom are expanded and the size of the FEM model is reduced to an intermediate value. They used 4 different optimal update methods in conjunction with the hybrid model reduction/eigenvector expansion technique for damage detection and found that the number of measurements is the most critical factor in locating the damaged element, followed by the number of test modes. Zimmerman *et al.*[24] showed that damage detection capability is enhanced if the DOF's directly affected by damage are instrumented.

Not all the modes of a structure can be measured or even detected. A number of local modes usually enter the FRF spectrum and only a small fraction of the total number of modes can be identified with a reasonable accuracy. There may be damage cases where the damage does not significantly affect the measured lower modes of vibration of the structure.

Modeling errors and measurement errors play a significant role in damage detection. Measurement errors in frequencies and mode shapes can be around 5% of their nominal values. Modeling errors result from manufacturing defects, variation of member properties, assumptions about structural damping, neglecting effects of temperature, neglecting nonlinearities in the structure, and errors in modeling boundary conditions. The measured mode shapes may not be orthogonal to one another for the undamaged model. Kashangaki *et al.*[25] found out that the damage detection is feasible for truss members that contribute significantly to the strain energy of measured modes and also depends upon the accuracy of the measured modes and frequencies. Usually 5% measurement errors should be expected and this severely hinders damage identification. Most truss members will only have small contributions to the strain energy of the structure. It is very difficult to measure partial damage in some of these locations without added instrumentation.

A number of researchers are trying to use hybrid approaches for damage detection in structures equipped with limited instrumentation. Kim and Bartkowicz[26] used a two step approach, in which the first step uses the optimal update method to find a general area of damage and the second step uses the sensitivity technique to locate the damaged element. Zimmerman *et al.*[24] showed that using multiple approaches not only provides a level of confidence in damage assessment but some types of damage are more easily revealed using one approach as opposed to others.

Measurement errors, modeling errors, limited instrumentation and noise affect the accuracy of the detection algorithms. Furthermore, identification has to be conducted in real time. The above approaches are either computationally expensive or require a large number of sensors to be able to locate damage successfully and hence may not be suitable for real time damage detection of space structures. In this study, we investigate a method which requires a limited amount of data that can be used in real time.

1.1.3 Updating the Model to Match Experimental Data

Most damage identification methods need a model of the structure which is in good agreement with the experimental data and use some system identification method to update the model. System identification approaches can be either in time domain (e.g. Ibrahim *et al.*[27]) or in frequency domain (e.g. Chen *et al.*[28]) and use the measured response to construct a new model of the system. Most system identification techniques can be classified into three categories: Eigenstructure Assignment (e.g., Zimmerman and Widengren[29], Minas and Inman[30]), Design Sensitivity (e.g., Flanigan[31]) and Optimal Update methods (e.g., Kabe[32], Berman and Nagy[21], Baruch and Bar Itzhack[33], Kammer[34], Smith and Beattie[35]). Two reviews of structural identification methods have been written by Ibrahim and Saafan[36] and Heylen and Sas[37].

1.2 *Anti-Optimization*

A number of experiments are usually conducted to validate or disprove a mathematical model. Since conducting experiments is usually expensive and time consuming, only a limited number of experiments can be performed. Haftka and Kao[38] pointed out some of the traditional approaches of verifying new models may be inherently flawed. A researcher

may inadvertently pick test conditions where the model agrees with the experiment. This may lead others to believe in the validity of the model. It was proposed that optimization be used to sharpen the differences between the existing and the new models of the same phenomenon. Optimization was used to obtain the points of maximum disagreement between the two models. This approach, using optimization to find weak points in models has been called anti-optimization. The term anti-optimization, however, has been introduced by Ben-Haim and Elishakoff[39] to denote the use of optimization to locate worst-case conditions.

Van Wamelen[40] used anti-optimization to design an experiment to find areas of extreme disagreement between two competing composite failure criteria. The Tsai failure criterion describes ply failure by employing an iterative ply degradation scheme and the Hart-Smith criterion is based on the fiber failure in shear. The failure predictions of the Tsai and the Hart-Smith failure criteria were found to have large differences in the prediction of biaxial compression failure loads and the prediction of combined axial-tension and in-plane shear failure load. By using anti-optimization, he found conditions where the difference between the failure loads was a factor of two. Tests then clearly established the advantage of the Tsai's criterion.

Ponslet[41] applied anti-optimization to design experiments to measure the difference in the probability of failure between probabilistic design and deterministic design of a truss. Two tuned absorbers were used to control two modes of vibration of the truss. The probabilistic formulation found the best locations of the tuned dampers on the truss to minimize the probability of failure and the deterministic formulation maximized the safety margin between the response of the nominal damped truss and the failure limit. Anti-optimization was successfully used to identify a design problem which created a large difference in the probability of failure between these two formulations. This avoided time consuming procedures to test small differences in failure probabilities.

A number of damage identification techniques either use vibration mode shapes in conjunction with some system identification method or the vibration mode is directly used as data to locate the damage. Instead of the vibration modes, we will use anti-optimization to generate contrast maximization excitation vectors that are most sensitive to damage. These excitation vectors are a kind of damage signature and have much smaller dimension

than the dimension of the vibration mode shapes. This decreases the time necessary to measure the structural response. Sensmeier *et al.*[19] used contrast maximization vectors in conjunction with neural networks to locate damage in composite beam. In this study, we use the contrast maximization vectors to locate damage in a 3-D truss. A simple methodology is developed to replace the use of neural networks to locate the damage.

1.3 *Objectives*

The study is targeted at applications which require immediate action if damage is detected in a structure. The first objective of the dissertation is to develop a technique which is computationally inexpensive and therefore applicable in real time. Since only a few degrees of freedom in a structure can be instrumented with sensors, the damage should be located with a limited amount of sensors and actuators. The technique should have a high success rate in locating the damage. The technique should be validated by numerical and laboratory experiments. The second objective is to develop the capability to predict what kind of damage will be detectable with the given number of sensors and actuators in the presence of modeling and measurement errors.

1.4 *Summary of Dissertation*

We formulate a technique for damage identification based on contrast maximization and then combine it with the frequency signature approach. This technique is described in detail in Chapter 2. The technique can be applied to structures equipped with collocated shakers/sensors or for an adaptive structure with active members. The measure of structural response can be the strain energy of the structure or the square of the measured displacement amplitudes or some other meaningful response quantity.

The contrast maximization problem of finding optimal excitations which makes the response of the structure most different from the response of the undamaged structure can be reduced to an algebraic eigenvalue problem. The optimal excitation of the damaged structure is compared to a database of optimal excitations from hypothetical damage scenarios. The frequency signature of the damaged structure is computed and matched against a database of frequency signatures from hypothetical damage scenarios. The results are combined with the results of the frequency signature approach to locate the damage.

This is defined as the *average angle* approach. To quantitatively measure the ability of the algorithm to detect damage, we define a success factor. The measurement errors and modeling errors strongly affect the damage detection ability of any method. We define a damage detectability measure which quantifies the influence of these errors on the ability of our method to detect damage.

In Chapter 3, we test the analytical feasibility of the proposed technique on a 3-dimensional, S-shaped space truss with 132 degrees of freedom and 128 members. The symmetric truss is modeled in free-free boundary conditions. The first 5 modes of the truss are used for damage identification. The technique is first tested when the structure is equipped with 3 active members and the response measure is chosen as the strain energy of the structure. The approach is also tested when the structure is equipped with 3 sets of collocated shakers/sensors and the measure of structural response is chosen as the square of the displacement amplitudes at the measured degrees of freedom.

Chapter 4 describes testing the feasibility of the proposed method by conducting numerical simulations on a 3-dimensional, 36 degree of freedom space truss with 30 members and equipped with 3 collocated shakers/sensors. Only 3 modes are used for damage identification. We test the viability of the proposed method with 20%, 45%, and 75% damage in a member. To take into account the measurement and modeling errors, we simulate noise in receptance matrix and natural frequencies of the undamaged and damaged structure. The objective of this chapter is also to find the members where we can expect to detect damage experimentally with a given amount of damage, and given amount of measurement noise. On the basis of success in locating damage in presence of errors, the members are classified into three groups for success in damage identification under experimental conditions.

Chapter 5 describes experiments conducted on the truss described in Chapter 4. This chapter shows how initially the modeling and measurement errors were so large compared to the damage that it was impossible to detect even the most detectable locations. The chapter shows the steps taken to rectify that, giving after each step the improvement in predicted damage detectability. The proposed method is successfully applied to detect damage in members in five different cases.

Chapter 6 contains some concluding remarks and recommendations for future research. Appendix A describes laboratory determination of the optimal excitations when strain energy is used as the measure of structural response. Appendix B describes the process of identifying the boundary conditions for the cantilevered laboratory truss. We test the predictive capability of the resulting model by checking it for a condition that was not used in fitting the data. Appendix C contains the glossary of some of the terms used in data acquisition and signal processing. Appendix D describes the method to determine the optimal location of shakers/sensors which will help us in the process of damage detection.

Chapter 2
Average Angle Technique

The method of contrast maximization is presented which determines harmonic excitations that maximize the difference between the response of the damaged structure and the response obtained from a model of the undamaged structure. The harmonic excitations are obtained by solving an eigenvalue problem at selected values of the excitation frequency. A set of hypothetical models with assumed damage in each member is generated analytically and for each such model, an excitation force vector is obtained using contrast maximization. This excitation vector is treated as a unique characterization of the damage. The optimal excitation force vector obtained from data from the real structure is matched against this database and it is expected that the model with the same damage as the actual structure will have the best match.

To increase the reliability of our approach, the resulting natural frequencies due to known damage in each member are also computed and stored in a database that can be matched against the natural frequencies obtained from the real structure. The results obtained by this frequency signature approach are combined with those obtained by contrast maximization to determine which member is damaged.

2.1 *Theory*

In order to identify the damage, the structure is assumed to be subjected to harmonic excitation by either a set of shakers or active members and the response of the structure is measured by collocated sensors. In this section, we derive the optimum excitation vector that creates the largest difference in a measure of the response between the damaged structure and the undamaged structure.

2.1.1 Derivation of Optimal Excitation Vector for Use with Shakers

We assume a structure instrumented with m collocated shakers/sensors which behaves linearly to the applied excitations. The measured displacement vector, **y**, can be expressed as

$$\mathbf{y} = C \, \mathbf{q} \qquad\qquad (2.1)$$

where C is the $m \times m$ symmetric matrix of the transfer functions for the given set of shakers and sensors and $\mathbf{q}$ is the m-vector of constant excitations. We need a scalar measure of structural response, U, to compare the response of the damaged structure (U_d) with the response of the undamaged structure (U_o). The response measure is assumed to be of the form,

$$U = \mathbf{y}^T H \, \mathbf{y} \qquad\qquad (2.2)$$

where H is an $m \times m$ symmetric matrix which depends upon the assumed form of the structural response. If the measure of structural response is taken as the square of measured displacements, then H assumes the form of an identity matrix.

The method of contrast maximization maximizes the difference between the response of the undamaged structure and the response of the damaged structure. We try to make the ratio of the measure

$$= \frac{U_d}{U_o} = \frac{\mathbf{q}^T C_d^T H C_d \, \mathbf{q}}{\mathbf{q}^T C_o^T H C_o \, \mathbf{q}} \qquad\qquad (2.3)$$

as different from unity as possible. The excitation vector $\mathbf{q}$ that extremizes the ratio of response measure is the solution of the algebraic problem,

$$\{C_d^T H C_d - C_o^T H C_o\} \, \mathbf{q} = 0 \qquad\qquad (2.4)$$

Now, we apply the method to linear undamped systems subjected to harmonic excitations. Neglecting damping, the equations of motion of a structure modeled using finite elements can be written as

$$M \, \ddot{\mathbf{x}} + K \, \mathbf{x} = \mathbf{f_0}, \qquad\qquad (2.5)$$

where $\mathbf{x}$ and $\mathbf{f_0}$ are n-vectors of nodal displacements and forces, and M and K are $n \times n$ symmetric mass and stiffness matrices, respectively. We assume that the structure is

11

excited by m shakers which subject the structure to harmonic excitation of the form, $\mathbf{f_0} = \mathbf{f}$ $e^{i\omega t}$. The response is also harmonic

$$\mathbf{x} = \mathbf{X} \, e^{i\omega t}, \tag{2.6}$$

where X is the n-vector of nodal amplitudes obtained by solving

$$[K - \omega^2 M]\, \mathbf{X} = \mathbf{f}. \tag{2.7}$$

For a structure with m shakers, the force amplitude f is given by,

$$\mathbf{f} = B \, \mathbf{q}, \tag{2.8}$$

where q is a m-vector of applied excitation amplitudes, B is n × m Boolean transformation matrix. The sensors read a vector y of nodal amplitudes and because they are collocated with the shakers,

$$\mathbf{y} = B^T \, \mathbf{X} \tag{2.9}$$

From Eqs. 2.7 - 2.10, we get

$$\mathbf{y} = B^T [K - \omega^2 M]^{-1} B \, \mathbf{q} \tag{2.10}$$

and comparing it to Eq. (2.1), the transfer function (receptance) matrix C can be expressed as

$$C = B^T [K - \omega^2 M]^{-1} B \tag{2.11}$$

We assume that we have a good model of the undamaged structure in the form of the stiffness and mass matrices K_u and M_u respectively. The damaged structure has the corresponding but unknown matrices K_d and M_d. It is assumed that there is no change in the mass matrix due to damage, i.e., $M_d = M_u$. The method of contrast maximization varies the excitation q for a fixed frequency ω which maximizes some measurable difference between the response of the undamaged structure (obtained by computer

simulation) and the response of the damaged structure (measured in situ). The response measure can be chosen as either the square of the displacement amplitude or the strain energy of the structure or some other equally meaningful quantity.

- **Response Measure as Square of Displacement Amplitude**

We use the square of the displacement amplitude U, as our response measure

$$U = \mathbf{y}^T \, \mathbf{y}.$$

Substituting Eq. 2.10, the response measure U can be expressed as

$$U = \mathbf{q}^T \, A \, \mathbf{q} \, ,$$

where
$$A = B^T \, [K - \omega^2 M]^{-1} \, B \, B^T \, [K - \omega^2 M]^{-1} \, B \qquad\qquad (2.12a)$$

Using the expression for the receptance matrix, C (Eq. 2.11), the above equation can also be expressed as,

$$A = C^T \, C$$

- **Response Measure as Strain Energy**

If we use the strain energy of the structure, U, as our response measure and following a similar procedure as before, we get

$$U = \frac{1}{2} \, \mathbf{X}^T \, K \, \mathbf{X} \, = \mathbf{q}^T \, A \, \mathbf{q}$$

where
$$A = \frac{1}{2} \, B^T \, [K - \omega^2 M]^{-1} \, K \, [K - \omega^2 M]^{-1} \, B \qquad\qquad (2.12b)$$

We see that choosing a different response measure of the structure changes the form of the A matrix. The process of selecting ω and $\mathbf{q}$ to maximize the difference between U_o and U_d is called contrast maximization because it seeks to make the analytical model that we have (K_o and M_o) yield results (U_o) which are at maximum variance with the experimental measurement (U_d). Here we try to make the ratio of the quadratic measures,

13

$$= \frac{U_d}{U_o} = \frac{\mathbf{q}^T A_d \mathbf{q}}{\mathbf{q}^T A_o \mathbf{q}}. \tag{2.13}$$

as different from unity as possible. The excitation vector $\mathbf{q}$ that extremizes the ratio of quadratic measures is the solution of the algebraic eigenvalue problem,

$$\{A_d - \lambda A_o\}\mathbf{q} = 0. \tag{2.14}$$

We seek the eigenvalue λ which is most different from unity, so that we may select λ such that λ or $1/\lambda$ is maximal. In the present work, we select frequencies which produce the highest value of λ. Both the matrices A_d and A_o are functions of the excitation frequency ω, hence the ratio λ also depends upon the forcing frequency. The forcing frequency is chosen at a fixed distance away from the natural frequency of the structure. Then the excitation vector, $\mathbf{q}$, is found by solving Eq. (2.14).

If the response measure is chosen as the sum of squares of the measured displacement amplitudes, constructing the A_d matrix (Eq. 2.12a) requires measuring only the receptance matrix C_d. The receptance matrix of the damaged structure is measured by applying a harmonic force of a unit magnitude by each shaker and measuring displacements at all the instrumented degrees of freedom. We need to measure the $m(m+1)/2$ independent elements of the receptance matrix C_d in order to construct the A_d matrix.

If the strain energy of the structure, U is selected as our response measure, it can be shown (Appendix A) that A_d corresponding to U_d is expressed as

$$A_d = C_d + \omega^2 \frac{\partial C_d}{\partial \omega^2}$$

The laboratory determination of A_d in this case would require measuring the receptance matrix and also the derivative of the receptance matrix with respect to the square of the excitation frequency. This doubles the experimental work and may add significant amount of errors into A_d matrix.

2.1.2 Derivation of Optimal Excitation Vector for Use with Active Members

We assume that the linear undamped structure is excited by m active members which subject the structure to harmonic excitation of the form, $\mathbf{f_0} = \mathbf{f}\,e^{i\omega t}$. The force amplitude f is given by,

$$\mathbf{f} = \tilde{B}\,K_a\,\mathbf{q}, \tag{2.15}$$

where $\mathbf{q}$ is a m-vector of applied excitation amplitudes, $\tilde{B}$ is n $\times$ m matrix of the direction cosines of the active members, and $K_a = \mathrm{Diag}[\dfrac{E_i A_i}{L_i}]$ is the m$\times$ m diagonal matrix of the stiffness of the active members. The sensors read a vector y of member elongations and because they are collocated with actuators

$$\mathbf{y} = \tilde{B}^T\,\mathbf{X} \tag{2.16}$$

The response measure can be chosen as either the square of the displacement amplitude or the strain energy of the structure or some other equally meaningful quantity.

- **Response Measure as Square of Displacement Amplitude**

When we use the square of the displacement amplitude U, as our response measure and following a similar procedure as before, we get

$$U = \mathbf{y}^T\,\mathbf{y} = \mathbf{q}^T A\,\mathbf{q}$$

where

$$A = K_a\tilde{B}^T[K - \omega^2 M]^{-1}\tilde{B}\tilde{B}^T[K - \omega^2 M]^{-1}\tilde{B}K_a \tag{2.17a}$$

- **Response Measure as Strain Energy**

When we use the strain energy of the structure, U, as our response measure and following a similar procedure as before, we get

$$U = \frac{1}{2}\mathbf{X}^T\,K\,\mathbf{X} = \mathbf{q}^T A\,\mathbf{q}$$

15

where

$$A = \frac{1}{2} K_a \tilde{B}^T [K - {}^2 M]^{-1} K [K - {}^2 M]^{-1} \tilde{B} K_a \qquad (2.17b)$$

As before, we try to make the ratio of the energies,

$$= \frac{U_d}{U_o} = \frac{\mathbf{q}^T A_d \mathbf{q}}{\mathbf{q}^T A_o \mathbf{q}}. \qquad (2.18)$$

as different from unity as possible.

2.1.3 Interpretation of Contrast Maximization Vector

The contrast maximization vector **q** maximizes the difference between the damaged structure and the undamaged model of the structure. This vector is used in conjunction with the natural frequencies of the structure to locate the damage. Most other damage detection algorithms based on system identification methods use the mode shapes and the natural frequencies of the structure to locate the damage. However, to measure vibration modes requires measurement of large number of degrees of freedom. Here, the optimal excitation vector is of considerably smaller dimension than the mode shape of the structure. This excitation vector can be regarded as a signature of the damage. The optimal excitations are obtained in the neighborhood of the natural frequency of the damaged structure. If the excitation frequency is chosen as the natural frequency of the structure, it can be shown that if the optimal excitation is applied to the structure, the spatial spectrum of the structure will be the mode shape of the damaged structure. The excitation vectors, in a sense, replace the mode shapes and are of a smaller dimension than the dimensions of the mode shapes.

2.2 *Detection Algorithm*

2.2.1 Generating the Database

The first set of experimental measurements are performed on the undamaged structure. Measurements of natural frequencies and receptance matrices at the selected frequencies are

16

used to improve the analytical model of the structure. A_o is constructed for later use, at a distance s from the corresponding natural frequency of the undamaged structure. Additionally, we construct a set of hypothetical models each with an assumed damage at a known location. For the truss structure studied in the dissertation, each model is constructed by assuming that one of the members is damaged with a particular damage scenario. These models are generated at *pre-determined frequencies*, i.e., frequencies which are at a fixed distance *s* from the natural frequency of each damage scenario and are given as

$$\omega_i^{*k} = (1-s)\,\omega_i^k; \quad i=1,2,...,n \;\; ; \;\; k=1,2,...,n_{ds}, \tag{2.19a}$$

where ω_i^k is the ith natural frequency of the kth damage scenario and n_{ds} represents the number of damage scenarios. This fixed distance, *s,* was initially chosen as 0.05 for damage identification experiments. Later, to improve the signal to noise ratio of the measured receptance matrix, C_d, the fixed distance was chosen as s=0.02. Contrast maximization is applied to each of these models and corresponding vectors, $\mathbf{q}_i^k$, are constructed using Eq. 2.14. No real time computation is required, as $\mathbf{q}_i^k$ are for hypothetical damage and are calculated and stored *a priori* in the form of a database.

Originally, we generated the hypothetical models at *experimental frequencies*, i.e., each model was generated at,

$$\omega_i^{*k} = \omega_i^* ; \qquad i=1,2,...,n \;\; ; \qquad k=1,2,...,n_{ds} \tag{2.19b}$$

where ω_i^* is the frequency at which the actual damaged structure is analyzed. Then we analyzed the hypothetical models at the *corrected frequencies*, i.e., each model is generated at

$$\omega_i^{*k} = \omega_i^* \left[\frac{\omega_i^k}{\omega_i}\right]; \qquad i=1,2,...,n \;\; ; \qquad k=1,2,...,n_{ds} \tag{2.19c}$$

The term ω_i^k / ω_i is a correction factor as now the distance between ω_i^k and ω_i^{*k} is the same as the distance between ω_i and ω_i^*. If experimental frequencies (Eq. 2.19b) or

17

corrected frequencies (Eq. 2.19c) are used to analyze the hypothetical model, then the frequencies at which the database of optimal excitations is generated depends upon the experimental measurements of the damaged structure. The database has to be generated in real time and the damage detection algorithm becomes computationally expensive. If the technique uses pre-determined frequencies instead of the corrected frequencies, the step of contrast maximization becomes much more efficient for real time application. The techniques based on either corrected frequencies or pre-determined frequencies yield similar success rate in identifying the location of the damage. Therefore, the technique based on pre-determined frequencies will be used in all our subsequent numerical simulations.

For each damage scenario, we have computed the natural frequencies of the structure. The changes in the natural frequencies due to damage for each damage scenario are also stored in the form of a database of frequency signatures. The percent change in the natural frequencies between the undamaged model and the kth damage scenario, is calculated for all the modes. We define the magnitude of the frequency change due to the kth damage scenario as $_i^k$, as

$$_i^k = _i^k - _i^o,$$
(2.20)

where the subscript i represents the mode and the superscript k represents the damage scenario.

Both databases are constructed *a priori*, which reduces the real-time computation requirements. The damage detection algorithm uses a frequency signature approach to complement the contrast maximization approach to locate the damage. We first describe the set of measurements required in the process of damage identification.

2.2.2 Necessary Experimental Measurements

The natural frequencies of the damaged structure are measured experimentally and only those which are at least moderately different from the corresponding natural frequencies of the undamaged model are considered. The excitation vector at $_i^*$ is the eigenvector $\mathbf{q}_i$ obtained as a result of contrast maximization. Using this excitation will create large differences between the two structures.

We also need to measure the elements of the receptance matrix. If strain energy is chosen as the measure of structural response, we also need to measure the derivatives of the receptance matrix with respect square of the excitation frequency. The elements of the receptance matrix can be measured by applying *m* (the number of collocated shakers and sensors) linearly independent forces on the structure and measuring their response. The next step is to match $\mathbf{q}_i$ against the database in order to identify the damage location.

2.2.3 Contrast Maximization Database Match

We compare the contrast maximization vector $\mathbf{q}_i$ from the actual damaged structure to the database of contrast maximization excitation vectors, $\mathbf{q}_i^k$. We compute the average angle, $(\theta_k)_{cm}$ between $\mathbf{q}_i$ and $\mathbf{q}_i^k$ (Fig. 2.1) over all the modes of interest,

$$(\theta_k)_{cm} = \frac{1}{n}\sum_{i=1}^{n} Cos^{-1}[\frac{\mathbf{q}_i^T\,\mathbf{q}_i^k}{\sqrt{(\mathbf{q}_i^T\mathbf{q_i})(\{\mathbf{q}_i^k\}^T\mathbf{q}_i^k)}}]$$ (2.21)

where n are the number of frequencies and the superscript T represents the transpose of the quantity. It is expected that the model which matches the damage site of the actual damaged member will have the best match with $\mathbf{q}_i$ and have the lowest average angle $(\theta_k)_{cm}$.

2.2.4 Frequency Signature Database Match

The natural frequencies of the damaged structure are measured experimentally and used indirectly in contrast maximization. We also use these frequencies to match the frequency signature of the damaged structure against a database of frequency signatures.

The natural frequencies of the actual damaged structure are used to determine the percent change in the natural frequencies between the undamaged model and the damaged structure for each mode,

$$\Delta\omega_i^d = \omega_i^d - (\omega_i^o)^{exp}.$$ (2.22)

19

The frequency signature of the damaged structure should be close to the frequency signature of the model of the damage scenario corresponding to the unknown damaged member. The degree of closeness of the frequency signature of the actual structure to the frequency signature of any one damage model from the database is measured by the angle between the two vectors. The angle between ϕ_i^d and ϕ_i^k, that is, $(\theta_k)_{freq}$, is expressed as,

$$(\theta_k)_{freq} = \text{Cos}^{-1}\left[\frac{\sum\limits_{i=1}^{n}(\phi_i^k \phi_i^d)}{\sqrt{\sum\limits_{i=1}^{n}(\phi_i^k)^2 \sum\limits_{i=1}^{n}(\phi_i^d)^2}}\right]; \qquad k=1,2,...,n_{ds}. \qquad (2.23)$$

It is expected that this angle will be smallest for the damaged member.

2.2.5 Average Angle

We combine the results of the frequency signature and contrast maximization by averaging the two angles to determine the damaged member. We define θ_k, the average angle as

$$\theta_k = \frac{[(\theta_k)_{cm} + (\theta_k)_{freq}]}{2} ; \quad k=1,2,...,n_{ds} \qquad (2.24)$$

It is expected that this angle will be the lowest for the damaged member.

2.2.6 Measuring Success in Damage Identification

One possible way to measure the success of the proposed technique in locating the damage is the qualitative approach: a simple "Yes" or a "No". If the average angle is lowest for the damaged member, then the technique was successful in damage identification. Otherwise our proposed technique failed to locate the damage.

A more quantitative success of damage can be represented by using the success factor, R, which is defined as,

$$R = \frac{dm}{\underset{k=1,..,n_{ds},k}{\mathrm{Min}} \; [\;_{dm}\;_k\;]} \tag{2.25}$$

where, the subscript *dm* represents the damaged member. R is the ratio of the angle of the damaged member and the smallest angle of an undamaged member. If the success factor is less than unity, then the technique probably located the damage and if it is greater than unity, the technique probably did not locate the damage. The greater the distance of R from unity, the greater is the confidence in the conclusion of the approach. If R is close to unity, then some more tests should be carried out to have confidence in the identified location of the damage.

2.2.7 Damage Detectability Measure

Under experimental conditions, there will be a mismatch between the experimental data and the corresponding analytical data. This may be due to modeling errors, measurement noise or signal processing errors. We need a measure which relates the signal to noise ratio (SNR) to the ability to detect damage. The measure should be independent of the contrast maximization function being used for damage detection. We first define the Euclidean distance between two matrices, C_1 and C_2 as,

$$[S(C_1,C_2)]^2 = \frac{||C_1 - C_2||^2}{||C_1||^2}$$

We define the damage detectability measure as the ratio of normalized error in the measurement of receptance matrix to the normalized amount of damage in the structure as

$$E = \sqrt{\frac{\underset{\mathrm{Modes}}{}[S(C_o^{exp},C_o^{FEM})]^2}{\underset{\mathrm{Modes}}{}[S(C_d^{FEM},C_o^{FEM})]^2}} \tag{2.26}$$

where $C(r,s)$ denote the components of the receptance matrix C. If the detectability measure is of order one or greater, then measurement errors can mask the change in the receptance matrix due to damage, and the damage may not be detectable. If the detectability

measure is substantially smaller than unity, then the effect of damage dominates the effect of errors on the receptance matrix and the damage should be detectable.
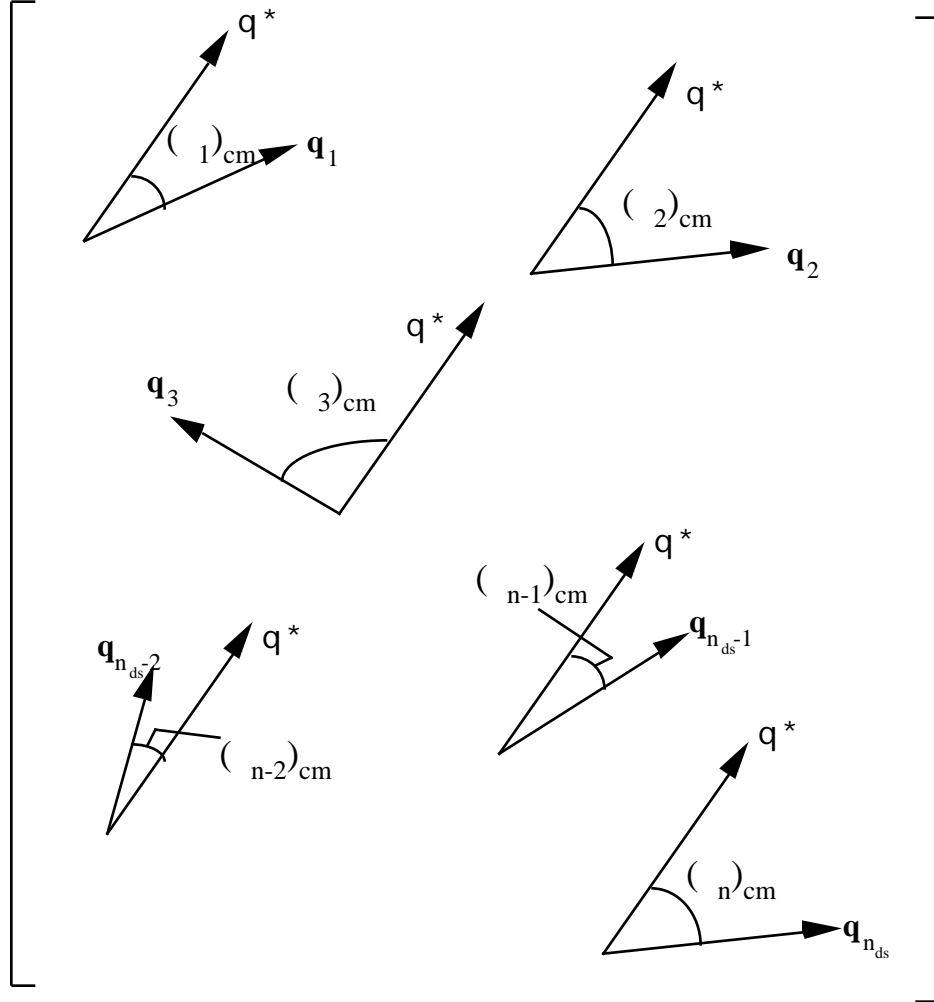
Figure 2.1 Computing angle between optimal excitation of actual structure and database of optimal excitations

2.2.8 Modifying the Contrast Maximization Function to Compensate for Modeling Errors

The contrast maximization based on the following contrast maximization function (Eq. 2.13 or Eq. 2.18) is represented as

$$
= \frac{\mathbf{q}^{\mathrm{T}} A_{d}^{\mathrm{exp}} \mathbf{q}}{\mathbf{q}^{\mathrm{T}} A_{o}^{\mathrm{FEM}} \mathbf{q}} ;
\tag{2.27}
$$

where the superscript *exp* represents the measured and hence noisy receptance matrix and the superscript *FEM* represents the receptance matrix with no noise. There will be a difference between the experimentally measured and the analytically computed receptance matrix of a structure. This difference can be partly due to a bias in the measurement of the receptance matrix or in modeling the structure. This bias can be reduced by compensating for errors common to the undamaged and the damaged structures. We modify the contrast maximization function as

$$\tilde{} = \frac{\mathbf{q}^{\mathrm{T}}\{A_{d}^{exp} - A_{o}^{exp}\}\mathbf{q}}{\mathbf{q}^{\mathrm{T}} A_{o}^{FEM} \mathbf{q}} \qquad (2.28)$$

The contrast maximization functions represented by Eq. 2.27 and Eq. 2.28 will be referred to as the uncompensated contrast maximization function and compensated contrast maximization function respectively. It is to be noted that in the absence of any noise and errors, i.e., if the experimental and analytical receptance matrices have a perfect match, the excitation vectors of the structure generated from the uncompensated and compensated contrast maximization functions will be identical.

2.2.9 Summary

In this chapter, we first describe the derivation of the optimal excitations which creates maximum difference between the response of the damaged and the undamaged structure. The contrast maximization approach for damage identification is formulated for use with either shakers or active members and combined with the frequency signature approach. This approach is defined as the average angle approach. To quantatively measure the ability of the approach to detect damage, a success factor is defined. We also define a damage detectability measure which quantifies the influence of the measurement errors modeling errors on the ability of our method to detect damage.

In the next chapter, using numerical simulations, we test the feasibility of the technique to locate the damage on a 132 degree of freedom space truss. The truss can be either equipped with active members or shaker/sensors.

Chapter 3
Analytical Feasibility Study with S Shaped Truss

In this study, we used numerical simulations of a 132 degree of freedom truss with 128 members, shown in Fig. 3.1, to determine the feasibility of the approach. The truss is made up of tubular aluminum members and solid aluminum nodes. The non-diagonal members are 10 inches long, have an effective stiffness, $k = 0.225 \times 10^8$ N/m, have a mass, m = 109.61 grams and have a mass moment of inertia about their center of gravity, $I_G = 5.1 \times 10^{-4}$ kg m^2. The diagonal members are 14.14 inches long, have an effective stiffness, $k = 0.148 \times 10^8$ N/m, have a mass, m = 128.15 grams and have a mass moment of inertia about their center of gravity, $I_G = 15.6 \times 10^{-4}$ kg m^2.
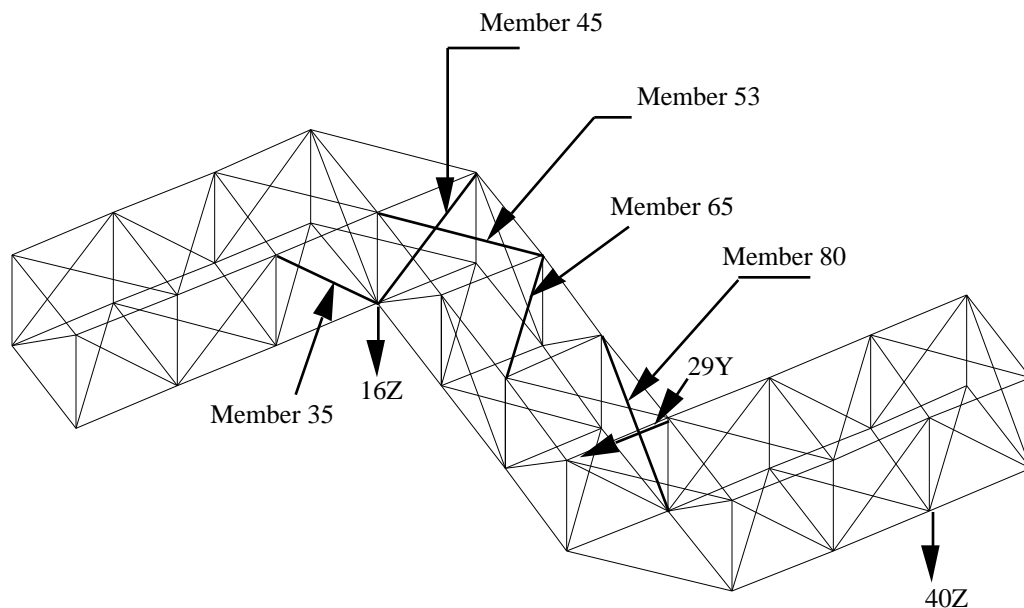
Figure 3.1. The 132 degree of freedom space truss.

The members of the truss are modeled as symmetric, non-uniform members and the metal nodes are modeled as rigid point masses. The structure is modeled as an undamped truss with free-free boundary conditions. The first five natural frequencies obtained from the FEM model of the truss are shown in Table 3.1.

24

Table 3.1. Natural Frequencies of S Shaped Truss	
Mode	Natural Frequency (Hz)
1	66.05
2	86.97
3	110.87
4	168.88
5	204.37

3.1 *Effect of Damage on Natural Frequencies*

We studied the effect of damage on the natural frequencies of the structure. Figure 2 shows the variation of the first natural frequency of the structure with the magnitude of damage in member 35.
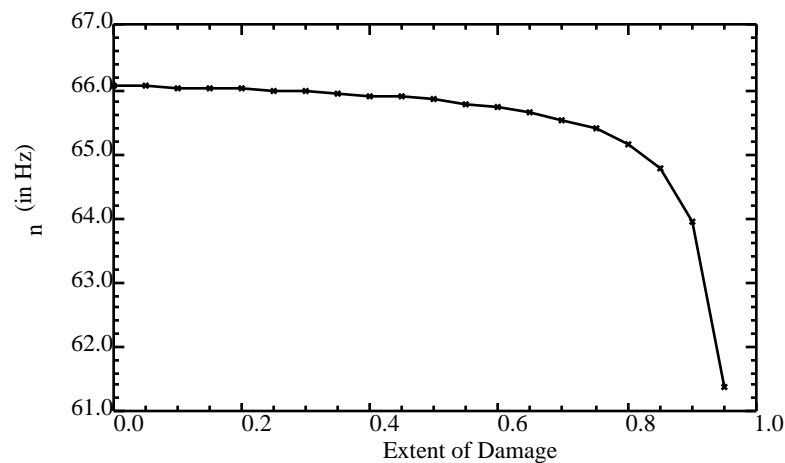
Figure 3.2. The effect of extent of damage in member 35 on the fundamental frequency

Both the damaged member and the mode considered were varied and it was observed that the nature of graph remains similar for all cases. The graph indicates that up to 50% damage, the slope of the curve remains approximately the same, and the effect of damage on natural frequency is small.

An example of the shift in natural frequencies due to damage is presented in Table 3.2. It is seen that damage does not affect all the modes of the truss. The first five natural

frequencies of both the undamaged truss and the truss with 50% damage in member 65 are shown in the table.

<div align="center">

Table 3.2. Natural frequencies (Hz) of undamaged structure and damaged structure with 50% damage in member 65.

</div>

Mode	Undamaged Structure	Damaged Structure
1	66.05	64.88
2	86.97	86.97
3	110.87	108.86
4	168.88	168.36
5	204.37	204.37

3.2 *Damage Detection with Active Members*

In this study, *active members* are used to excite and sense the response of the structure. The collocated actuators/sensors were located at members 45, 53 and 80. The first 5 modes were considered for damage identification. The contrast maximization approach combined with the frequency signature approach was applied for damage detection with the database damage scenarios being represented by 30% and 70% damage in a member. A member was damaged with 80% stiffness reduction and the technique was applied to locate the damage. The *strain energy* of the structure was used as the measure of the response of the truss. The frequency signature angles and contrast maximization angles were then computed for all members. The average angle was used to sort the members and the members were then stored in the form of a list. It was expected that the damaged member will have the smallest average angle and will be first in the list. The database is represented by two damage levels, 30% and 70% damage. The damage level which gives the smallest average angle is chosen to represent the actual damaged structure. The location of damage was then changed and the technique was again applied to locate the damage. The technique is not applied to detect damage at the location of active members.

The results of using only the frequency signature approach for damage detection are summarized for the 128 members of the truss in Fig. 3.3. This technique was unable to identify damage in 10 different locations out of 128 locations. The symmetry in the structure and in its boundary conditions resulted in two members symmetrically located

having the same frequency signature angles. The frequency signature approach is unable to differentiate between damage in symmetrical members. The frequency signature approach was able to identify the damaged member with 80% damage in 92.2% of the cases.
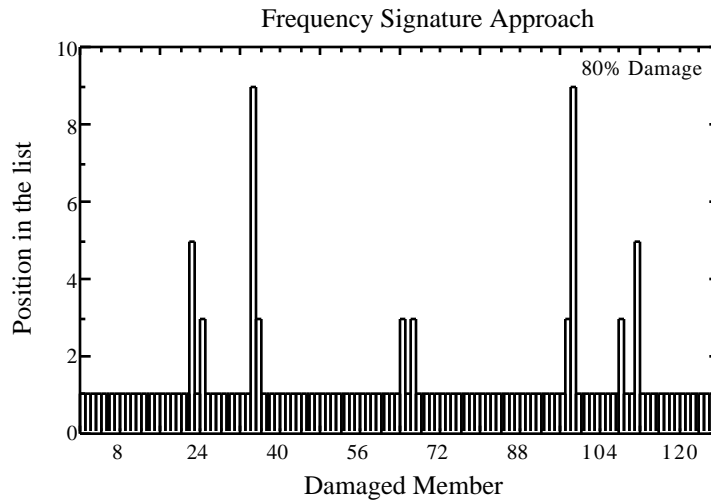
**Figure 3.3. Damage identification by frequency signature approach
when truss is excited by active members.**

If only contrast maximization was used for damage detection, then the technique (Fig. 3.4) was unable to identify damage in 8 different locations. The contrast maximization approach was able to differentiate between damage in symmetrical members. The contrast maximization approach was able to identify the damaged member with 80% damage in 94% of the cases. However, the proposed technique based on the average angle approach was able to identify damage in **all** the different locations when 80% damage was inflicted on a member.

We also computed the success factor based on the average angle (Fig. 3.5) technique to quantitatively estimate the success of the technique in locating the damage. For damage in one of the active members, the success factor is given a value of unity to indicate that the method is inconclusive. We see that damage at any other location is successfully located by the technique.

Contrast Maximization Approach
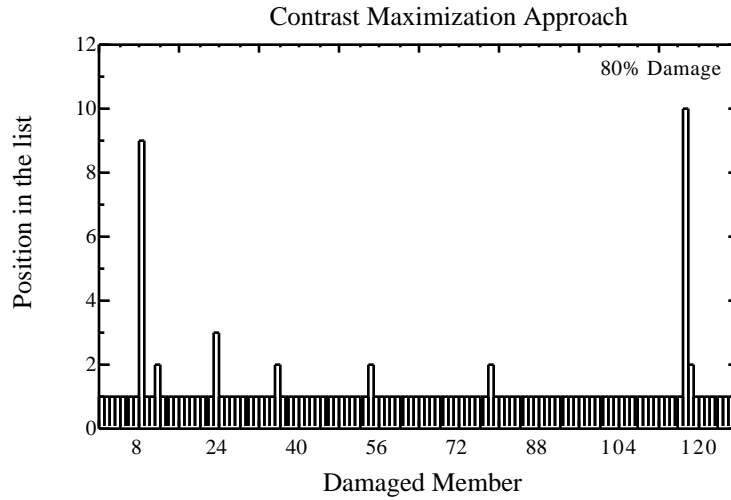
**Figure 3.4. Damage identification by contrast maximization approach
when truss is excited by active members.**
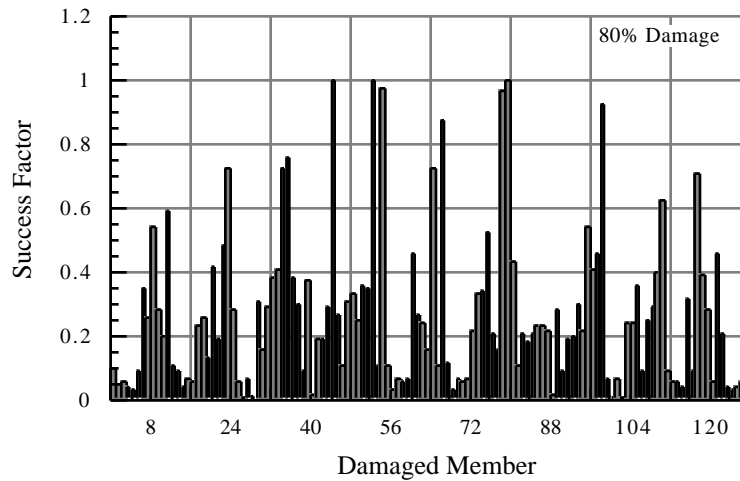
**Figure 3.5. Success factor based on average angle for 80% damage
when truss is excited by active members.**

To check the *robustness* of the technique, we need to take into account measurement errors. We generated noise in the measurement of natural frequencies of the actual truss and also in the components of the contrast maximization vectors. The measurement noise is simulated by using a pseudo-random number generator with coefficient of variation, (COV), of 1%. The proposed technique was able to identify damage in all the locations. Figure 3.6 shows the success factor based on the average angle approach in the presence of

28

noise for all the locations of damage.   Comparing Figures 3.5 and 3.6, we observed that there was very little effect in the results due to the measurement noise. This is observed because the noise was generated for the contrast maximization vectors and not for the elements of the C_d matrix. We carried out a more elaborate robustness study in Chapter 4 on a smaller truss.
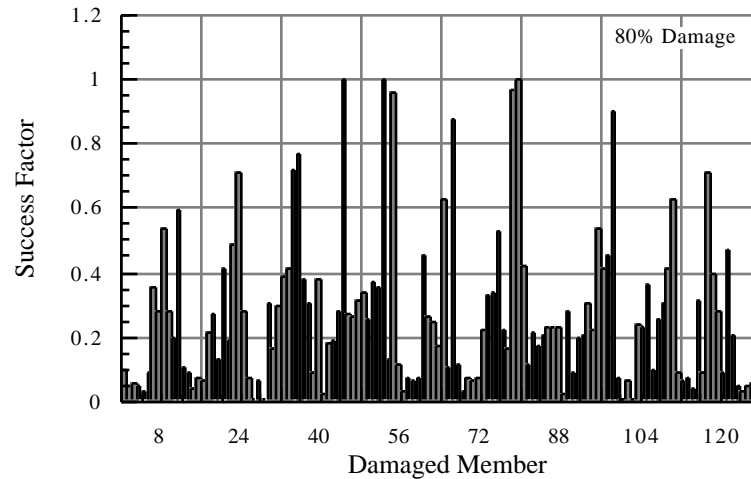
Figure 3.6. Success factor based on average angle approach in the presence of noise for 80% damage when truss is excited by active members.

3.3 *Damage Detection with Shakers/Sensors*

In this study, we used collocated *shakers/sensors* to excite and sense the response of the structure. The first 5 modes were considered for damage identification. The shakers/sensors were located at degrees of freedom 16Z, 29Y and 40Z (Fig. 3.1). A member was damaged with 80% stiffness reduction and the technique was applied to locate the damage. The contrast maximization approach combined with the frequency signature approach was applied for damage detection with the database damage scenarios being represented by 30% and 70% damage in a member. The square of *measured displacement amplitudes* of the structure was used as the measure of the response of the truss.

The damage identification results are shown in Fig. 3.7. The technique was unable to locate damage in members 37 and 67. The damaged members were second most likely members to have the damage. This shows that the technique may not always be able to

locate the damage. The technique was able to identify the damaged member with 80% damage in 98.4% of the cases. The success factor based on average angle approach is shown in Fig. 3.8.
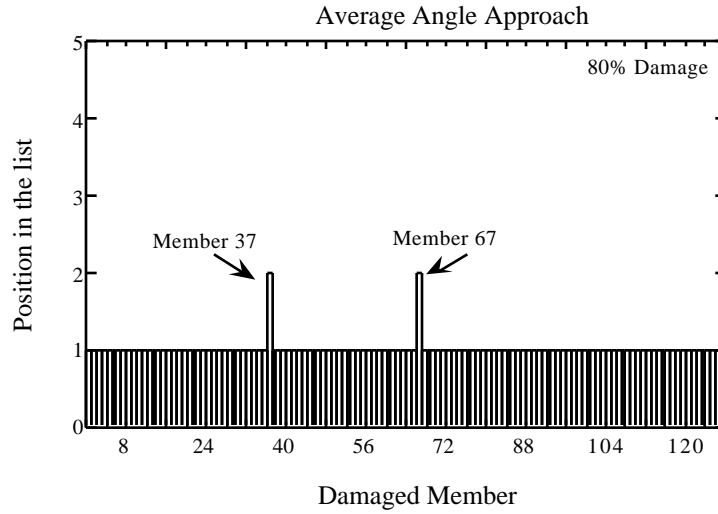
Figure 3.7. Damage identification by average angle approach when truss is excited by shakers.
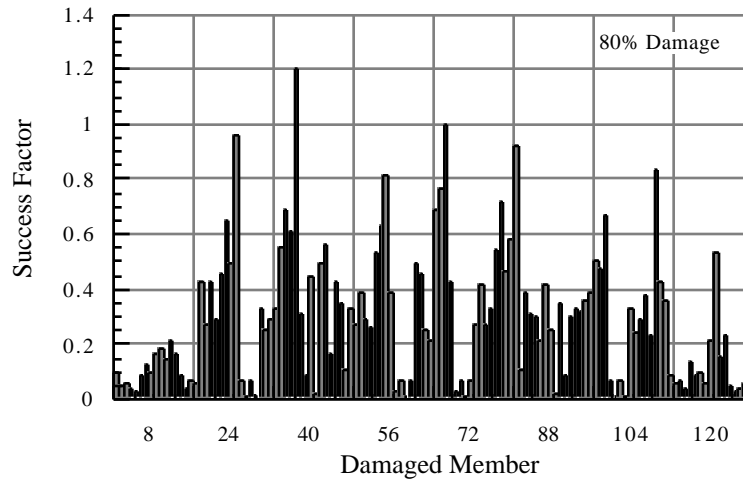
Figure 3.8. Success factor based on average angle approach for 80% damage when truss is excited by shakers.

Chapter 4
Numerical Simulations on Laboratory Truss

We have demonstrated the feasibility of the method for the 132 degree of freedom space truss in Chapter 3. Now our objective is to apply the method to the laboratory truss, and use numerical simulations to find the members in which we can expect to detect damage experimentally with a given amount of damage, and given amount of measurement noise.

In this chapter we first develop a finite element model of the truss. We will study the effect of damage on a truss member and will show that for a given mode, there is a high correlation between the strain energy stored in a member and the change in the natural frequencies due to damage in the same member. We study the variation of the frequency signature angle, contrast maximization angle and average angle for the truss members when a member (member 4) is damaged. The feasibility of the average angle approach is tested for 20%, 45% and 75% damage in a member in the absence of noise.

Using only the contrast maximization approach, we compare the results from the uncompensated and compensated contrast maximization functions in the presence of noise in the receptance matrix. We check the effect of noise in the measurement of natural frequencies on the success factor based on frequency signature alone. The average angle approach is then applied to locate damage in the presence of errors in both the receptance matrix and natural frequencies. A relationship between the damage detectability measure and the success factor based on average angle approach with and without noise is established. The damage detectability measure is combined with the success factor, which indicates the likelihood that a given damage scenario will be detected with a given magnitude of modeling and measurement errors.

4.1 *Finite Element Model of the Truss*

The truss (Fig. 4.1) is made up of tubular aluminum members and solid aluminum nodes. The non-diagonal members are 0.254 m (10 inches) long, have an effective stiffness, k = 0.225×10^8 N/m, a net mass, m = 109.61 grams and a mass moment of inertia about their center of gravity, $I_G = 5.1 \times 10^{-4}$ kg m^2. The diagonal members are 0.359 m (14.14 inches)

long, have an effective stiffness, $k = 0.148 \times 10^8$ N/m, a net mass, m = 128.15 grams and a mass moment of inertia about their center of gravity, $I_G = 15.6 \times 10^{-4}$ kg m^2.

The members of the truss are modeled as symmetric, non-uniform members, and the metal nodes are modeled as rigid point masses. The boundary conditions at each node at the wall are modeled as three massless springs, orthogonal to each other with stiffness, $k_x = 1.7 \times 10^8$ N/m, $k_y = 0.51 \times 10^8$ N/m and $k_z = 1.27 \times 10^8$ N/m. The first three natural frequencies of the undamaged truss obtained from the resulting FEM model are shown in Table. 4.1.

<div align="center">

Table 4.1. Natural frequencies of the truss.

Mode	Natural Frequency (Hz)
1	100.15
2	129.86
3	192.44

</div>
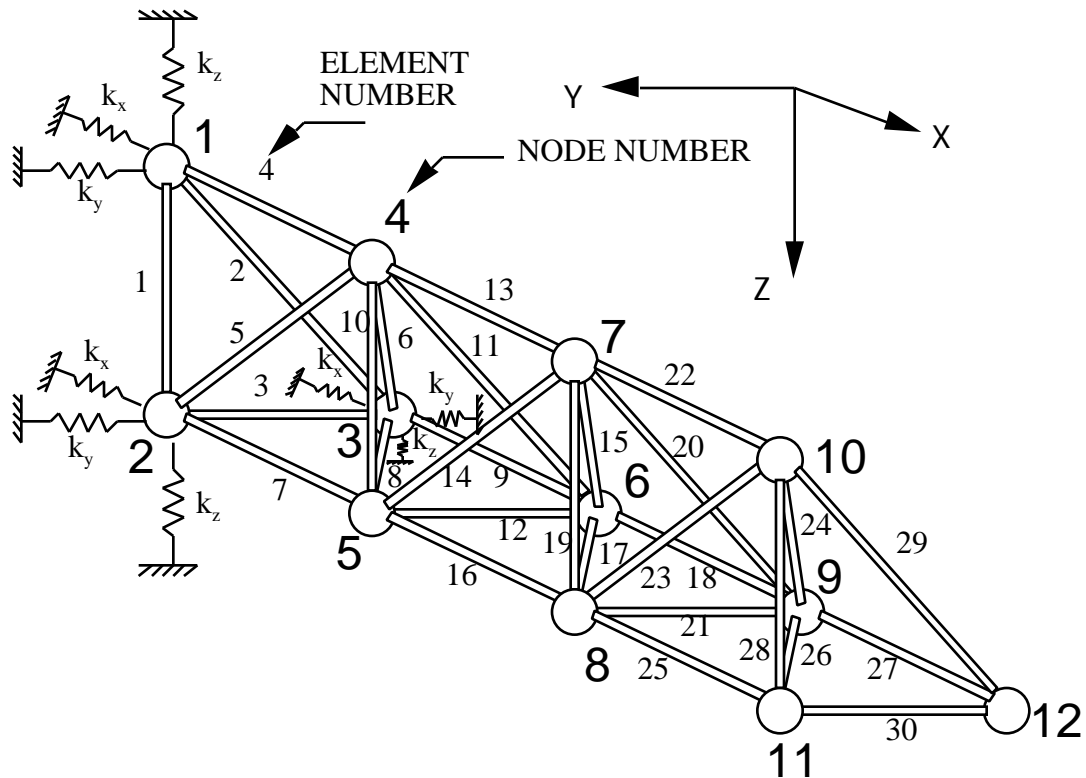
Figure 4.1. The 36 degree of freedom truss with springs at the wall

4.2 *Effect of Damage on Natural Frequencies*

We numerically studied the effect of extent of damage on the natural frequencies of the structure. Figure 4.2 shows that the variation of the first natural frequency of the structure with the magnitude of damage in member 4.   The graph indicates that up to 40% damage, the amount of change remains small. Both the damaged member and mode considered were varied and it was observed that the nature of graph remains similar for damage in most of the members.

Figure 4.3 shows the variation of the third natural frequency of the structure with the extent of damage when the damaged member is 18. It is seen that for damage in some members and for certain modes, there is little change in the natural frequency of the structure. These members have small contributions to the strain energy of the structure in that mode of vibration.
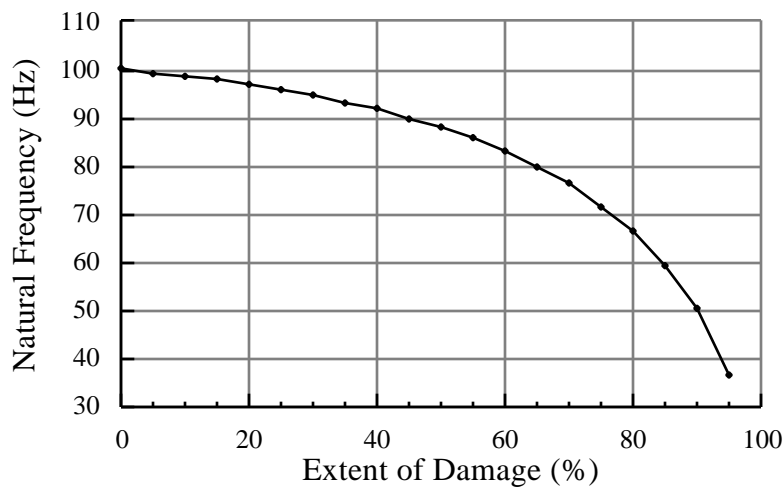
Figure 4.2. Effect of damage in Member 4 on Mode 1 of the truss

We computed the strain energy stored in a member when the undamaged truss is in its fundamental mode of vibration. Figure 4.4 shows that members 4, 7, 13 and 16 contribute a high percentage of strain energy in the fundamental mode. Members 9,18, 24, 26 and 27 have a negligible contribution to the strain energy in this vibration mode. We also simulate damage to each member of the truss with a 50% stiffness reduction and compute

the change in first natural frequency. Fig. 4.5 shows that maximum change in fundamental natural frequency of the truss occurs when the members 4, 7, 13 and 16 are damaged, where as a small change in fundamental natural frequency of the truss occurs when the members 9, 18, 24, 26 and 27 are damaged

The correlation coefficient between the strain energy stored in a member of the undamaged structure for the fundamental mode and the change in the fundamental natural frequency for 50% damage in a member was calculated to be 97%. This shows that if a member has a high contribution to the strain energy of the undamaged structure for a vibration mode, the change in natural frequency of the structure when the same member is damaged is also high. It can be shown analytically[43] that the derivative of the strain energy with respect to the area of a member is proportional to the derivative of the strain energy and kinetic energy in the member with respect to the area of the member. Since damage does not affect the mass of the element, the derivative of frequency is proportional to the derivative of the strain energy in the member.
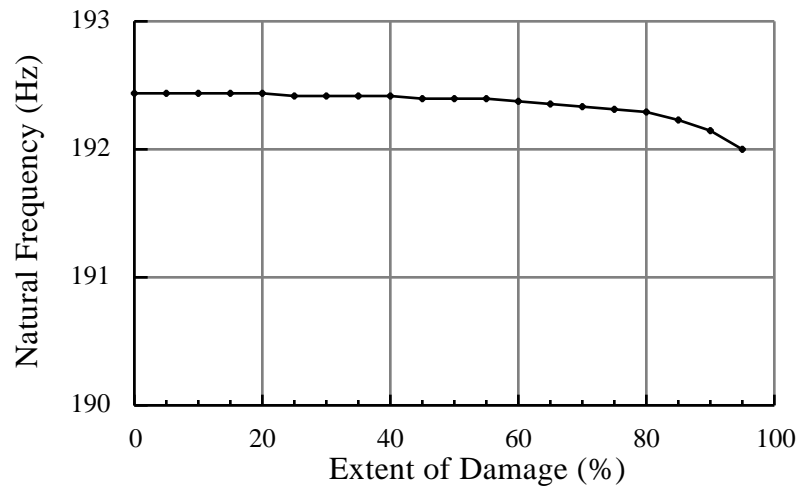
Figure 4.3. Effect of Damage in member 18 on Mode 3 of the truss.
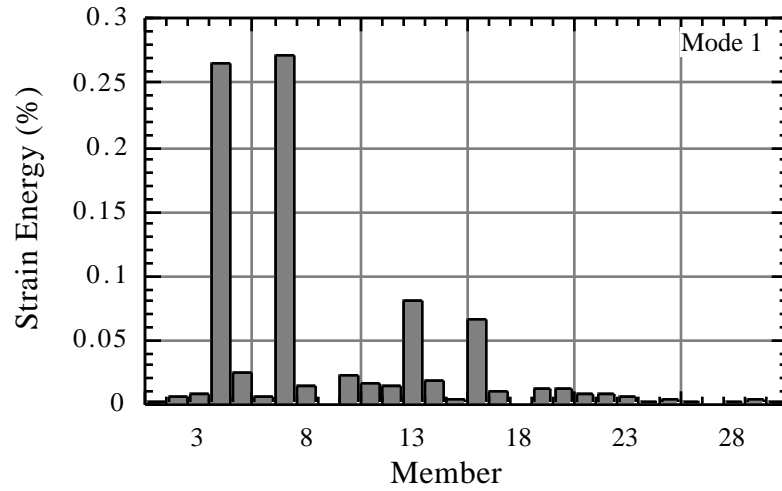
Figure 4.4. Strain Energy (percent) in a member of undamaged truss for mode 1.
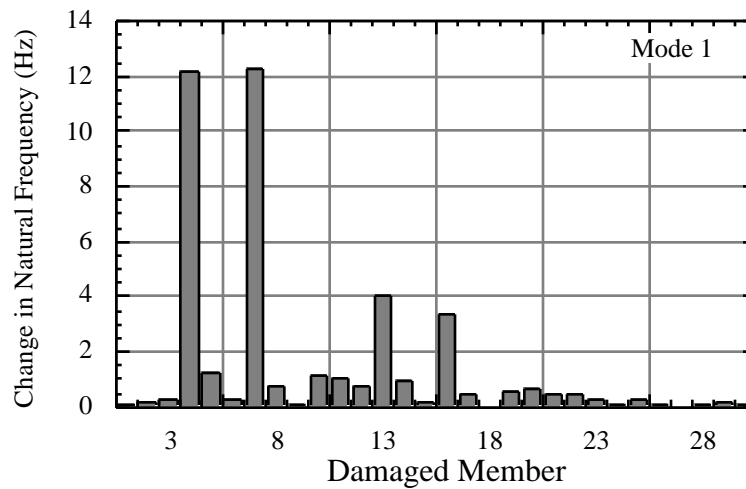
Figure 4.5. Change in natural frequency for 50% damage in a member.

4.3. *Measuring Structural Response*

To generate the contrast maximization excitations, which will create the maximum difference between the actual damaged structure and the model of the undamaged structure, we need to measure the structural response. For the technique to be efficient in real time, we need a measure of structure response which is easy to accurately measure in the field or

laboratory, takes little computation time, and is a physically meaningful quantity. Two possible choices are the strain energy of the structure and the square of measured displacement amplitudes. It was shown in Chapter 2 that the technique based on square of the measured displacement amplitudes takes less experimental time than the technique based on strain energy of the structure.

4.4 *Damage Identification with No Errors*

In the laboratory work, we will use collocated shakers/sensors rather than active members. For all the numerical simulations on the laboratory truss, we assume that the structure is excited by shakers and the response is measured by collocated sensors. The collocated shakers/sensors were located at degrees of freedom 6Z, 7Z and 12Z. Only the first three modes, which are bending, bending and torsion modes, were considered for damage identification.

Hypothetical models of damage scenarios corresponding to damage in a member with 30% or 70% stiffness reduction are created. The technique was based on pre-determined frequencies (Eq. 2.19a) and no real-time computation was required to generate the database. We first damaged member 4 and computed the various angles for all the members. The damage level (30% or 70%) which gives the *smallest average angle* is chosen to represent the actual damaged structure. Member 4 was chosen as the first candidate for damage identification as the damage at this location has maximum effects on the fundamental natural frequency, i.e., this member has a high strain energy in the fundamental mode of vibration.

4.4.1 Damage in Member 4 - Numerical

Member 4 was damaged with a stiffness reduction of 20% and the natural frequencies of the damaged structure were:

$$\omega_1^d = 96.87 \text{ Hz}, \qquad \omega_2^d = 128.48 \text{ Hz}, \qquad \omega_3^d = 191.63 \text{ Hz}$$

The excitation frequencies for the contrast maximization approach were 5% away from the natural frequencies of the damaged truss. The average angle approach was applied and the

smallest average angle obtained for 30% database was 2.9˚ (Fig. 4.8) and 15.7˚ (Fig. 4.9) for 70% database. The 30% damage level was hence chosen to represent the actual damaged structure. The average contrast maximization angle was calculated and it is observed (Fig. 4.6) that member 4 had the smallest contrast maximization angle. The frequency signature angles for the truss members are shown in Fig. 4.7 and we see that member 4 had the smallest frequency signature angle. The average angle for the 30%
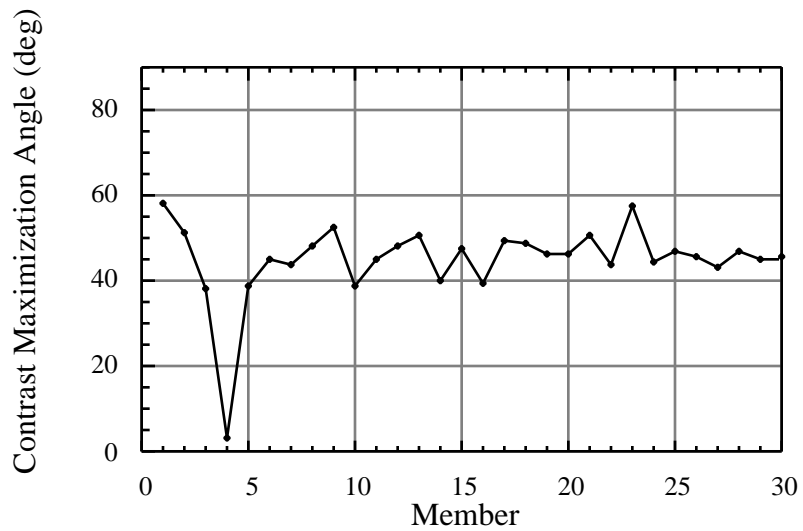
Figure 4.6. Contrast maximization angles for all members when member 4 is damaged
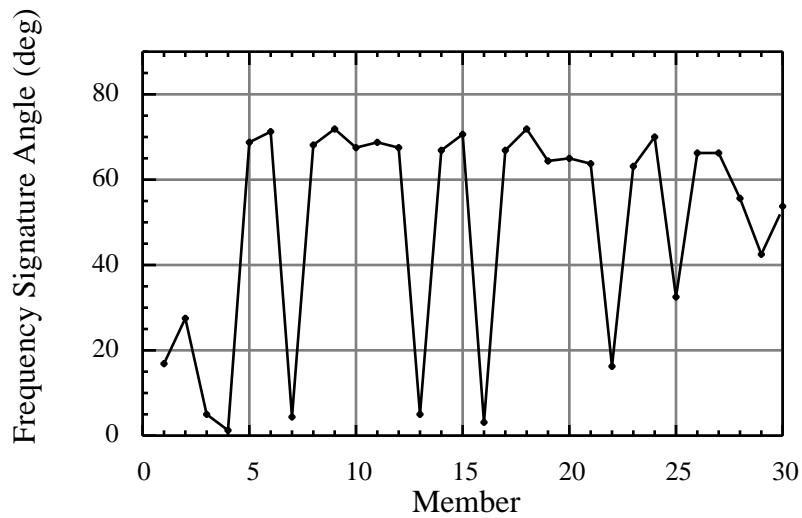
Figure 4.7. Frequency Signature Angle for all members when member 4 is damaged

damage level are shown in Fig. 4.8. The success factors were calculated to be 0.44, 0.10, and 0.12 for the frequency signature approach, contrast maximization approach, and the average angle approach respectively. The contrast maximization approach, frequency signature approach and the average angle approach were all able to identify the damaged member. For comparison, the average angle for the 70% damage level are shown in Fig. 4.9.
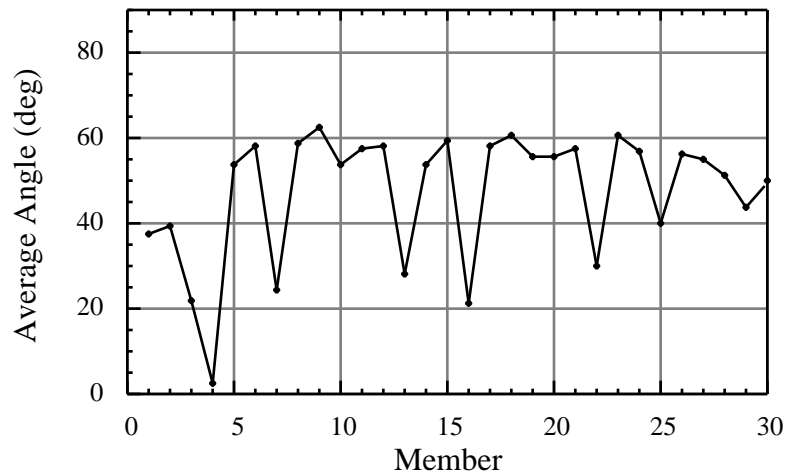
Figure 4.8. Average angle for all members (using 30% database) when member 4 is damaged.
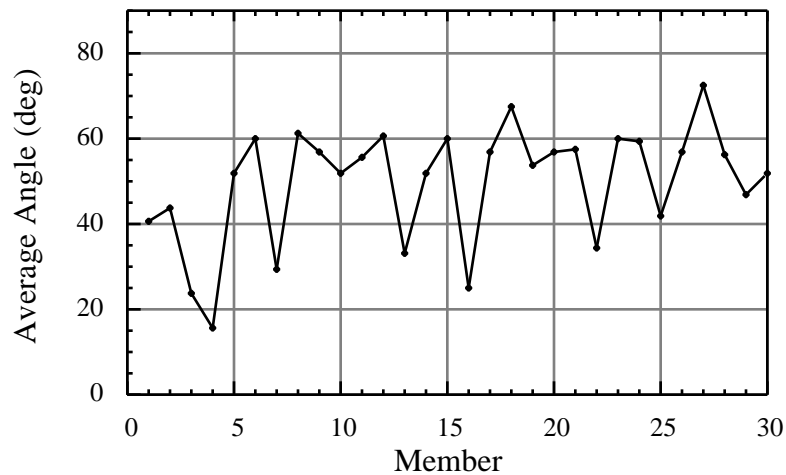
Figure 4.9. Average angle for all members (using 70% database) when member 4 is damaged.

38

4.4.2 20% Damage in an arbitrary member

One member was damaged with 20% reduction in its stiffness and the technique was applied to locate the damage. The average angle was used to sort the members in an ascending order and the members were then stored in the form of a list. It was expected that the damaged member will have the smallest average angle and will be first in the list. As before, the damage scenarios were represented by 30% and 70% damage level. The database (30% or 70% damage) which gives the smallest average angle is chosen as the database which best represents the damaged structure. The location of damage was then changed and the technique was then applied to locate the damage. The average angle technique (Fig. 4.10) was able to identify the damage in all the different locations. It was observed that the smallest average angle was obtained for 30% database for all the locations of damage. The following results are with database represented by 30% damage in a member.

The frequency signature approach (Fig. 4.11) and the contrast maximization approach (Fig. 4.12) were also able to locate the damage for all members. We observe that most of the members with a very small value of success factor based on average angle approach are either at the wall or near the free end of the truss.
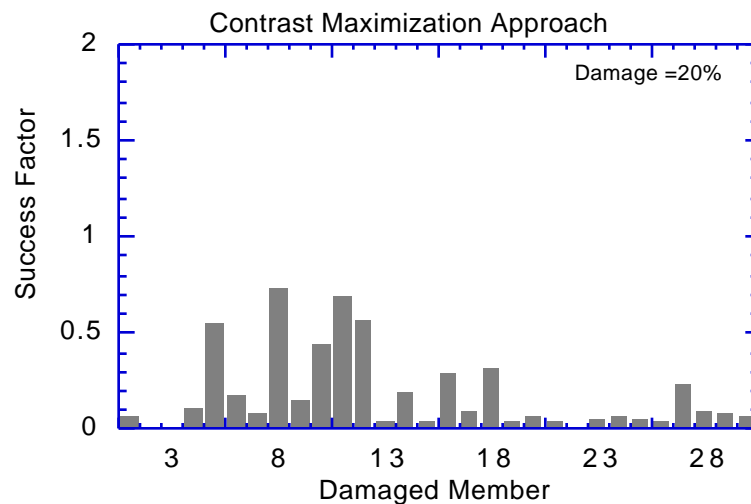
Figure 4.10. Contrast maximization approach for 20% damage in a member
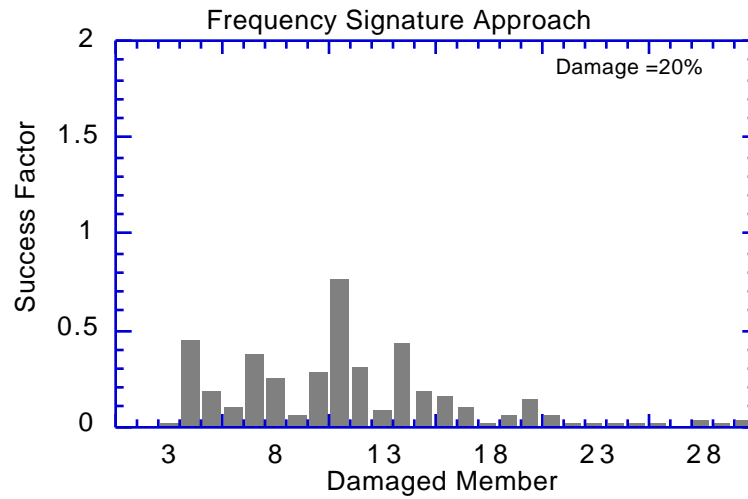
Figure 4.11. Frequency signature approach for 20% damage in a member.
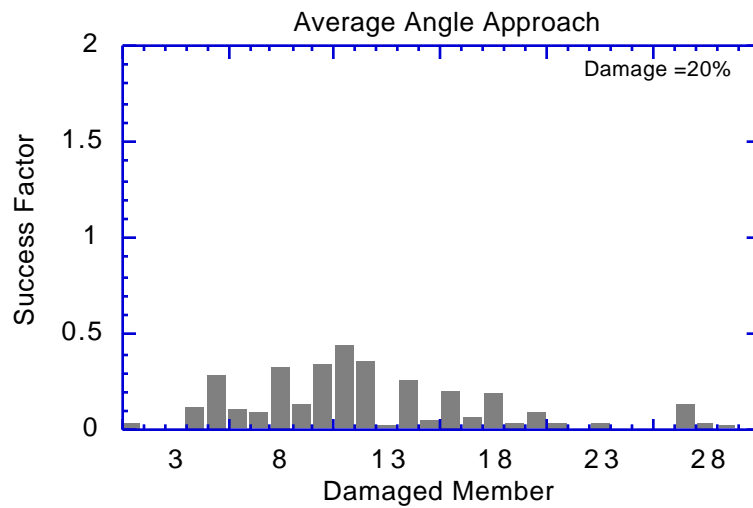
Figure 4.12. Average angle approach for 20% damage in a member.

4.4.3 45% Damage in a member

A member was damaged with 45% reduction in its stiffness and the technique was applied to locate the damage. It was expected that the damaged member will have the smallest average angle and will be have a success factor smaller than unity. The damage level (30% or 70%) which gives smaller average angle is chosen to represent the damaged structure.

Since the actual damage level falls in between 30% and 70% damage level, for some damage locations 30% database will give smallest average angle and for other damage locations, 70% database will give smallest average angle. The location of damage was then changed and the technique was then applied to locate the damage.

The contrast maximization approach (Fig. 4.13) were unable to locate the damage at member 11 where the success factor was 3.94. The frequency signature approach (Fig. 4.14) was unable to identify damage at members 10 and 11 and had a success factor of 2.4
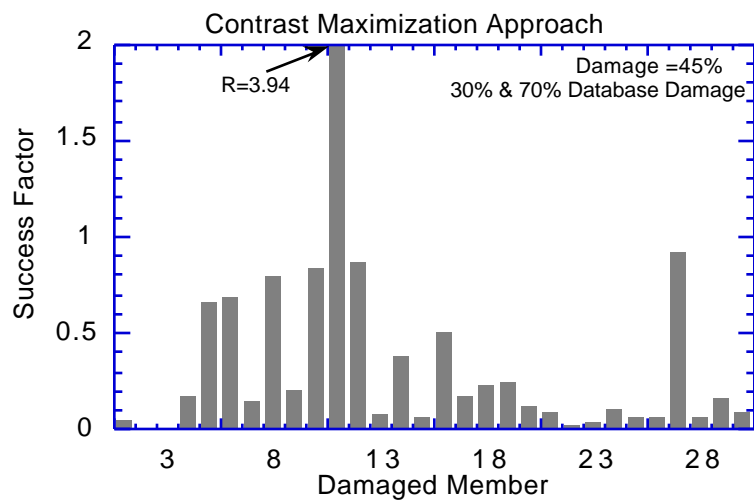
Figure 4.13. Contrast maximization approach for 45% damage in a member.
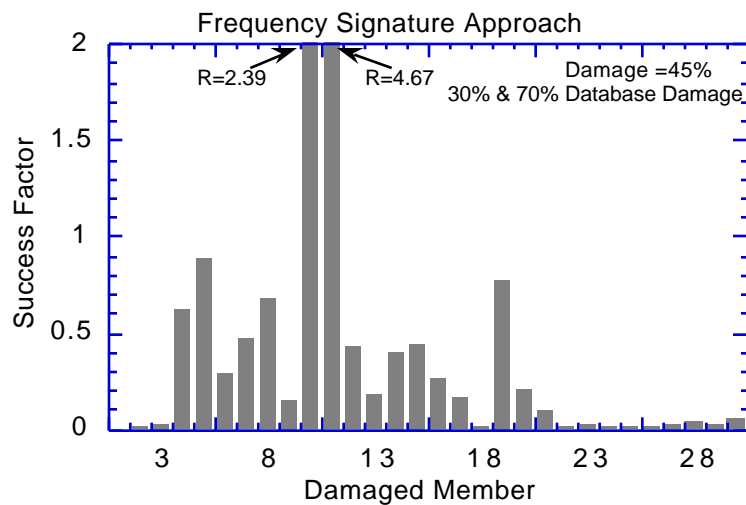
Figure 4.14. Frequency signature approach for 45% damage in a member.

and 4.7 respectively. The average angle technique (Fig. 4.15) was able to identify the damage in all locations except for member 11. Combining the frequency signature approach with the contrast maximization approach helped increase the reliability of the damage detection algorithm.
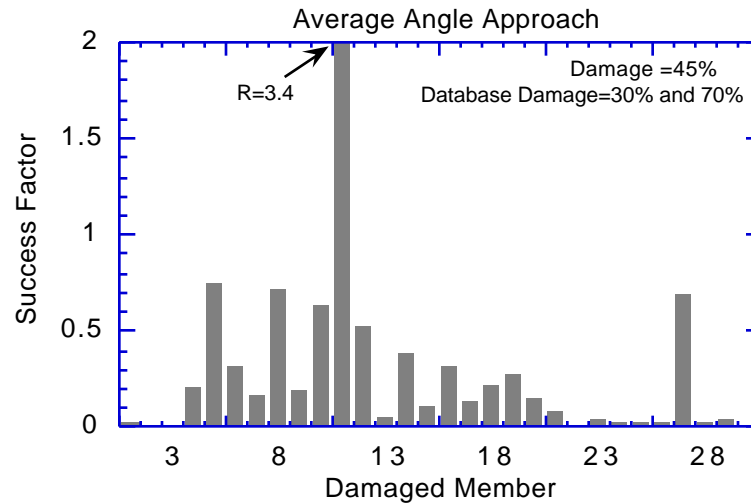
Figure 4.15. Average angle approach for 45% damage in a member.

4.4.4 75% Damage in an arbitrary member

Each member was damaged with 75% reduction in its stiffness and the technique was applied to locate the damage. The contrast maximization approach (Fig. 4.16) were unable to locate the damage at members 10 and 12. The frequency signature approach (Fig. 4.17) was unable to identify damage at members 5 and 10. The success factor based on frequency signature approach for damage in member 5 was 26.7. The large value for the success factor was obtained because the member (member 10) which had the smallest angle had an angle of 0.03˚ compared to 0.99˚ for the damaged member 5.

The average angle technique (Fig. 4.18) was able to identify the damage in 29 of the 30 locations. The technique was unable to locate the damage in member 5, but it predicted the damaged member as the 2nd most likely member to have the damage with a success factor

of 1.2. Combining the frequency signature approach with the contrast maximization approach helped in increasing the reliability of the damage detection algorithm.
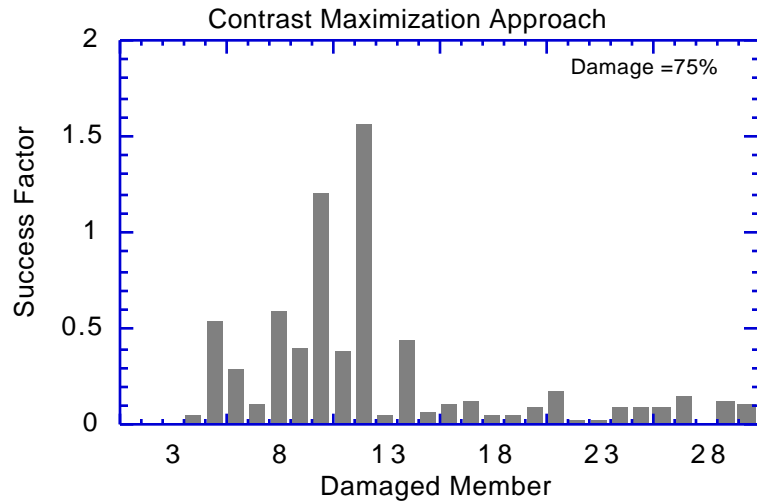
Figure 4.16. Contrast maximization approach for 75% damage in a member.
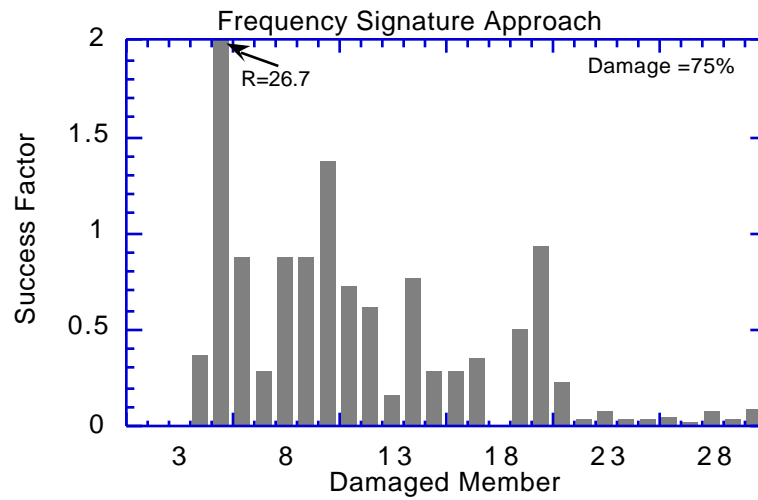
Figure 4.17. Frequency signature approach for 75% damage in a member.
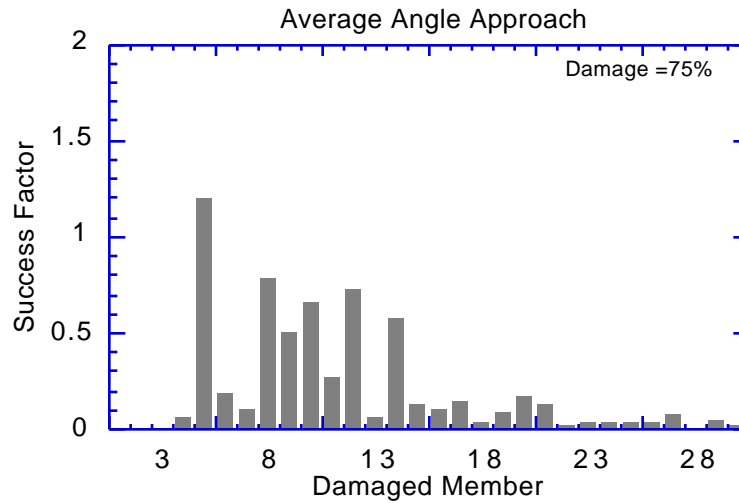
Figure 4.18. Average angle approach for 75% damage in a member.

4.5 *Damage Identification in Presence of Errors*

To check the robustness of the technique, we considered measurement errors and noise in the acquired signal. To study the effect of noise on damage detection by *contrast maximization* only, we generated measurement noise in the measurements of the receptance matrix of both the undamaged structure and the damaged structure. The noise was simulated by generating a pseudo random number from a standard normal distribution (subroutine RNNOF in the IMSL MATH/LIBRARY) with a coefficient of variation (COV) of 1%. To model any bias in the measurements or modeling errors, we constrained the noise to be positive.

Later, we study the effect of noise on the estimates of the natural frequencies and apply the *frequency signature approach* to locate the damage. Under experimental conditions, we have noise in both the receptance matrix and the natural frequencies and we use the *average angle approach* to locate the damage. For all the cases studies in this section, the database is represented by only 30% damage level. The amount of damage in a member is either 20% or 45%.

44

4.5.1 20% Damage with Noise in Receptance Matrix

In this section we will compare the damage detection results for the uncompensated (Eq. 2.27) and the compensated (Eq. 2.28) contrast maximization functions. Since the results from the frequency signature approach are the same for both the approaches, we will not use the average angle approach for comparison. For 20% damage in a member, eight sets of receptance matrices having noise were generated and for each set, we applied only *contrast maximization* to detect the damage. Both the uncompensated and compensated contrast maximization functions were used for generating the excitation vectors. For a chosen damage location, the success factor and the damage detectability measure were computed for each set of receptance matrices and the results were then averaged over the eight sets of receptance matrix.

If the uncompensated contrast maximization is used, there were 16 members (Fig. 4.19) where a 20% damage could not be identified (R > 1.0) in the presence of measurement noise with a 1% COV. The mean value and the standard deviation of the success factor based on contrast maximization over the different locations of damage is computed to be,

$$R_\mu = 2.08 \quad \text{and} \quad R = 0.47 \tag{4.1}$$

The number of members which could not be identified by each of the eight sets were also calculated and averaged. The average number of members which could not be identified in the presence of noise was obtained to be 16.6. We obtained the same success rate in damage identification when we averaged R based on contrast maximization over the eight sets and perform damage identification or average the number of successfully identified members by each set.

For successful detection of damage at a particular location, the value of success factor should be much less than unity. The mean value, $R_\mu = 2.08$ indicates that on average, the damage will not be detectable using this contrast maximization function.

If the damage detectability measure is approximately greater than 0.5, then we believe that the effect of noise is large and our confidence in damage detection is low. The damage detectability measure (Fig. 4.20) indicates that damage in 17 members where the damage

detectability is greater than 0.5. These are the members of the structure with negligible strain energy.

If the compensated contrast maximization is used for damage identification, there are 13 members (Fig. 4.21) where a 20% damage could not be identified in the presence of measurement noise of 1% COV. The mean value and the standard deviation of the success factor over all locations of damage is computed to be,

$$R_\mu = 1.07 \quad \text{and} \quad R = 0.59 \tag{4.2}$$

For successful detection of damage at a particular location, the value of success factor should be much less than unity. The mean value, $R_\mu = 1.07$ is a big improvement over $R_\mu = 2.08$ for the uncompensated contrast maximization function. The success factors for the uncompensated and compensated contrast maximization function and the damage detectability measure are also shown in Table 4.2. It shows that the compensated contrast maximization is more effective in locating damage than the uncompensated contrast maximization. Note that in this section on damage identification in the presence of errors, we are using only 30% database.
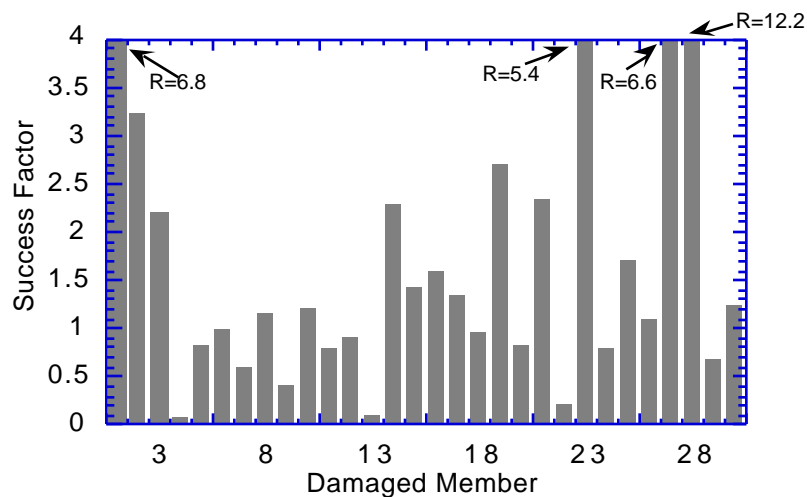
Figure 4.19. Success factor based on uncompensated contrast maximization for 20% damage with numerical noise.
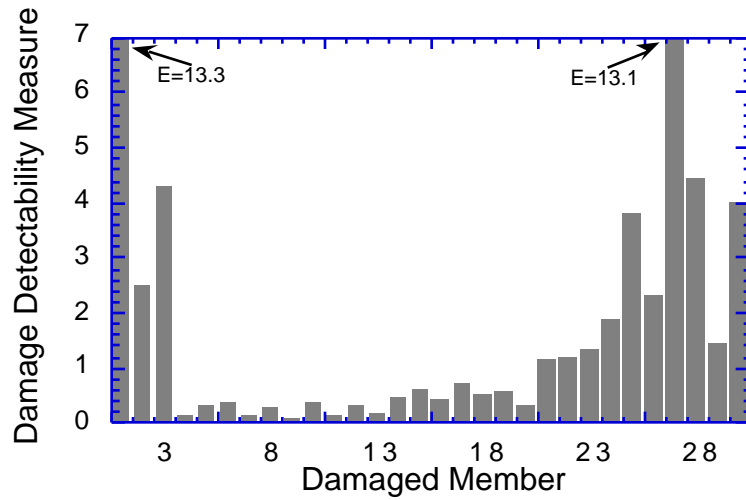
Figure 4.20. Damage Detectability measure for 20% damage with numerical noise.
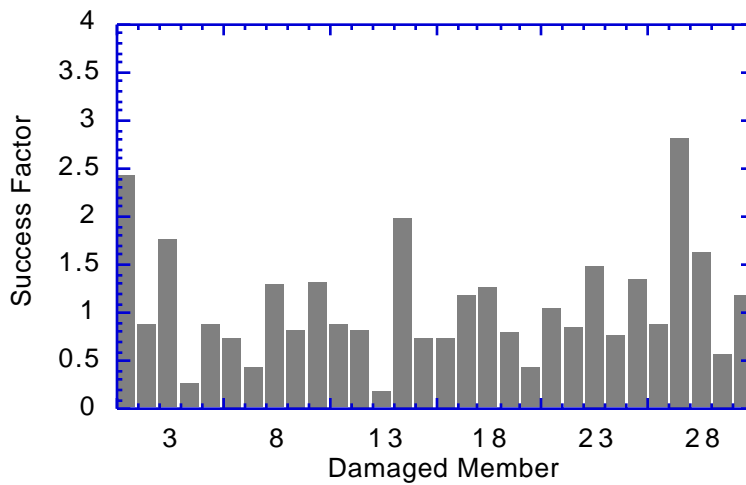
**Figure 4.21. Success factor based on compensated contrast
maximization for 20% damage with numerical noise.**

The detectability measure is independent of the contrast maximization function and has the
same values as those obtained for the previous contrast maximization function. For the
compensated contrast maximization problem, the correlation coefficient between success
factor based on contrast maximization and damage detectability measure was calculated to
be 76%. This indicates that a member which should not be detected due to noise (E > 0.5)
can still be detected sometimes (R < 1.0) and vice-versa. The success factor based on

compensated contrast maximization in the absence of noise was also calculated and the correlation coefficient between success factor with and without noise was calculated to be 5%. We believe that we obtained a low value for the correlation due to the small amount of damage (20% damage) in the damaged member.

Table 4.2 Effect of noise on the success factors for uncompensated and compensated contrast maximization approach

Damaged Member	R (Contrast Maximization) for no noise - R_o	Damage Detectability Measure, E	R (Uncompensated Contrast Maximization)	R (Compensated Contrast Maximization)
1	0.06	13.3	6.84	2.41
2	0.01	2.5	3.22	0.87
3	0.01	4.3	2.20	1.75
4	0.10	0.1	0.07	0.25
5	0.05	0.3	0.80	0.86
6	0.18	0.4	0.98	0.73
7	0.07	0.1	0.61	0.42
8	0.72	0.3	1.14	1.29
9	0.14	0.1	0.39	0.80
10	0.43	0.4	1.19	1.30
11	0.69	0.1	0.78	0.87
12	0.56	0.3	0.90	0.82
13	0.04	0.1	0.09	0.17
14	0.19	0.4	2.27	1.96
15	0.04	0.6	1.43	0.74
16	0.28	0.4	1.58	0.72
17	0.10	0.7	1.32	1.19
18	0.31	0.5	0.96	1.26
19	0.03	0.6	2.71	0.80
20	0.06	0.3	0.81	0.42
21	0.03	1.1	2.34	1.02
22	0.01	1.2	0.20	0.83
23	0.04	1.3	5.35	1.49
24	0.07	1.8	0.79	0.75
25	0.04	3.8	1.69	1.34
26	0.03	2.3	1.09	0.85
27	0.23	13.1	6.59	2.82
28	0.09	4.4	12.2	1.62
29	0.08	1.4	0.67	0.57
30	0.06	4.0	1.22	1.18

4.5.2 45% Damage with Noise in Receptance Matrix

We also performed numerical simulations for 45% damage in a member in the presence of noise. The measurement noise was again simulated by a pseudo-random number generator

with COV=1%. Only the compensated contrast maximization was applied to locate the damage. The damage detectability measure and the success factor are shown in Figs. 4.22 and 4.23.
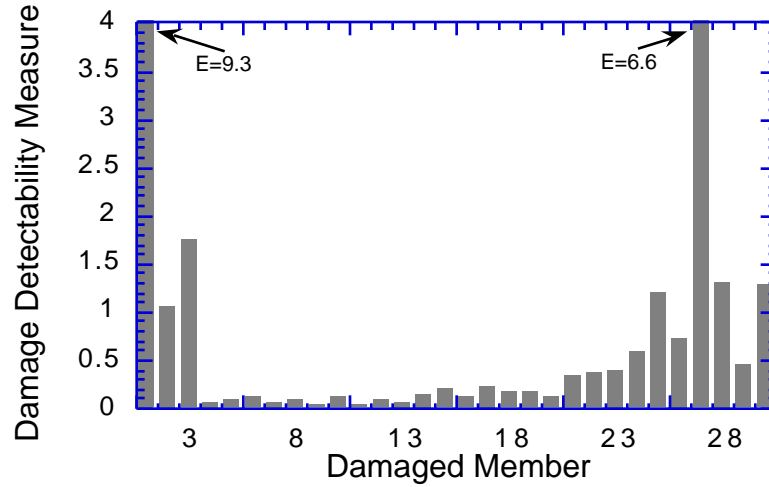
Figure 4.22. Damage Detectability measure for 45% damage in a member with numerical noise in receptance matrix.

The number of members where damage detectability measure is greater than unity decreased to 7 and the number of members which could not be identified in the presence of noise decreased to 10. The mean value and the standard deviation of the success factor based on contrast maximization over different locations of damage is computed to be,

$$R_\mu = 0.82 \qquad \text{and} \qquad R_\sigma = 0.64 \tag{4.3}$$

We see that the technique is able to locate the damage in the presence of noise for most members with small values of damage detectability measure. The correlation coefficient between success factor based on contrast maximization and damage detectability measure was calculated to be 62%. The correlation coefficient between the success factor with and without noise was calculated to be 57%. We see that the success in damage detection in presence of noise depends upon the success in damage detection in absence of noise and the damage detectability measure. Increases in damage, decreases damage detectability measure and increases the chances of damage identification.
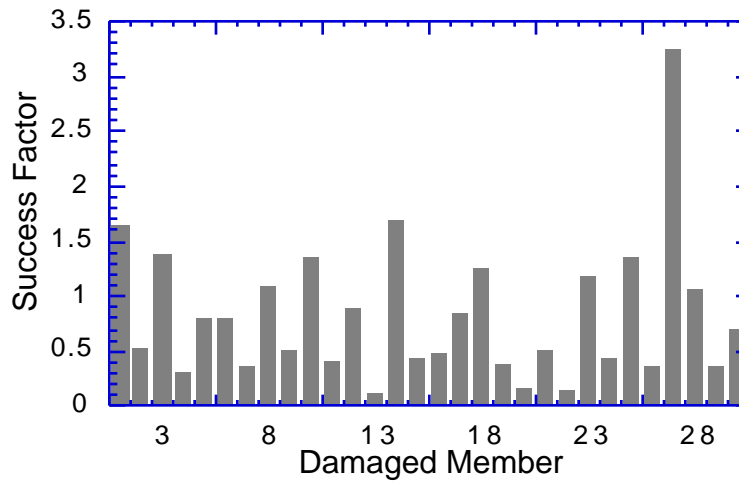
Figure 4.23. Success factor based on compensated contrast maximization for 45% damage in a member in presence of noise.

4.5.3 45% Damage with Noise in Natural Frequencies

Under experimental conditions in our particular test set up, we estimated that we can expect errors of approximately 0.15 Hz in measuring the natural frequencies. Eight sets of natural frequencies having noise were generated for both the undamaged and the damaged structure. The *frequency signature approach* was applied to locate the damage. For a chosen damage location, success factor based on frequency signature approach and damage detectability measure was calculated for each set and the results were then averaged over the eight sets. Note that errors in measured natural frequencies will result in an error in the elements of receptance matrix, and that we can compute damage detectability measure from Eq. 2.27.

We obtained the same success rate in damage identification when we averaged success factor over the eight sets and performed damage identification or averaged the number of successfully identified members for each set. The following results were obtained when we averaged success factor over eight sets to locate the damage.

The number of members not identified (R > 1.0) by the frequency signature approach (Fig. 4.24) in the presence of noise increased to 7. The number of members where damage

50

detectability measure (Fig. 4.25) was greater than 0.5 was 7. The correlation coefficient between success factor based on frequency signature and damage detectability measure was calculated to be 33%. This indicates that small errors in measuring natural frequencies do not severely effect the measured receptance matrix. The success factor in the absence of noise was also calculated and the correlation coefficient between success factor with and without noise was found to be 60%.
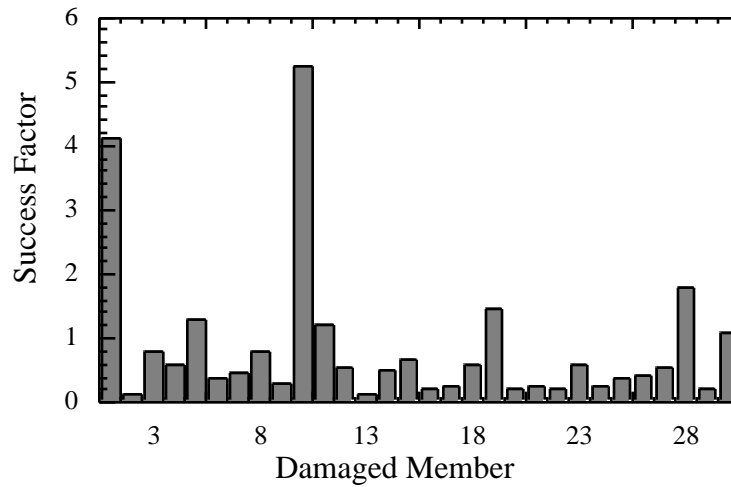
Figure 4.24. Success factor based on Frequency Signature Approach in the presence of noise for 45% damage.
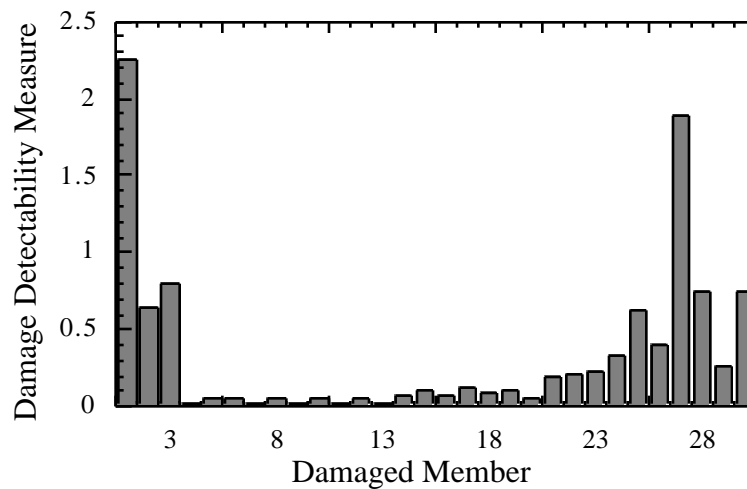
Figure 4.25. Damage detectability measure for 45% damage in a member with noise in natural frequencies.

51

4.5.4 20% Damage with Noise in Natural Frequencies and Receptance Matrix

We generated noise in the receptance matrix and the natural frequencies of both the undamaged and the damaged structure. Eight sets of data having noise was generated for both the undamaged and the damaged structure. The *average angle approach* was applied to locate the damage. For a chosen damage location, success factor based on average angle approach (Fig. 4.26) and damage detectability measure (Fig. 4.27) was calculated for each set and the results were then averaged over the eight sets. The results indicate that the technique was unable to detect damage in 11 locations and damage detectability measure was greater than 0.5 in 19 locations. Note that the damage detectability measures shown in Fig. 4.27 are different from the corresponding damage detectability measures shown in Fig. 4.20. The damage detectability measures in Fig. 4.27 were computed for random noise in natural frequencies and receptance matrix, where as, the damage detectability measures in Fig. 4.20 was computed for random noise in receptance matrix alone. It seems that the way we generated noise in natural frequencies helped decrease the damage detectability measure for damage in some locations.
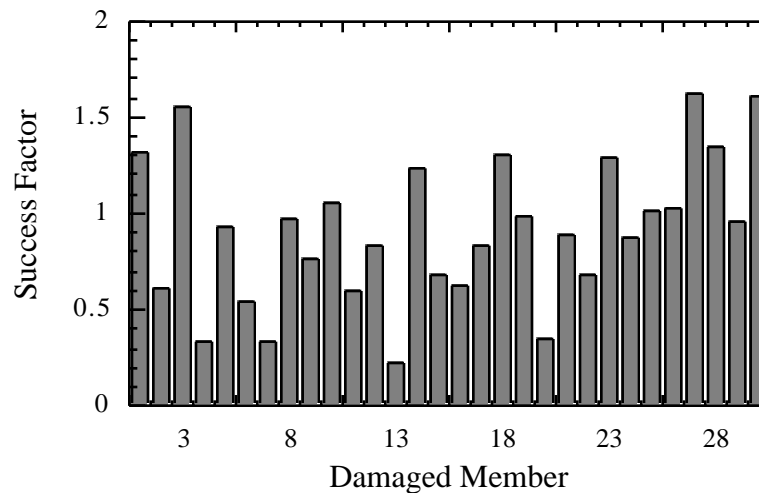
Figure 4.26. Success factor based on average angle approach for 20% damage in a member in the presence of noise.
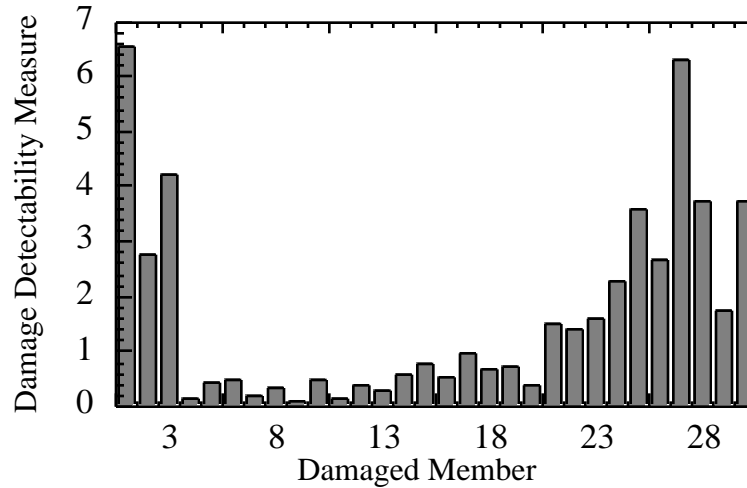
Figure 4.27. Damage Detectability measure for 20% damage in a member with noise in natural frequencies and receptance matrix.

4.5.5 45% Damage with Noise in Natural Frequencies and Receptance Matrix

Eight sets of data having noise was generated for both the undamaged and the damaged structure. The *average angle approach* was applied to locate the damage. For a chosen damage location, success factor based on average angle approach (Fig. 4.28) and damage detectability measure (Fig. 4.29) was calculated for each set and the results were then averaged over the eight sets. The results indicate that the based on the success factor, the technique was unable to detect damage in 6 locations. The average value of success factor over all locations of damage was computed to be $R_\mu = 0.63$. The damage detectability measure was greater than 0.5 in 11 locations. Our confidence in the results at these 11 locations is low as the effect of noise is of the same order of magnitude as the effect of the damage. The correlation coefficient between the success factor in the presence of noise and damage detectability measure was found to be 47%.

From the numerical simulations in the presence of errors, we make the following conclusions:

i) based on the success factor (R < 1.0), the compensated contrast maximization approach has a higher success rate in damage identification than the uncompensated contrast maximization approach.

ii) the success factor in the presence of noise depends upon the damage detectability measure and the success factor in the absence of noise.

We will now try to establish a relationship between damage detectability measure, success factor in the presence of noise (R) and success factor in the absence of noise (R_O).
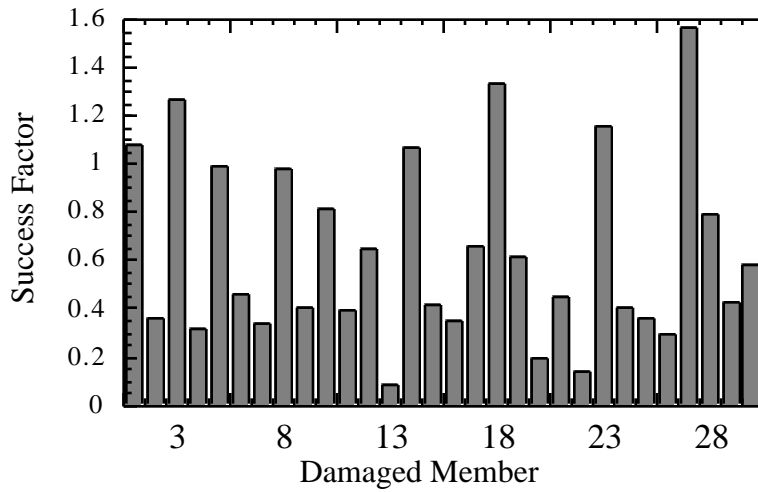
Figure 4.28. Success factor based on average angle approach for 45% damage in a member.
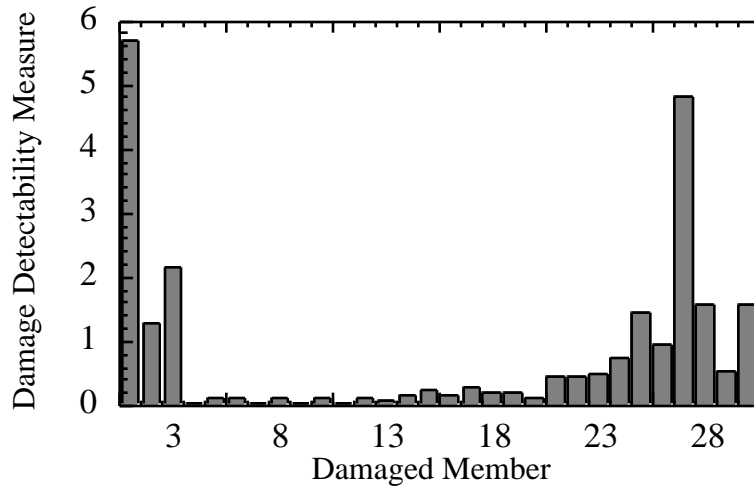
**Figure 4.29. Damage Detectability measure for 45% damage in a member
with noise in natural frequencies and receptance matrix.**

4.6 Establishing Relationship between R, E and R_0

Since R in the presence of noise depends upon E and R without noise (R_O), we applied linear regression to the data for 20% damage in a member to obtain an expression for the relationship. We have the calculated values of damage detectability measure and the success factor in the presence and absence of noise. The estimated success factor in the presence of noise is assumed to take the form,

$$\hat{R} = c\ E\ \ R_o \tag{4.4}$$

Taking logarithm on both the sides, we get a linear equation,

$$Ln(\hat{R}) = Ln(c) + \ \ Ln(E) + \ \ Ln(R_o) \tag{4.5}$$

The difference between the right and left hand sides of the above equation is minimized to obtain a fit between the Eq. 4.6 and the data by using Mathematica function (Fit). The best fit is obtained by,

$$\hat{R} = 1.482\ E^{0.434}\ R_o^{0.183} \tag{4.6}$$

The error between the measured success factor (R) and estimated success factor ($\hat{R}$) for 20% damage in a member in the presence of noise for each location is calculated,

$$(i) = |\frac{\hat{R}(i) - R(i)}{R(i)}| \tag{4.7}$$

and then averaged over the 30 possible damage locations. The average error for 20% damage, $^-(20\%)$ is calculated to be 25%. To further decrease the average error, the response surface is assumed to take the form of quadratic function of logarithm in E and R_o,

$$Ln(\hat{R}) = \ Ln(a) + b\ Ln(E) + c\ Ln(R_o) + d\ (Ln(E))^2 + e\ (Ln(R_o))^2 + f\ Ln(E)Ln\ (R_o)$$

The best fit is obtained by

$$Ln(\hat{R}) = 0.1639 + 0.0048\ Ln(E) + 0.023\ Ln(R_O) - 0.063\ (Ln(E))^2 - 0.0303(Ln(R_O))^2$$
$$- 0.151\ Ln(E)Ln\ (R_O) \tag{4.8}$$

The average error between estimated and calculated success factor for 20% damage in a member, $\bar{\ }(20\%)$ decreased to 21%. In section 4.8, we will check the predictive capability of the response surface given by Eq. 4.8 for the case of 45% damage.

4.7. *Classification of Members in Groups*

The success factor based on the average angle approach in the presence of errors is expected to simulate the success of the technique in locating damage under experimental conditions. Though the amount of errors and bias in the experimental measurements would be different from the simulations, we expect that there will be a close match between the success factor obtained by simulations in the presence of noise and the success factor obtained experimentally for the same amount of damage. If damage in a member yields success factor much smaller than one, we expect that it will be easier to locate the damage in this member while conducting experiments and vice-versa. If the success factor is close to unity then depending upon the errors, we may or may not be able to locate the damage under experimental conditions.

Based on the success factor obtained from numerical simulations in the presence of noise, we try to classify the members into 3 groups.

i) Group A: Damage in a member belonging to this group should be easy to locate under experimental conditions. For such members, success factor based on the average angle approach is less than 0.5.

ii) Group B: Damage in a member belonging to this group may or may not be located under experimental conditions. For such members success factor based on the average angle approach belongs to a range $\{0.5 < R < 1.5\}$.

iii) Group C: Damage in a member belonging to this group will be difficult to locate under experimental conditions. For such members, success factor based on the average angle approach is greater than 1.5.

Table 4.3 shows the members classified into the three groups for 45% damage in a member. We see that 16 members belong to Group A, 13 members belong to Group B and

Table 4.3. Classification of members by calculated success factor for 45% damage in a member

Group	Range of R	Members in the group
A	$R < 0.5$	2, 4, 6, 7, 9, 11, 13, 15, 16, 20, 21, 22, 24, 25, 26, 29
B	$0.5 < R < 1.5$	1, 3, 5, 8, 10, 12, 14, 17, 18, 19, 23, 28, 30
C	$R > 1.5$	27
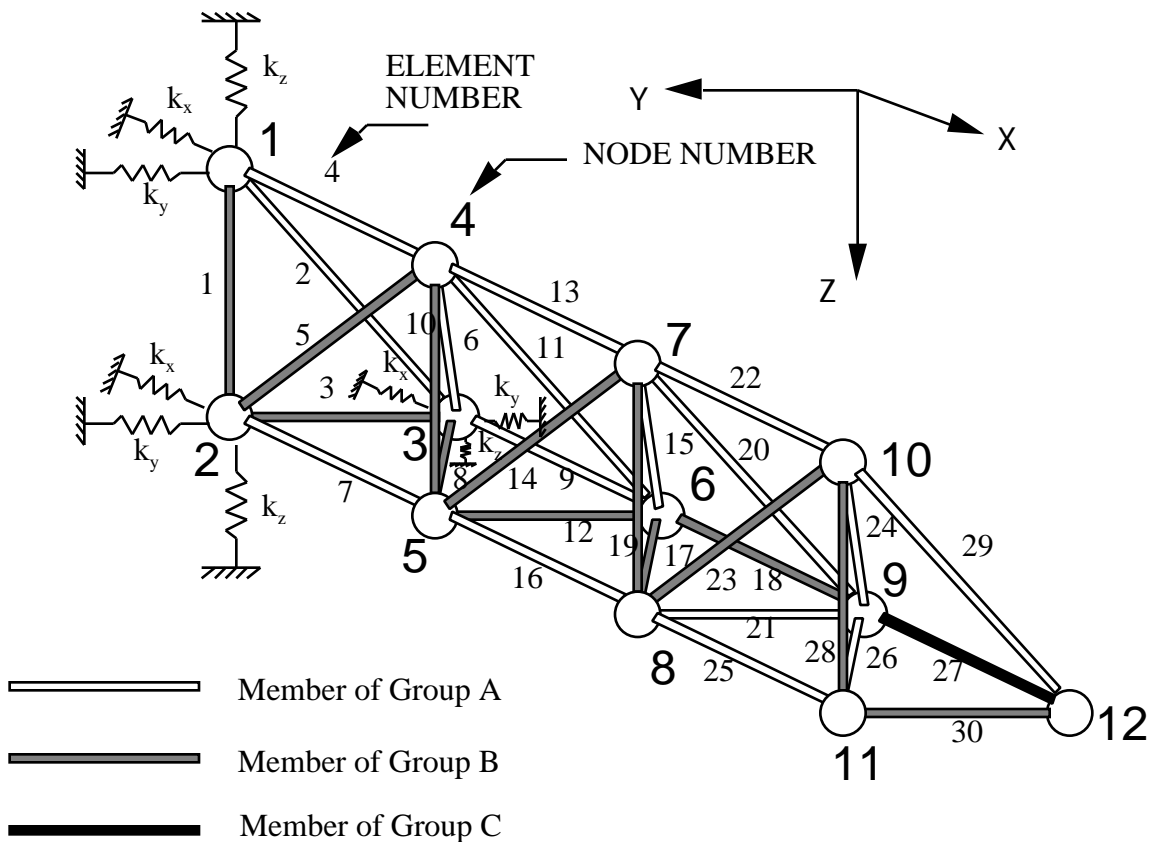
Figure 4.30. The members belonging to Groups A, B and C shown on the truss.

one member belongs to Group C. The location of members belonging to the three groups are shown in Fig. 4.30. We see that the longerons (members like 4, 13, 22, 7,...) have a low value of success factor in the presence of noise and it is easy to locate damage in these members. Most of the members aligned with the Y or Z axis belong to Group B and it may not be able to identify them in the presence of noise for the given number and location of shakers and sensors and with the use of first 3 vibration modes.

4.8 *Prediction of Damage Detectability*

In the previous section, we classified the members into 3 groups based on calculated success factor in the presence of noise. In section 4.6, we obtained an expression for estimating the success factor for a given value of damage detectability measure and success factor in the absence of noise for 20% damage in a member. In this section, we will check the predictive capability of Eq. 4.8 by comparing the estimated and calculated success factor for 45% damage in a member.

We used Eq. 4.8 to estimate the success factor for 45% damage and compared it with the calculated success factor. The average error between the estimated success factor ($\hat{R}$) and calculated success factor (R), $\bar{}(45\%)$ was calculated to be 45%. We observed the errors,
  (i) for the case of 45% damage are similar to the errors for 20% damage. To increase the predictive value of the expression given by Eq. 4.8, the equation is modified by multiplying by a factor which will eliminate any errors for the case of 20% damage. For any amount of damage and for a given damage location, we modify the estimated success factor as

$$\tilde{R} = \hat{R} \left[\left. \frac{R}{\hat{R}} \right|_{20\%} \right] \tag{4.9}$$

The estimated success factor $\tilde{R}$ and R are compared in Table 4.4. We see that $\tilde{R}$ is closer to the calculated success factor, R than $\hat{R}$. The average error between the estimated success factor $\tilde{R}$ and calculated success factor R decreased from 45% damage to 35%.

58

Table 4.4. The estimated success factor and the calculated success factor for 45% damage in a member

Damaged Member	$\dfrac{R}{\hat{R}}\bigg|_{20\%}$	$\hat{R}$	$\tilde{R}$	R
1	0.82	1.57	1.35	1.08
2	0.72	0.51	0.39	0.36
3	1.21	0.80	0.93	1.27
4	0.78	0.40	0.33	0.32
5	1.06	0.80	0.83	0.99
6	0.76	0.59	0.48	0.46
7	0.81	0.30	0.26	0.34
8	1.12	0.77	0.84	0.97
9	2.14	0.25	0.47	0.41
10	1.12	0.79	0.86	0.82
11	0.83	0.35	0.31	0.39
12	0.92	0.70	0.65	0.65
13	0.85	0.16	0.14	0.07
14	1.31	0.72	0.89	1.07
15	0.92	0.53	0.49	0.42
16	0.68	0.64	0.47	0.35
17	0.96	0.62	0.60	0.66
18	1.44	0.60	0.80	1.34
19	1.48	0.76	1.04	0.61
20	0.55	0.44	0.27	0.20
21	0.98	0.63	0.62	0.45
22	1.15	0.30	0.33	0.14
23	1.28	0.56	0.68	1.16
24	0.91	0.56	0.53	0.40
25	0.84	0.79	0.69	0.36
26	1.02	0.60	0.61	0.30
27	1.14	1.05	1.17	1.56
28	0.98	0.93	0.92	0.79
29	1.09	0.55	0.59	0.43
30	1.36	0.74	0.95	0.58

The estimated success factor given by Eq. 4.9 is a function of the damage location and the amount of damage. Using this equation, we estimated the success factor for 45% damage in a member and classified them into the 3 groups (Table 4.5). We observed that members 21, 24, 25, 27 and 29 were wrongly classified into Group B. We observe that Eq. 4.9 correctly classified 25 of the 30 members and has a good predictive value in classifying the members for any amount of damage.

Table 4.5. Classification of members by estimated success factor for 45% damage in a member

Group	Range of R	Members in the group
A	R < 0.5	2, 4, 6, 7, 9, 11, 13, 15, 16, 20, 22, 26
B	0.5 < R < 1.5	1, 3, 5, 8, 10, 12, 14, 17, 18, 19, 21, 23, 24, 25, 27, 28, 29, 30
C	R > 1.5	-

To summarize, for a given amount of errors and a given location of damage, we can compute the damage detectability measure, E, and the success factor in the absence of errors, R_o. We can estimate the success factor in the presence of noise, $\tilde{R}$ and check if the average angle approach has a chance at locating the damage. We can find the members where we can expect to detect damage experimentally with a given amount of damage, and given amount of measurement noise. In next section, we will describe the measures which can be taken to increase the ability of the method to locate damage.

4.9 *Effect of Increasing Number of Shakers and Sensors*

For a given set of shakers/sensors and given detectability measure, we can find members where it is not easy to detect damage. In this section, we will briefly study the effect of increasing the number of collocated shakers/sensors on the ability of the technique to locate damage.

We increase the number of collocated shakers/sensors by attaching a 4th set of collocated shaker/sensor at 10Y. This location was arbitrarily chosen and hence the location of shakers and sensors may not be good for our method of damage detection (Appendix D). The amount of damage in the damaged member was 45%. Random noise was introduced in the receptance matrix and in measurement of natural frequencies. Eight sets of data having noise were generated for both the undamaged and the damaged structure. The average angle approach was applied to locate the damage. For a chosen damage location, the success factor (Fig. 4.31) was calculated and then averaged over the eight sets of data.

The results are compared with the results obtained in section 4.5.5 with 3 pairs of shakers and sensors (Fig. 4.28). The members were then classified into three group and we

observed that the number of members in group A increased from 16 to 17 and the number of members in group B decreased from 13 to 11. The average value of success factor over all the locations of damage (R_μ) decreased from 0.63 using 3 pairs of shakers and sensors (Fig. 4.28) to 0.52 for 4 pairs of shakers and sensors (Fig. 4.31). There is an improvement in the ability of the technique to locate the damage by adding an extra shaker and sensor and we believe that the improvement can be further pronounced by optimally choosing the location of 4 pairs of shakers and sensors.
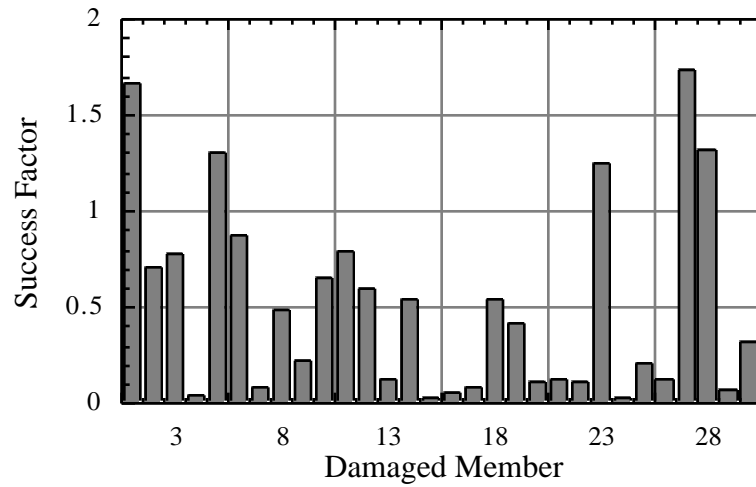
Figure 4.31. Success factor in presence of noise by using 4 sets of collocated shakers/sensors.

4.10 *Summary*

In this chapter we conducted a series of numerical experiments on a 36 degree of freedom cantilevered truss. We first showed that if a member has a high contribution to the strain energy of the undamaged member for a vibration mode, the change in natural frequency of the structure when the same member is damaged is also high. We successfully conducted numerical damage identification tests on the structure in the absence of noise by assuming a member is damaged by either 20%, 45% or 75% stiffness reduction.

We generated noise in the receptance matrix and by using only contrast maximization, we showed that compensated contrast maximization is more effective in locating damage than the uncompensated contrast maximization. By increasing the damage without changing the

amount of noise, we showed that the damage detectability measure decreases, which increases the chances of damage identification. We then performed damage identification tests using the average angle approach in both the presence of noise in natural frequencies and receptance matrix. It was shown that the success factor in the presence of noise (R) depends upon success factor in the absence of noise (R_o) and the damage detectability measure (E). A relationship between R, R_o and E was then established using linear regression. The members were classified into 3 groups depending upon the ability of the technique to detect damage in the presence of noise. We showed that we can find the members where we can expect to detect damage experimentally with a given amount of damage, and given amount of measurement noise. We conducted a study to see if increasing the number of shakers and sensors would increase the number of members where we can expect to locate damage for a given amount of damage and noise. We could detect 2 more members even when we arbitrarily placed the 4th pair of shaker and sensor.

In the next chapter, we will show how the technique performed in the laboratory.

Chapter 5
Experimental Validation

In this chapter we concentrate on the application of the average angle technique to locate damage in a member of the experimental truss. Here we show how the magnitude of the modeling and measurement errors was initially large compared to the damage so that it was impossible to detect damage in the most detectable locations. The chapter describes the steps taken to rectify that, giving after each step the improvement in the predicted damage detectability measure. Finally, the amount of damage was increased and the amount of noise and errors decreased so that the damage in the members could be located.

5.1 *Laboratory Truss*

5.1.1 Description

The truss structure used in this study is shown in Fig. 5.1. The structure is a cantilevered truss consisting of 12 solid spherical aluminum nodes and 30 aluminum members. The truss is bolted to a 0.4064 m $\times$ 0.4064 m (16" $\times$ 16") aluminum plate at nodes 1, 2 and 3 and the aluminum plate is bolted into the wall.

Each member is made of a tubular part in the middle and two end fittings on each side. The end fitting consists of an aluminum insert with a 0.00635 m (1/4") threaded steel rod. The aluminum node is a spherical node with 18 flat faces. A 0.00635 m (1/4") threaded hole has been drilled into each face. The member can go into any of these 18 holes which are at angles of 45˚, 60˚, 90˚, 120˚, 135˚ or 180˚ to one other. The members are designed in such a way that the threaded rods can move in and out of the tubular part so that the member can be removed and installed on to the truss without disassembling it. This feature is important for damage identification experiments as the undamaged member has to be replaced by a damaged member.

The truss has 2 bays in the middle with a half bay at each end. The bays are pyramids with a 0.254 m (10") square base. Each middle bay and each half bay have a diagonal member of length 0.359 m (14.14") in the square base (members 2, 11, 20 and 29). The remaining

26 members of the truss are non-diagonal members. The truss is about 1 m long and weighs about 4.4 kg.
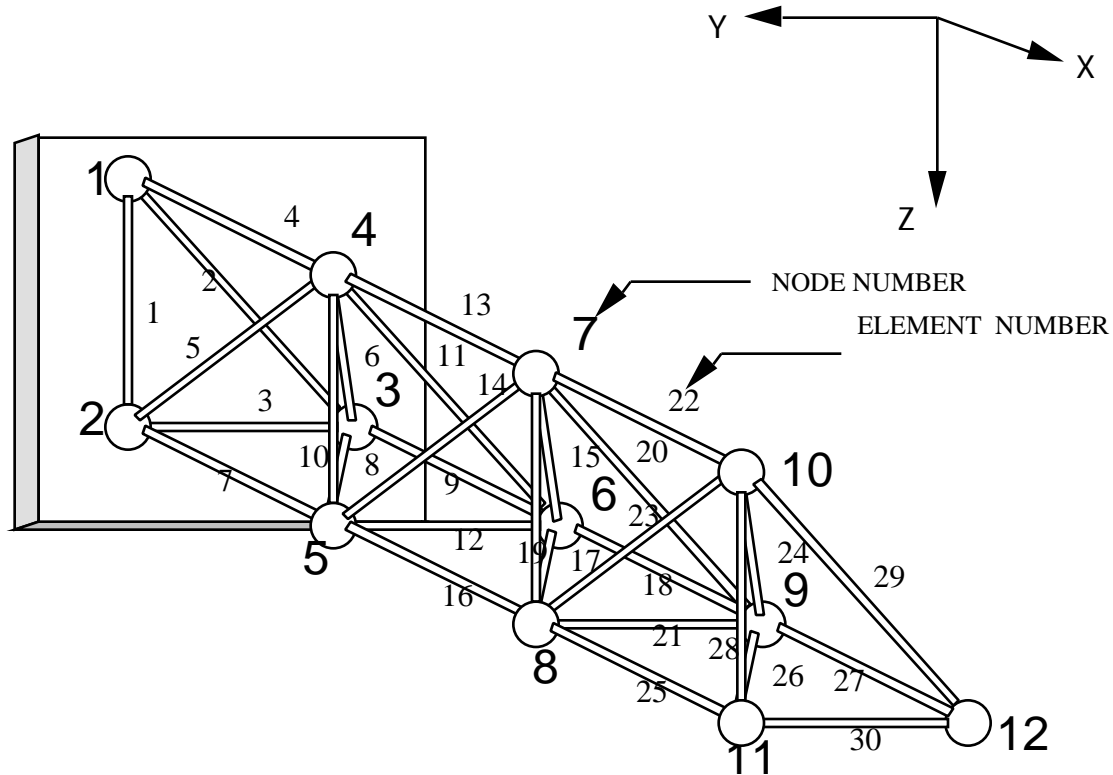
Figure 5.1. The laboratory truss with 30 members mounted on the wall.

Figure 5.2 shows a plot of the magnitude of a measured frequency response function (FRF), the ratio of the response acceleration to the excitation force in the frequency domain. The first three modes are well separated and clearly identified at about 100, 128 and 193 Hz. The local bending modes occur at frequencies greater than 275 Hz making the truss model accurate only for the first three modes. The sharpness of the peaks suggests that the truss is lightly damped. The damping ratios for the first three modes were measured by measuring the sharpness of resonance, i.e., the damping ratio of the ith mode, ζ_i is expressed as

$$\zeta_i = \frac{(\omega_2)_i - (\omega_1)_i}{2\,\omega_i} \qquad (5.1)$$

64

where $(\omega_1)_i$ and $(\omega_2)_i$ are the side bands (half power points) corresponding to ω_i, the ith natural frequency. The measured damping ratios are 0.15%, 0.18% and 0.10% for the first three modes.
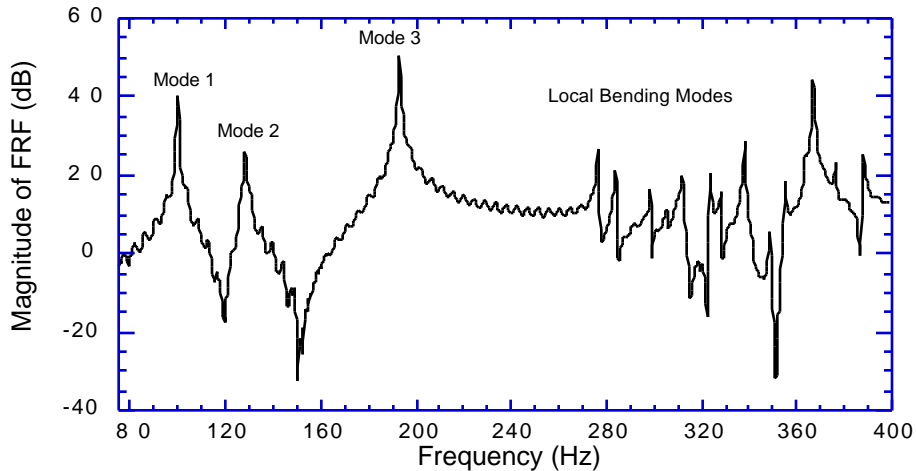
Figure 5.2. The FRF of the experimental truss showing the vibration modes

5.1.2 Instrumentation

The truss was initially excited by an electromagnetic shaker (Ling Dynamic Systems, model V203) mounted on a tripod and connected to a node of a truss through a stinger orthogonal to the face of the node. The response amplitude was measured by a subminiature accelerometer (PCB, model 303-A03). The data acquisition and FFT analysis were performed on a Tektronix 2630, PC controlled analyzer.

For our experiments, we needed to apply force at 3 different locations and it required moving the shaker assembly from one node to another. This resulted in a change in the natural frequencies of the structure. We calculated the mass below the gauge of the shaker and attached an equal mass at the 3 shaker locations. The mass at a shaker location was replaced by the shaker assembly when the excitation was applied at that node. The change

in the natural frequency of mode 3 was still observed to be more than 1 Hz even when we accounted for the moving mass.

To circumvent the above problem, the truss is excited by an impulse hammer (Kistler, model 9724A2000). The locations of the excitation and response measurement were selected to help in the damage identification process.

5.1.3 Finite Element Model

A finite element model of the truss is developed based on nonuniform, symmetric members and infinitely stiff nodes. The global axes frame is defined as follows (see Fig. 1): X axis is orthogonal to and pointing out of the wall, Y axis is pointing from node 3 to node 2 and Z axes completes the right -handed coordinate system.

Each member is modeled as a nonuniform, symmetric, straight, 6-degree of freedom rod element. The element is defined by its stiffness, mass and rotational inertia about its center of mass. The solid spherical nodes are assumed to be infinitely stiff. A similar truss was built by Ponslet[29]. He carried out experiments to estimate the mass, rotational inertia, and the stiffness of the members. The moment of inertia about the center of mass was measured for a member with a node attached to each end. The properties of the truss elements obtained in that work are shown in Table 5.1.

<div align="center">

Table 5.1. The measured properties of the truss members and nodes.

Truss element	Mass (g)	Stiffness (MN/m)	Centroidal Moment of Inertia ($g\ m^2$)
Node	88.62	-	-
Short member	107.37	22.51	0.51
Diagonal member	125.91	14.82	1.56

</div>

An FEM model which produces the best match with the experimental data for the undamaged structure is needed. Since we constructed the FEM model of the cantilevered truss based on measured FEM element properties, the uncertainties in the model are primarily in the boundary conditions. Instead of updating the entire model, we used

optimization methods to identify the boundary conditions. The process of obtaining the boundary conditions is described in detail in Appendix B.

Each of the three nodes at the wall are assumed to attached to the wall by three springs having mass. The 3 stiffness parameters to be adjusted were the wall stiffness along X, Y and Z direction, k_x, k_y and k_z. The mass of each of the three springs at a node is equal and is represented by m_1, m_2 and m_3. The experimental data was initially chosen as the natural frequencies and the mode shapes of the truss. An objective function (Eq. B.9) was minimized to obtain the design variables (Eq. B.10) as,

$$\mathbf{k}^*=\{k_x, k_y, k_z\} = \{1.44\times 10^8, 0.48\times 10^8, 2.80\times 10^8\}\text{N/m} \quad \text{and}$$
$$\mathbf{m}^*=\{m_1, m_2, m_3\}= \{0.0, 0.0, 61.0\} \text{ kg} \tag{5.2}$$

Later, to get a better match, we included the measured elements of the receptance matrix of the undamaged structure in the objective function (Eq. B.11) and the design variables which minimized the objective function were obtained to be

$$\mathbf{k}^{**}=\{k_x, k_y, k_z\} = \{1.30\times 10^8, 0.61\times 10^8, 3.26\times 10^8\}\text{N/m} \quad \text{and}$$
$$\mathbf{m}^{**}=\{m_1, m_2, m_3\}= \{25.0, 0.0, 56.1\} \text{ kg} \tag{5.3}$$

The wall parameters given by Eq. 5.3 resulted in an FEM model which is in good agreement with the experimental data and also has a high predictive value to changes made in the structure. An experiment we conducted to verify this is shown in Appendix B.

5.2 Damage Detection - Low Damage Level

In this section, we describe how a damaged member with a damage of 25% is obtained. This member was then installed at location of member 13 in the undamaged truss. The average angle approach was then applied to locate the damage. We checked the correlation between the experimentally obtained matrices and the FEM matrices and concluded that there is a need to decrease the damage detectability measure. This can be achieved to some extent by selecting the frame size for signal processing which will have the least error in the symmetry of measured receptance matrix of the truss. The Zoom mode with a frame size of 128 data points is selected. (Appendix C contains the glossary of some of the signal

processing terms being used in this section.) Damage identification is then performed to locate damage in member 4. In the section on damage detectability, we observe that measurement and modeling errors overwhelm the effect of damage on the structural response. There is a need to increase the amount of damage in the damaged member. The location of shakers/sensors and the distance of the selected frequency also need to be changed to improve the quality of the response signal.

5.2.1 Identification of Magnitude of Damage

One way to decrease the stiffness of a member is by a saw cut. This preserves the mass distribution of the member and primarily affects the member stiffness. A member was saw cut to obtain a partially damaged member. The undamaged member at location 4 was replaced with this member. The natural frequencies of this damaged truss and the change in natural frequency due to damage were

$$\omega_1^d = 96.10 \text{ Hz}, \qquad \omega_2^d = 126.94 \text{ Hz}, \qquad \omega_3^d = 193.02 \text{ Hz}$$

and

$$\Delta\omega_i^{exp} = \{3.95,\ 1.62,\ 0.17\} \text{ Hz}$$

The amount of damage in the member was estimated analytically by matching $\Delta\omega_i^{exp}$ to $\Delta\omega_i^{FEM}$, the change in the analytical natural frequency due to damage in member 4. The data of mode 3 was discarded as the change in the natural frequency was of the same order as measurement noise. Matching $\Delta\omega_i^{exp}$ to $\Delta\omega_i^{FEM}$ for modes 1 and 2, resulted in an estimated change in member stiffness due to damage to be 23.2% and 25.0% respectively.

To obtain an estimate of damage by matching experimental and analytical data of mode 3, the same damaged member was then used to replace member 5 of the undamaged truss. The change in the 3rd natural frequency due to damage, $\Delta\omega_3^{exp}$ was 2.75 Hz. Matching $\Delta\omega_3^{exp}$ to $\Delta\omega_3^{FEM}$ resulted in a damage of 26.2% in the member.

The damage in the member was taken as the average of estimated damage by matching modes 1, 2 and 3,

$$\text{amount of damage} = (23.2+25.0+26.2)/3 = 24.8\%.$$

It is to be noted that the magnitude of the damage was found so that we will know how much stiffness reduction was caused by the saw cut. The magnitude of damage will not be used in any of the computations to determine the location of the damaged member.

5.2.2 Damage Detection in Member 13

The undamaged member 13 was replaced by the damaged member with an estimated damage of 24.8%. The first three modes were considered for damage identification. The 3 sensors were arbitrarily placed at 6Z, 7Z and 12Z. Impulse hammer was used to apply the force to the structure at the locations of the sensors. The response was measured in the frequency range of 200 Hz with a frame size of 4096 data points. To reduce the effect of noise in the measurements, the data was averaged over 20 measurements. The natural frequencies of the damaged truss were measured to be

$$\omega_1^d = 99.07 \text{ Hz}, \qquad \omega_2^d = 128.03 \text{ Hz}, \qquad \omega_3^d = 192.38 \text{ Hz}$$

The experimental frequencies which are the frequencies at which the damaged truss is excited were selected to be 5% away from resonance,

$$\omega_1^* = 94.11 \text{ Hz}, \qquad \omega_2^* = 134.43 \text{ Hz}, \qquad \omega_3^* = 182.76 \text{ Hz}$$

The 3×3 receptance matrix, $C_d(k,l)$ was measured at the 3 selected frequencies. The matrix was observed to be non-symmetric and it was made symmetric by taking the average of the matrix and its transpose. The FEM model was based on the boundary condition parameters (Appendix B, Eq. 5.2), $\mathbf{k}^*$ and $\mathbf{m}^*$. The uncompensated contrast maximization function was used for damage identification. The optimal excitation, $\mathbf{q}^*$ was compared to the database of optimal excitations and the contrast maximization angles were computed. The contrast maximization angles, frequency signature angles and the average angles were arranged in an ascending order, i.e., they were sorted in the form of a list.

The damaged member, member 13, came 6th in the list based on contrast maximization angles, 3rd in the list of frequency signature angles and 1st in the list of average angles. The success factor based on uncompensated contrast maximization approach, frequency

69

signature approach, and the average angle approach was 1.36, 1.69, and 0.95 respectively. The contrast maximization approach of the frequency signature approach in itself was unable to locate the damage, but combining the two approaches by using the average angle we were able to identify the damaged member.

The average contrast maximization angle and the frequency signature angle for member 13 were 21.75˚ and 10.68˚, respectively. The contrast maximization angles for the first three modes were 50.7˚, 13.2˚ and 1.3˚ respectively. To reduce the effect of measurement noise, we averaged 3 sets of the contrast maximization matrix for the undamaged structure, A_o^{exp}, and used it for contrast maximization. There was no improvement in the damage identification results.

We also used the compensated contrast maximization for damage identification. The contrast maximization angle and the average angle is computed and the results did not show any improvement over the previous results. Member 13 came 16th in the list based on contrast maximization and 3rd in the list based on the average angle. The average contrast maximization angle corresponding to member 13 was 38˚. Changing the contrast maximization function to

$$= \text{Max } [q^T \{A_d^{exp} - A_o^{exp}\}q] \tag{5.4}$$

and applying the algorithm to detect damage, did not improve the results. Member 13 came 15th in the list based of contrast maximization and 3rd in the list based on average angle approach.

The *damage detectability measure*, E was calculated to be 1.14, which is greater than unity. This implies that measurement errors mask the effect of damage. Further, we observed that irrespective of the contrast maximization function being used, the contrast maximization angle was high for one of the modes. A plausible explanation for this behavior is that the experimentally measured A_d and A_o matrices are not in good agreement with the corresponding matrices from the finite element model. This issue is addressed in the next section.

5.2.3 Discrepancy between Experimental and Analytical Contrast Maximization Matrices

We need to check the discrepancy between the experimentally measured matrices and the corresponding FEM matrices. We have two extremes, the FEM matrices and the experimentally obtained matrices. We define,

$$A_d(\gamma) = A_d^{exp}(1-\gamma) + A_d^{FEM}\gamma$$

and

$$A_o(\gamma) = A_o^{exp}(1-\gamma) + A_o^{FEM}\gamma .$$

where γ, the parameter to be varied, is the weighting function of the analytical matrices. Contrast maximization is performed using $A_d(\gamma)$ and $A_o(\gamma)$ matrix and the angle between the optimal excitation and the database of optimal excitations is obtained for the three modes. Figure 5.3 to 5.5 show the variation of the contrast maximization angles with γ, for 3 different contrast maximization functions. Such plots are referred in the future as an γ-plot. In Fig. 5.3, there is a jump in the contrast maximization angle corresponding to mode 1 at γ=0.656. A similar jump is also observed in the contrast maximization angle of mode 2 in Fig. 5.5 at γ=0.12. This is due to a switch in the eigenvectors corresponding to the largest eigenvalue.

The contrast maximization process yields 3 eigenvalues, λ_1, λ_2 and λ_3 for each selected excitation frequency. We select the optimal excitation as the eigenvector corresponding to the largest eigenvalue. At γ=0.656 in Fig. 5.3, there is a crossover in the eigenvalues. That is, for γ<0.656, λ_1 is the largest eigenvalue and it has a corresponding eigenvector q_1. For γ>0.656, λ_2 is becomes greater than λ_1 and q_2, the eigenvector corresponding to λ_2 replaces q_1 as the optimal excitation. The angle between the optimal excitation and the database suddenly changes and a jump in the contrast maximization angle is observed.

It is seen from Figs. 5.3-5.5, that if γ is closer to unity, that is, if $A_d^{exp}(\gamma)$ and $A_o^{exp}(\gamma)$ are close to A_d^{FEM} and A_o^{FEM}, then the contrast maximization angles are low. But for small values of γ, where the correlation between the experimentally obtained matrices and the corresponding FEM matrices is low, the contrast maximization angles are high. The large discrepancy between the experimental and FEM matrices needs to be reduced. This

discrepancy was thought to be due to poor signal to noise ratio (SNR) of the measured data.   In the next section, we address this issue from a perspective of signal processing.

$$\text{Max}\left[\frac{q^T\{A_d \quad A_o\}q}{q^T A_o q}\right]$$
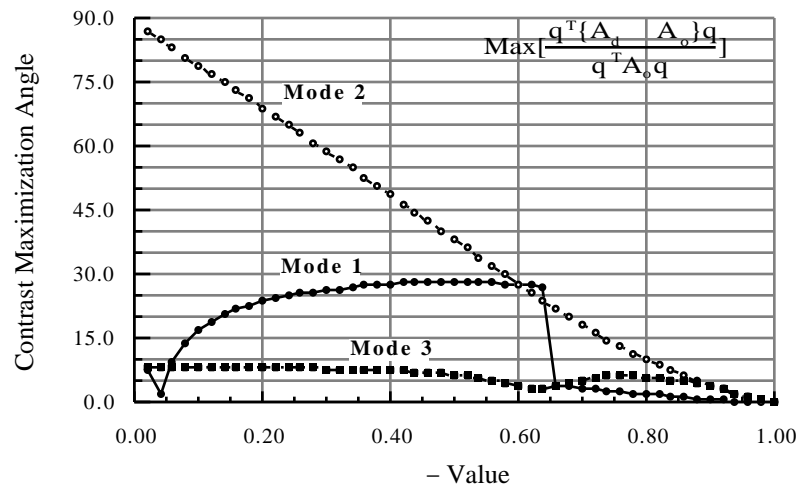
Figure 5.3. The α-plot for the compensated contrast maximization problem.
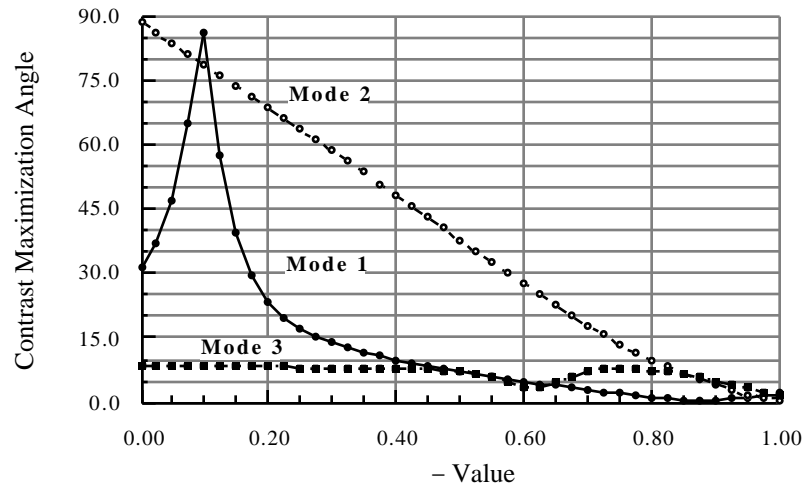
Figure 5.4. The α-plot for the uncompensated contrast maximization problem.
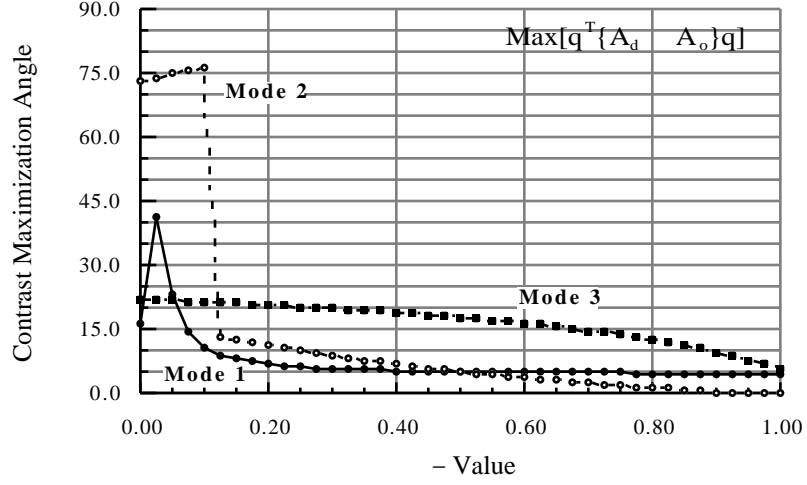
Figure 5.5. The α-plot for the contrast maximization problem defined by Eq. 5.4.

5.2.4 Selection of Frame Size for Signal Processing

The receptance matrix $C_d(k,l)$ is measured at the 3 selected excitation frequencies. We have used a frame size (Appendix C) of 4096 data points to measure the signal. Theoretically, it should be a symmetric matrix, but the experimentally obtained $C_d(k,l)$ is not symmetric. It is made symmetric by taking the average of receptance matrix and its transpose. The measured receptance matrix $C_d(k,l)$ can be expressed as

$$C_d = \frac{C_d + C_d^T}{2} + \frac{C_d - C_d^T}{2} \tag{5.5}$$

The first part of the term is assumed to represent the receptance matrix from which A_d^{exp} is calculated. The second part of the term is viewed as an error term. One possible way of decreasing this error term is by selecting the optimal data frame size when the signal is being processed. It was observed that the response signal decays to zero in about 2 seconds. If a frame size of 4096 is used for the 200 Hz baseband mode, then the signal is measured for approximately 8 seconds. For 6 seconds, the system is measuring only the noise and the FFT (Appendix C) of this corrupted signal is taken. This results in an erroneous value of the frequency response function (FRF) and hence an inaccurate value of $C_d(k,l)$.

73

To minimize the signal processing error, we should select the best frame size from a list of 4096, 2048, 1024, 512 frame size in the baseband mode (Appendix C) and 128 frame size in the zoom mode (Appendix C). The frame size 2048 will suffer from the same drawbacks as 4096 and was not considered in the selection process. The frame size which yields the lowest value of the error term in symmetry of the receptance matrix will be selected. For each mode, we define the error terms as,

$$S_1 = \frac{|\,C_o(1,2) - C_o(2,1)\,|}{\min[C_o(1,2), C_o(2,1)]} , \; S_2 = \frac{|\,C_o(1,3) - C_o(3,1)\,|}{\min[C_o(1,3), C_o(3,1)]} , \; S_3 = \frac{|\,C_o(2,3) - C_o(3,2)\,|}{\min[C_o(2,3), C_o(3,2)]}$$

The average value of the error terms was found for each mode, by

$$S_{av} = \frac{S_1 + S_2 + S_3}{3} \qquad\qquad (5.6)$$

These error terms were found for each frame size by measuring the receptance matrix of the undamaged truss. The results are summarized in Table 5.2.

Table 5.2. The error in measurement of receptance matrix for various frame size.

Frame Size	# of Averages	S_{av} in %			Average over
		Mode 1	Mode 2	Mode 3	3 modes
4096	50	21.2	4.3	4.6	10.0
1024	20	9.9	8.3	7.6	8.6
1024	160	7.4	7.1	10.4	8.3
512	20	7.2	3.4	6.7	5.8
128 Zoom	20	1.2	3.4	8.0	4.2

We observe that the zoom mode with 128 frame size gives the least error in making the receptance matrix a symmetric matrix. The frequency resolution given by the zoom mode of ±5 Hz is 0.2 Hz and is much better than 1.0 Hz for 512 frame size of baseband mode in the range of 200 Hz. The zoom mode with 128 frame size is then used to detect damage in member 4.

74

5.2.5 Damage Detection in member 4

Member 4 has high strain energy in modes 1 and 2. The damaged member with damage of 24.8% was then installed at location of member 4. The average angle technique was applied to locate the damage. The uncompensated contrast maximization function was used. The damaged member came 1st in the list of frequency signature angle, 4th in the list of contrast maximization angle and 1st in the list of average angle. The success factor based on contrast maximization, frequency signature and the average angle was calculated to be 0.91, 1.0 and 0.89 respectively. The damage detectability measure was calculated to be 1.55.

A possible reason that the damaged member did not come 1st in the list of contrast maximization angle is that the effect of modeling and measurement errors was of the same order of magnitude as the damage. Further, given the current location of excitations/sensors, is not a good location for exciting mode 2. The process of selecting another good location of shakers and sensors follows the section on damage detectability. To improve the SNR, the distance between the selected excitation frequency and the natural frequency of the structure is decreased.

5.3 *Improving Signal to Noise Ratio*

5.3.1 Damage Detectability

To compare the effect of modeling and measurement error to the damage, we compute the damage detectability measure. For damage in member 4 with a damage of 24.8%, the value of the damage detectability measure, E, is 1.55. For the damage to be detected, the effect of damage on the structural response should be greater than the magnitude of modeling and measurement errors, that is, E<1. For damage of 24.8% in member 4, the inequality is not satisfied and so we should try to increase the damage.

5.3.2 Location of Shakers/Sensors

The location of shakers/sensors was initially arbitrarily chosen at degrees of freedom, 6Z, 7Z and 12Z. It was observed experimentally (Fig. 5.6), that this location is not a good

location for exciting mode 2. The FRF in Fig. 5.6 was obtained by applying the force at 12Z and measuring the response at 7Z. The location of shakers/sensors should give different analytical optimal excitation vectors for varying damage locations and for all modes of interest. It should also be robust with respect to errors in the direction of the applied force. An optimal location (Appendix C) was obtained at degrees of freedom 7Y, 8Y and 10Y. This location of shakers/sensors is able to excite all the 3 modes (Fig. 7) and was selected for damage identification experiments. The FRF in Fig. 5.7 was obtained by applying the excitation at 10Y and measuring the response at 7Y.
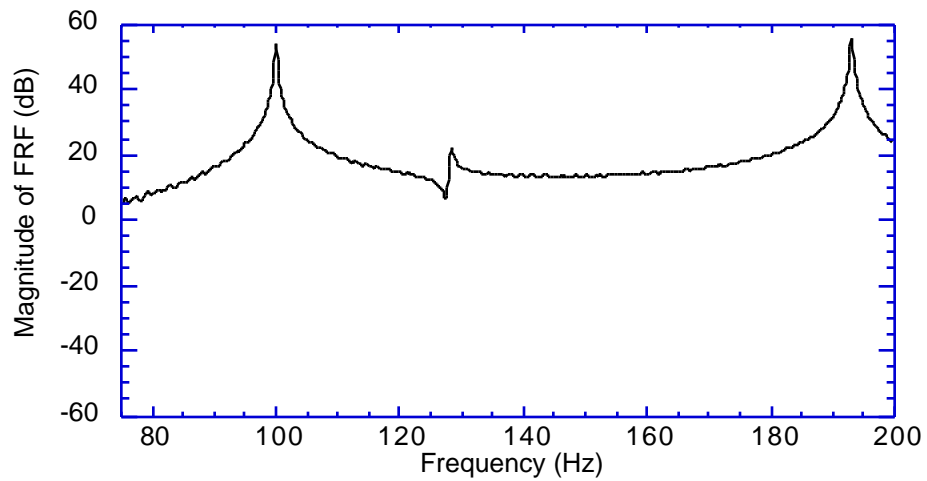
Figure 5.6. The FRF by applying force at 12Z and measuring response at 7Z
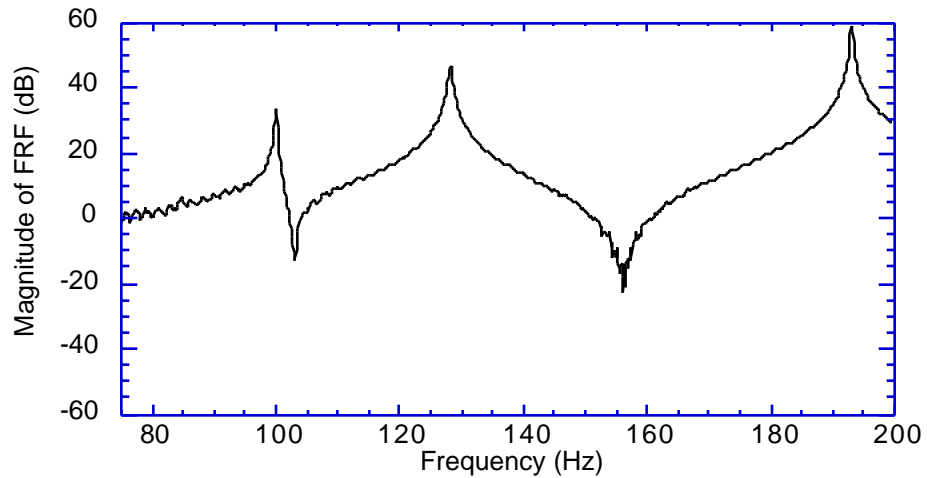
Figure 5.7. The FRF by applying force at 10Y and measuring response at 7Y

5.3.3 Distance of Selected Frequency from Natural Frequency

The selected frequency at which the truss is analyzed was 5% away from the natural frequency of the truss. It was observed that for the sensor location at 6Z, 7Z and 12Z, the SNR was poor for mode 2 and for the sensor location at 7Y, 8Y and 10Y, the SNR was poor for mode 1. The signal quality could be improved if we choose the selected frequency to be 2% away from natural frequency of the truss.

In the next section, we damage a member with a damage such that it will be detectable. The location of shakers/sensors is chosen as 7Y, 8Y and 10Y. The structure response is processed using a 128 frame size, zoom mode. The truss is analyzed at the selected natural frequency which is 2% away from the resonant frequency of the truss.

5.4 *Damage Detection - High Damage Level*

In this section, we describe how a damaged member with an estimated damage of 58.7% is obtained. This member was then installed at location of member 4 in the undamaged truss. Three different contrast maximization functions were used to locate the damage in member 4. The contrast maximization function which gave the best damage identification results was selected for more damage identification tests. Damage identification was then performed at locations 7, 9 and 13. These are the members belonging to Group A of member classification based on success factor for 45% damage in the presence of numerical noise. We also applied the technique to locate damage in member 14 which belongs to Group B. These damage locations are shown in Fig. 5.8. The average angle approach and the contrast maximization approach were able to locate the damage. The frequency signature approach was able to identify the damage at locations 4, 7 and 13. The results are presented in detail in the following section.

5.4.1 Damaging a Member

A member was saw cut to obtain a partially damaged member. The undamaged member 4 was then replaced with this member. The natural frequencies of this damaged truss and the change in natural frequency due to damage were

$$\omega_1^d = 83.75 \text{ Hz}, \qquad \omega_2^d = 124.0 \text{ Hz}, \qquad \omega_3^d = 190.25 \text{ Hz}$$

and

$$\Delta\omega_i^{exp} = \{16.25, \; 4.38, \; 2.75\} \text{ Hz}$$

The amount of damage in the member was estimated analytically by matching $\Delta\omega_i^{exp}$ to $\Delta\omega_i^{FEM}$, the change in the analytical natural frequency due to damage in member 4. Matching $\Delta\omega_i^{exp}$ to $\Delta\omega_i^{FEM}$ for the three modes resulted in a damage of 58.7%. The magnitude of damage will not be used in any of our computations.
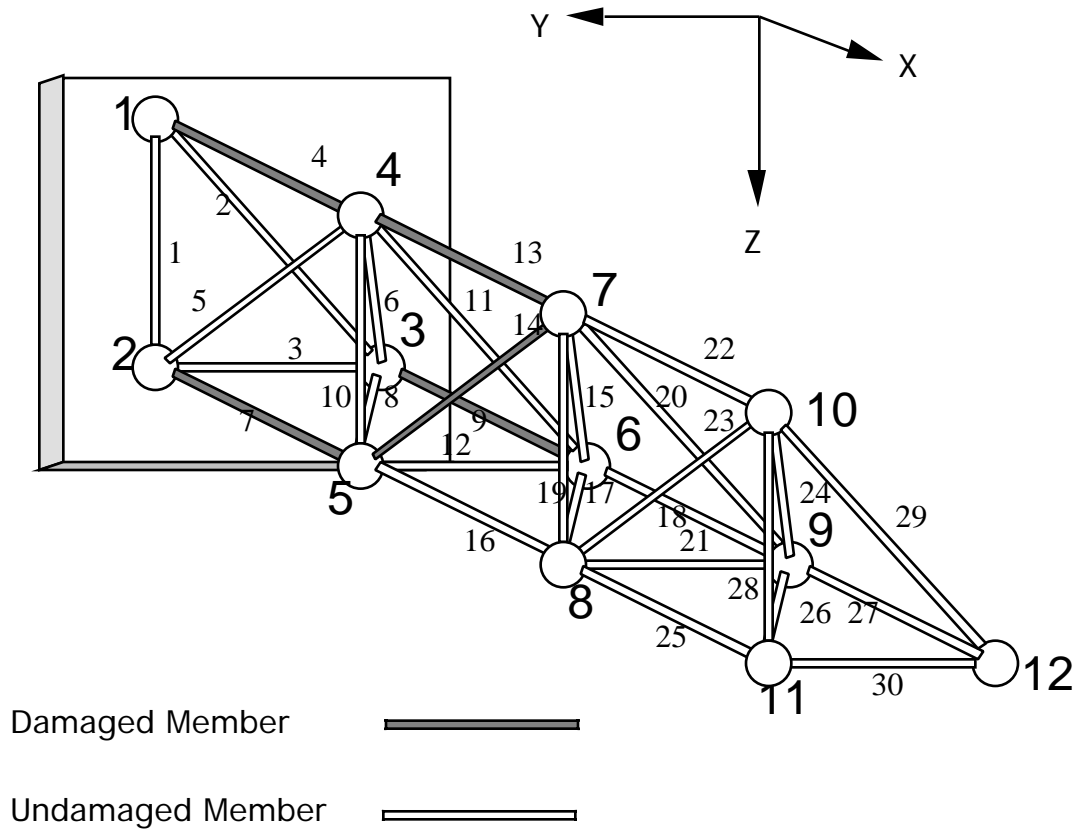
Figure 5.8. The five locations of damage on which the method was applied.

5.4.2 Damage in Member 4

The undamaged member 4 was replaced by the damaged member with an estimated damage of 58.7%. The first three modes were considered for damage identification. The 3 sensors

were located at degrees of freedom 7Y, 8Y and 10Y and the impulsive excitations were applied at the same locations. The impulse hammer was used to apply the force to the structure. The response was measured in the frequency range of ±5 Hz with a frame size of 128 data points. The natural frequencies of the damaged truss were measured to be

$$\omega_1^d = 83.75 \text{ Hz}, \qquad \omega_2^d = 124.0 \text{ Hz}, \qquad \omega_3^d = 190.25 \text{ Hz}$$

The experimental frequencies which are the frequencies at which the damaged truss is excited were selected to be 2% away from resonance. The 3×3 receptance matrix, $C_d(k,l)$ was measured at the 3 selected frequencies. The FEM model was based on the boundary condition parameters, $\mathbf{k^{**}}$ and $\mathbf{m^{**}}$ (Eq. 5.3). Three different contrast maximization functions were used to locate the damage.

If the uncompensated contrast maximization function is used for damage identification the damaged member, member 4 came 11th in the list based on contrast maximization angles. The success factor based on the uncompensated contrast maximization was calculated to be 1.42.

If the compensated contrast maximization approach is applied, the technique is able to identify the location of the damage. The success factor based on contrast maximization was calculated to be 0.48. The compensated contrast maximization function will be used for the balance of our damage identification tests.

The frequency signature approach was applied and the success factor based on frequency signature was calculated to be 0.76. It is to be noted that the frequency signature results are independent of the contrast maximization function.

The average angle approach was applied to locate the damage by matching the frequency signatures and contrast maximization vectors for the damaged structure with the damage scenarios represented by 30% and 70% damage level. It was observed that for both damage levels, the damaged member had the smallest average angle with the 30% damage level giving a smaller average angle for the damaged member as compared to 70% damage level. The average angle approach was able to locate the damage with a success factor (for damage scenarios represented by 30% damage) of 0.38. Figures 5.9 to 5.11 shows the

frequency signature angle, contrast maximization angle and the average angle for each member. It is seen that member 4 had the lowest angle in each of the three approaches. The damage detectability measure, E, was computed to be 0.28 which is smaller than 1.0 and hence increases the confidence in the results.

Figure 5.9. Frequency signature angles when member 4 is damaged.

Figure 5.10. Contrast maximization angles when member 4 is damaged.
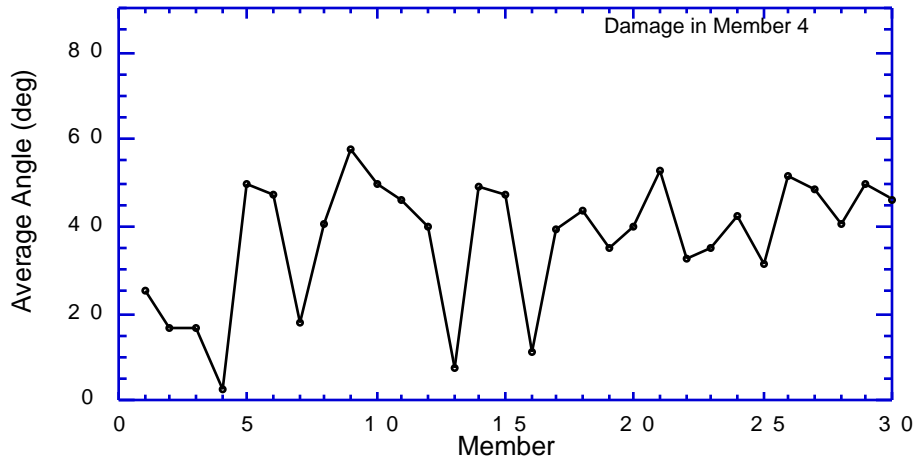
Figure 5.11. Average angle approach when member 4 is damaged.

5.4.3 Damage in Member 7

The damaged member was installed in the truss at location of member 7. The natural frequencies of the truss were measured to be

$$\omega_1^d = 82.78 \text{ Hz}, \qquad \omega_2^d = 123.75 \text{ Hz}, \qquad \omega_3^d = 192.30 \text{ Hz}$$

The selected frequencies were taken to be 2% away from the natural frequencies of the truss. The average angle approach was applied to locate the damage. As before, both databases (30% and 70% damage level) correctly identified the damaged member with 70% database giving the smallest average angle. The following results are with database represented by 70% damage. Figures 5.12 to 5.14 shows the frequency signature angle, contrast maximization angle and the average angle for each member. All the three approaches are able to locate the damage. The success factor based on contrast maximization approach, frequency signature approach and the average approach was 0.62, 0.77 and 0.32 respectively. The damage detectability measure was computed to be 0.16.

For comparison, Fig. 5.15 shows the average angles for each member using 30% database. We see that there is not much difference between the results of the two databases.

81

Figure 5.12. Frequency signature angles when member 7 is damaged.

Figure 5.13. Contrast maximization angles when member 7 is damaged.

82
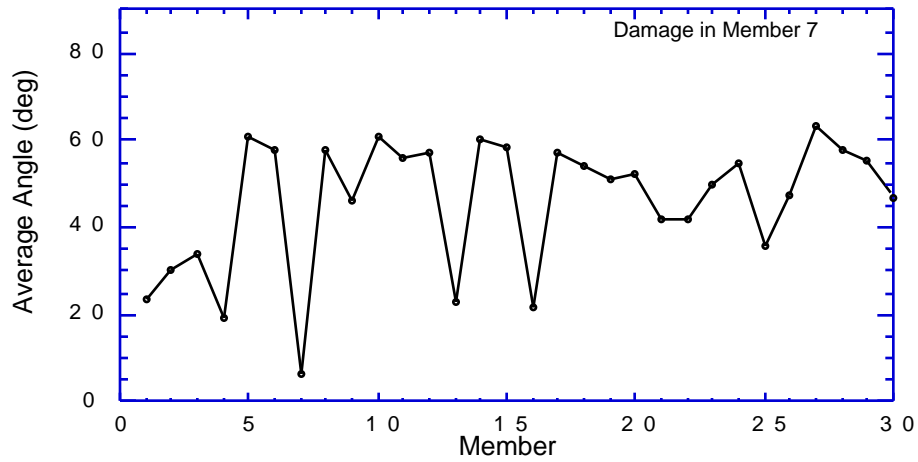
Figure 5.14. Average angle approach using 70% database when member 7 is damaged.
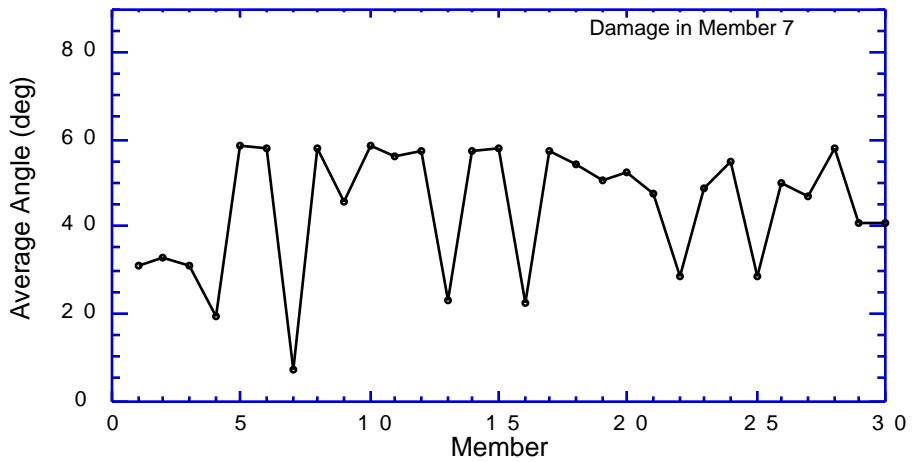
Figure 5.15. Average angle approach using 30% database when member 7 is damaged.

5.4.4 Damage in Member 9

The damaged member was installed in the truss at location of member 9. The natural frequencies of the truss were measured to be

$$d_1 = 99.69 \text{ Hz}, \qquad d_2 = 103.20 \text{ Hz}, \qquad d_3 = 192.50 \text{ Hz}$$

The selected frequencies were taken to be 2% away from the natural frequencies of the truss. The average angle approach was applied to locate the damage. As before, both databases (30% and 70% damage level) correctly identified the damaged member. The following results are with database represented by 30% damage. Figures 5.16 to 5.18 shows the frequency signature angle, contrast maximization angle and the average angle for
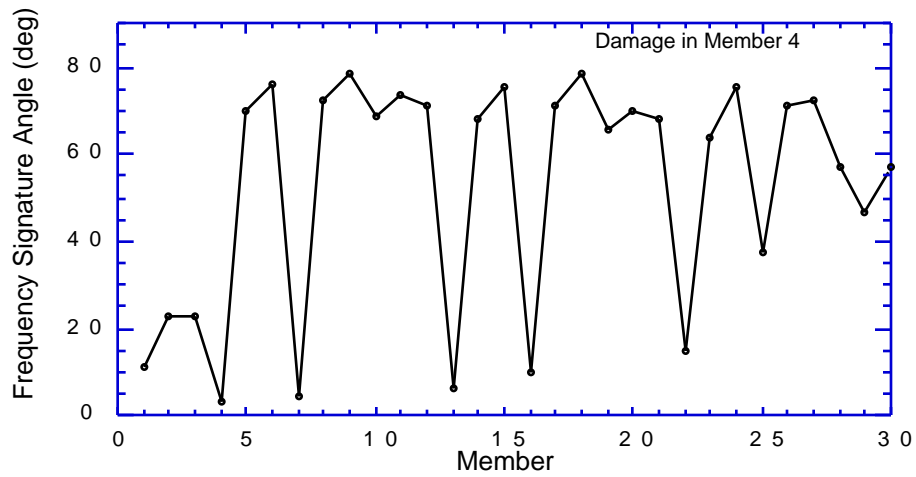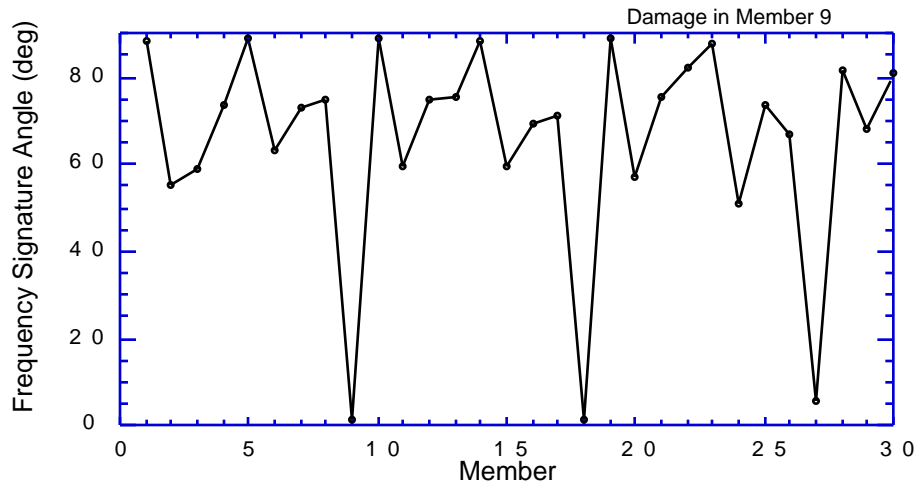

Figure 5.16. Frequency signature angles when member 9 is damaged.
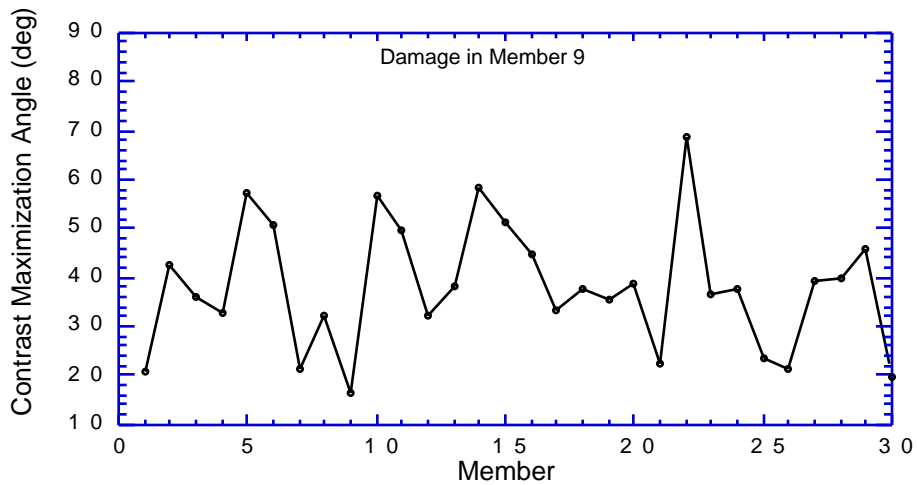
Figure 5.17. Contrast maximization angles when member 9 is damaged.

each member. The contrast maximization approach and the average angle approach were able to locate the damage. The frequency signature approach identified the damaged member as the 2nd most likely candidate for damage. The success factor based on contrast maximization approach, frequency signature approach and the average approach was 0.83, 1.17 and 0.46 respectively. The damage detectability measure, E was computed to be 0.11.
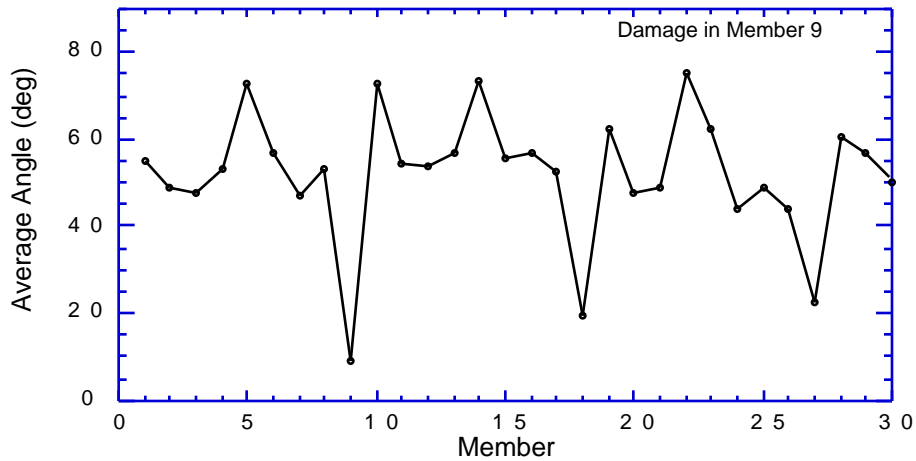
Figure 5.18. Average angle approach when member 9 is damaged.

5.4.5 Damage in Member 13

The damaged member was installed in the truss at location of member 13. The natural frequencies of the truss were measured to be

$$\omega^d_1 = 93.92 \text{ Hz}, \qquad \omega^d_2 = 126.47 \text{ Hz}, \qquad \omega^d_3 = 190.50 \text{ Hz}$$

The selected frequencies were taken to be 2% away from the natural frequencies of the truss. The average angle approach was applied to locate the damage. As before, both databases (30% and 70% damage level) correctly identified the damaged member. The following results are with database represented by 30% damage. Figures 5.19 to 5.21 shows the frequency signature angle, contrast maximization angle and the average angle for each member. The contrast maximization approach, the frequency signature approach and

85

the average angle approach were able to locate the damage. The success factor based on contrast maximization approach, frequency signature approach and the average approach was 0.74, 0.23 and 0.40 respectively. The damage detectability measure was computed to be 0.48.
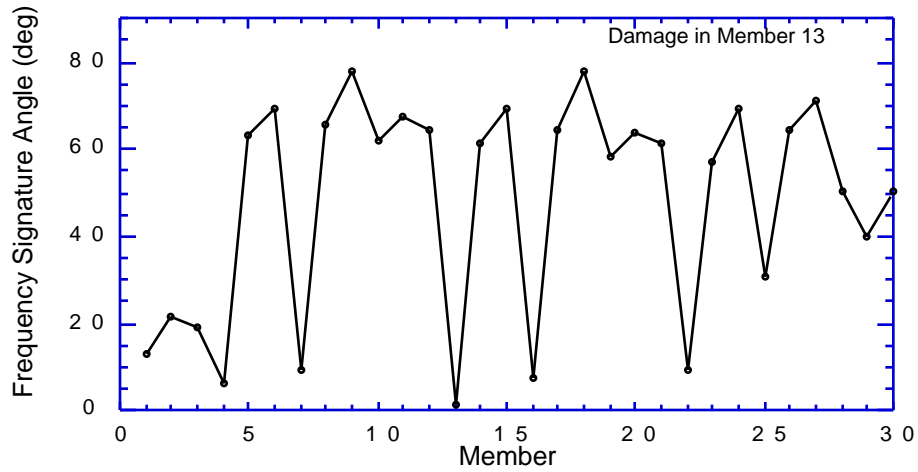
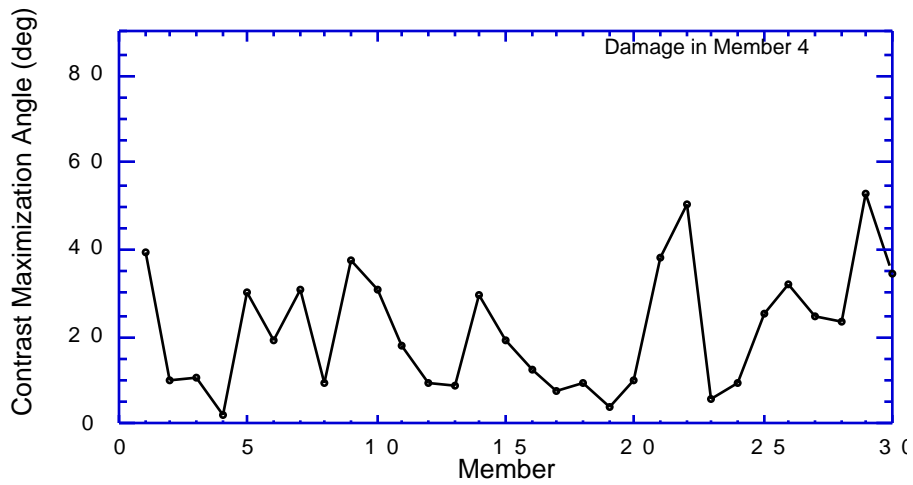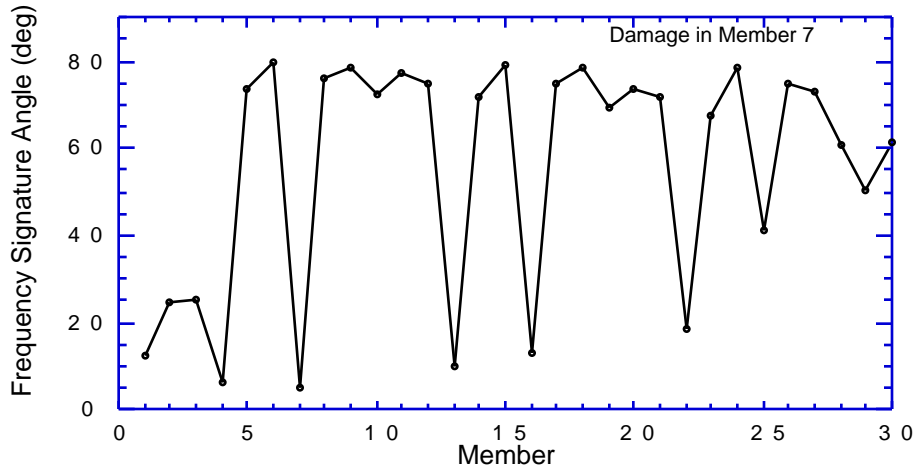**Figure 5.19. Frequency signature angles when member 13 is damaged.**
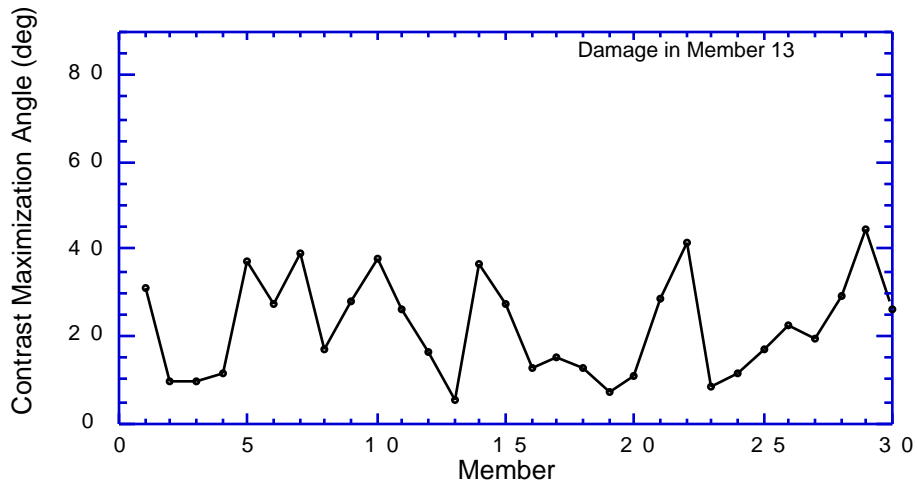
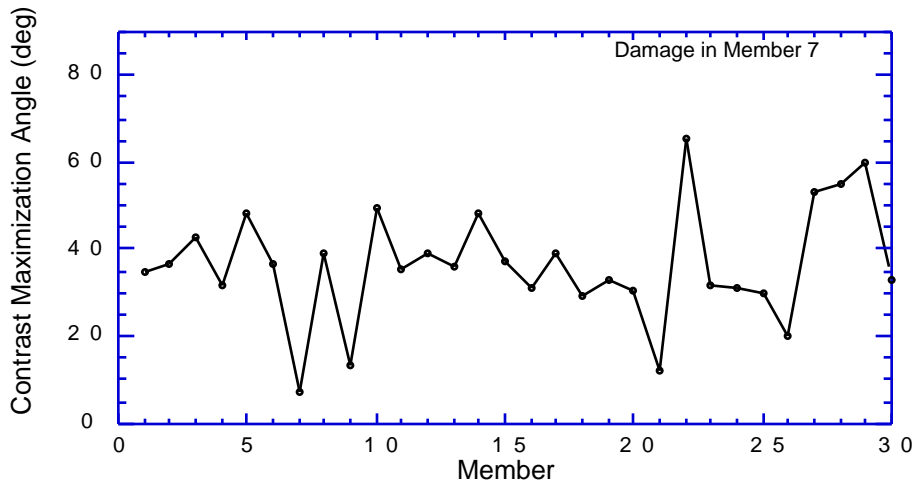**Figure 5.20. Contrast maximization angles when member 13 is damaged**
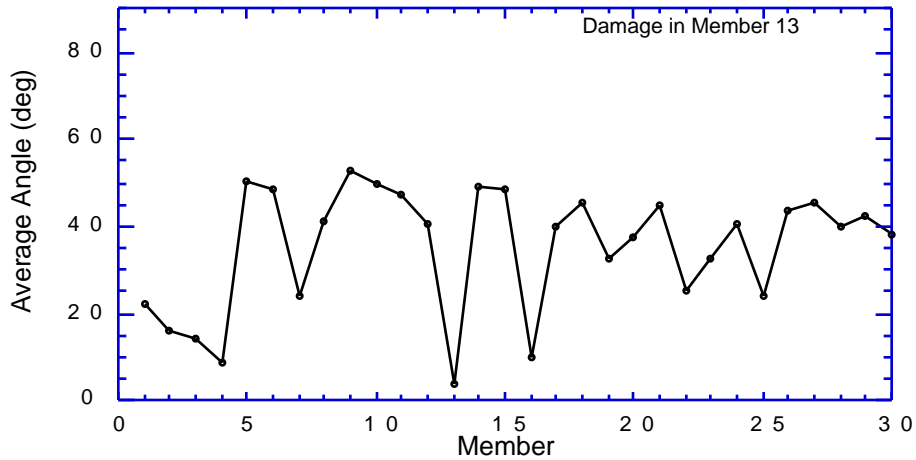
Figure 5.21. Average angle approach when member 13 is damaged.

5.4.6 Damage in Member 14

The damaged member was installed in the truss at location of member 14. Member 14 belongs to Group B of member classification based on success factor of 45% damage in presence of noise. The natural frequencies of the truss were measured to be

$$\omega_1^d = 98.38 \text{Hz}, \qquad \omega_2^d = 128.56 \text{ Hz}, \qquad \omega_3^d = 183.25 \text{ Hz}$$

The selected frequencies were taken to be 2% away from the natural frequencies of the truss. It is seen that mode 2 is unaffected by damage. This mode was not used for contrast maximization approach. The average angle approach was applied to locate the damage. The database corresponding to 30% damage level correctly identified the damaged member with an average angle of 4.18° where as the database represented by 70% damage level had members 10 and 14 with identical average angles of 4.86°.

The following results are with database represented by 30% damage. The frequency signature approach and the average angle approach were able to locate the damage. The success factor based on contrast maximization approach, frequency signature approach and the average approach was 1.65, 0.67 and 0.91 respectively. The damage detectability

measure was computed to be 0.54. The following results are with database represented by 70% damage. The contrast maximization and frequency signature approaches were unable to locate the damage on their own. The success factors based on frequency signature and contrast maximization were 1.18 and 3.15 respectively. But when the two approaches are combined using the average angle approach, the success factor is 1.0.

To summarize this sub-section, we conducted damage identification tests on member 14, which belongs to Group B of member classification and the damage detection was indeed marginal. It was marginally successful (R=0.91) with the 30% database, and borderline with 70% database (R=1.0).

5.5 *Summary*

The average angle technique is used to locate damage in a member of the experimental truss. We tried to locate damage in member 13 when the member is damaged by 25%. The damage detectability measure was found to be greater than unity and this showed that the measurement and modeling errors overwhelm the effect of the damage. By constructing an a-plot, we learned that there is a large discrepancy between the experimental and analytical receptance matrix. In order to achieve higher experimental/analytical correlation, we conducted experimental tests to determine the best frame size for signal processing.

Member 4 was damaged and the technique was applied to detect the damage. The damage detectability measure was found to be greater than unity. To decrease the detectability measure, we increased the damage in the member to 59%, obtained an optimal location of shakers/sensors and reduced the distance of excitation frequency from the natural frequency of the structure. The detectability measure for members 4 and 13 were now found to be smaller than unity. The average angle technique was successfully applied to locate damage in members 4, 7, 9 and 13. These members belong to Group A of member classification. Damage detection was also performed for damage in member 14 which belonged to Group B of member classifications, and the damage detection results were marginal.

Chapter 6
Conclusions

A damage detection technique based on combining a frequency signature approach with a contrast maximization approach was presented. The contrast maximization approach designs the experiment such that it will help us in the process of damage identification. A success factor is defined to quantitatively measure the success of the average angle technique in locating the damage. A damage detectability measure is defined, which compares the effect of modeling and measurement errors to the amount of damage.

To check the analytical feasibility of the method, the technique is first applied on a 132 degree of freedom space truss with 128 members. The excitations could be provided by either active members or by set of collocated shakers/sensors. The results indicate that irrespective of the type of excitation (active members or shakers), the technique had a high success in locating the damage.

The technique is then tested numerically on a 36 degree of freedom space truss equipped with 3 collocated shakers/sensors. In presence of errors, the compensated contrast maximization problem neutralized common errors to measurements of damaged and undamaged structure and produced higher success rate than the uncompensated contrast maximization problem. The average angle technique had a higher success rate in locating the damage than either the contrast maximization approach or the frequency signature approach alone. We developed a relationship between the damage detectability measure and the success factor with and without noise. We found members where we can expect to locate damage experimentally, for a given amount of damage and given amount of measurement and modeling errors.

A similar structure was then built in the laboratory and an FEM model which closely matches the experimental data was constructed. We checked the predictive capability of the model by checking it for a condition that was not used in fitting the data. Optimal locations for sensors/shakers were found and the technique was successfully applied to locate the damage in one member. Five different cases of damage were tried for 58.7% damage in a member for members with good detectability measures.

89

From numerical simulations and laboratory experiments, we observed that the technique using just 3 shakers/sensors is sensitive to measurement noise and modeling errors. One possible way to decrease the effect of noise on the ability to detect damage is by increasing the number of shakers and/or sensors and placing them optimally. The other possibility is to decrease the amount of measurement noise and modeling errors by generating a model of the structure which agrees more with the data and utilizing better signal processing and measurement techniques.

The current work focused on damaged structure with a single damaged member. The damage was represented as a decrease in stiffness of the damaged member. Though the current work is applicable for damage identification in any linear structure, the analytical feasibility and experimental validation were conducted on truss structures. One other practical application of the method is for damage identification in bridges. Further research can incorporate more complex types of damage and apply it to more complex structures.

References

[1]Malla, R. B., and Nalluri, B. B., "Response of Truss Structures Subjected to Dynamic Loads During Member Failure," *Proceedings of the IASS-ASCE International Symposium*, Atlanta, Georgia, 1994, pp. 249-257.

[2]Housner, G.W., and Brady, A.G.,"Natural Periods of Vibrations of Buildings," *Journal of the Engineering Mechanics Division, Proceedings of ASCE*, Vol. 89, No. EM4, August 1963, pp. 31-65.

[3]Vandiver, J.K., "Detection of Structural Failure on Fixed Platforms by Measurement of Dynamic Response," *Proceedings of the Seventh Annual Offshore Technology Conference*, Houston, Texas, May 1975, pp. 243-252.

[4]Cawley, P., Adams, R.D., "The Location of Defects in Structures from Measurements of Natural Frequencies," *Journal of Strain Analysis*, Vol. 14, No. 2, 1979, pp. 49-57.

[5]Yao, J.T.P., "Damage Assessment and Reliability Evaluation of Existing Structures," *Engineering Structures*, Vol. 1, October 1979, pp. 245-251.

[6]Adams, R.D., and Cawley, P., "Vibration Techniques in Nondestructive Testing," *Research Techniques in Nondestructive Testing*, Vol. 8, Chapter 7, 1985, pp. 304-360.

[7]Smith, S. W., and Hendricks, S.L., "Damage Detection and Location in Space Trusses," *AIAA SDM Issues of the International Space Station: A Collection of Technical Papers,* Williamsburg, Virginia, 1988, pp. 56-63.

[8]Lindner, D. K., Twitty, G., and Goff, R., "Damage Detection, Location and Estimation for Large Truss Structures," *AIAA/ASME/ASCE/AHS/ASC 34th Structures, Structural Dynamics, and Materials Conference*, La Jolla, CA, April 1993, pp. 1539-1548.

[9]Baruch, M., "Damage Detection Based on Reduced Measurements," Technion, Israel Report TAE No. 754, 1995.

[10]Chen, J.C. and Garba, J.A., "On-Orbit Damage Assessment for Large Space Structures," *AIAA Journal*, Vol. 26, No. 9, September 1988, pp. 1119-1126.

[11]Rickles, J.M., and Kosmatka, J.B., "Damage Detection in Elastic Vibratory Structures Using Residual Forces and Weighted Sensitivity", *AIAA Journal*, Vol. 30, No. 9, September 1992, pp. 2310-2316.

[12]Lin, C.S., "Unity Check Method for Structural Damage Detection," *Proceedings of 35th AIAA/ASME/ASCE/AHS/ASC Structures, Structural Dynamics and Materials Conference*, Hilton Head, South Carolina, April 1994, pp. 347-354.

[13]Pandey, A.K., Biswas, M., and Samman, M.M.,"Damage Detection from Changes in Mode Shapes," *Journal of Sound and Vibration*, Vol. 145, No. 2, 1991, pp. 321-332.

[14]Pabst, U., and Hagedorn, P., "On the Identification of Localized Losses of Stiffness in Structures," *Structural Dynamics of Large Scale and Complex Systems*, Vol. 59, 1993, pp. 99-104.

[15]Barga, R.S., Friesel, M.A., and Melton, R.B.,"Classification of Acoustic Emission Waveforms for Nondestructive Evaluation using Neural Networks," *SPIE Applications of Artificial Neural Networks*, 1990, Vol. 1294, pp. 545-556.

[16]Tsou, P., and Shen, M.H.H., "Structural Damage Detection and Identification using Neural Networks," *Proceedings of the 34th AIAA/ASME/ASCE/AHS/ASC Structures, Structural Dynamics and Materials Conference*, La Jolla, CA, 1993, pp. 3551-3560.

[17]Povich, C.R., and Lim, T.W., "An Artificial Neural Network Approach to Structural Damage Detection Using Frequency Response Functions,"*Proceedings of the 35th AIAA/ASME/ASCE/AHS/ASC Structures, Structural Dynamics and Materials Conference*, Hilton Head, SC, 1994, pp. 151-159.

[18]Rhim, J., and Lee, S.W., "A Neural Network Approach for Damage Detection and Identification of Structures," *Computational Mechanics*, Vol. 16, 1995, pp. 437-443.

[19]Sensmeier, M. D., Sensharma, P. K., Haftka, R. T., Griffin, O. H., and Watson, L. T., "Experimental Validation of Anti-optimization Approach for Detecting Delamination Damage," Proceedings of 36th AIAA/ASME/ASCE/AHS/ASC Structures, Structural Dynamics and Materials Conference, New Orleans, April 1995, pp. 3171-3184.

[20]Gangadharan, S. N., Nikolaidis, E., Lee, K., and Haftka, R. T., "The Use of Antioptimization to Compare Alternative Structural Models," *Proceedings of 34th AIAA/ASME/ASCE/AHS/ASC Structures, Structural Dynamics and Materials Conference*, La Jolla, CA, April 1993, pp. 534-543.

[21]Berman, A. and Nagy, E. J., "Improvement of Large Analytical Model Using Test Data," *AIAA Journal*, Vol. 21, No. 8, Aug. 1983, pp. 1168-1173.

[22]Guyan, R.J., "Reduction of Stiffness and Mass Matrices," *AIAA Journal*, Vol. 3, No.2, 1965, pp. 380.

[23]Kim, H.M., and Bartkowicz, T.J., "Damage Detection and Health Monitoring of Large Space Structures," *Sound and Vibration*, Vol. 27, No. 6, June 1993, pp. 12-17.

[24]Zimmerman, D.C., Smith, S.W., Kim, H.M., and Bartkowicz, T.J., "An experimental Study of Structural Damage Detection using Incomplete Measurements," *Proceedings of*

35th AIAA/ASME/ASCE/AHS/ASC Structures, Structural Dynamics and Materials Conference, Hilton Head, SC, April 1994, pp. 307-317.

[25]Kashangaki, T.A., Smith, S.W., and Lim, T.W., "Underlying Modal Data Issues for Detecting Damage in Truss Structures," *Proceedings of 33rd AIAA/ASME/ASCE/AHS/ASC Structures, Structural Dynamics and Materials Conference*, Dallas, TX, April 1992, pp. 1437-1446.

[26]Kim, H.M., and Bartkowicz, T.J., "A Two-Step Structural Damage Detection Approach with Limited Instrumentation," *Proceedings of 35th AIAA/ASME/ASCE/AHS/ASC Structures, Structural Dynamics and Materials Conference*, Hilton Head, SC, April 1994, pp. 318-324.

[27]Ibrahim, S.R., and Pappa, R.S., "Large Modal Survey Testing Using Ibrahim Time Domain Identification Technique," *Journal of Spacecraft and Rockets (AIAA)*, Vol. 19, No. 5, September 1982, pp. 459-465.

[28]Chen, C.W., Juang, J.N., and Lee, G., "Frequency Domain State Space System Identification," *Journal of Vibration and Acoustics*, October 1994, Vol. 116, pp. 523-528.

[29]Zimmerman, D. C., and Widengren, M., "Correcting Finite Element Models Using a Symmetric Eigenstructure Assignment Technique," *AIAA Journal*, Vol. 28, No. 9, September 1990, pp. 1670-1676.

[30]Minas, C. and Inman, D. J., "Matching Finite Element Models to Modal Data," *Journal of Vibrations and Acoustics, Transactions of the ASME*, Vol. 112, No. 1, January 1990, pp. 84-92.

[31]Flanigan, C. C., "Test/Analysis Correlation of the STS Centaur Using Design Sensitivity and Optimization Methods," *Proceedings of the 5th International Modal Analysis Conference (IMAC)*, London, England, April 6 - 9, 1987, pp. 99-107.

[32]Kabe, A. M., "Stiffness Matrix Adjustment Using Mode Data," *AIAA Journal*, Vol. 23, No. 9, Sept. 1985, pp. 1431-1436.

[33]Baruch, M., and Bar Itzhack, I. Y., "Optimal Weighted Orthogonalization of Measured Modes," *AIAA Journal*, Vol. 16, No. 8, 1978, pp. 346-351.

[34]Kammer, D. C., "Optimum Approximation for Residual Stiffness in Linear System Identification," *AIAA Journal*, Vol. 26, No. 1, 1988, pp. 104-112.

[35]Smith, S. W., and Beattie, C. A., "Optimal Identification Using Inconsistent Modal Data," *AIAA/ASME/ASCE/AHS/ASC 32nd Structures, Structural Dynamics, and Materials Conference*, Baltimore, MD, April 8-10, 1991, pp. 2319-2324.

[36]Ibrahim, S. R. and Saafan, A. A., "Correlation of Analysis and Test in Modeling of Structures Assessment and Review," *Proceedings of 5th International Modal Analysis Conference*, London, England, April 1987, pp. 1651-1660.

[37]Heylen, W. and Sas, P., "Review of Model Optimization Techniques," *Proceedings of 5th International Modal Analysis Conference*, London, England, April 1987, pp. 1177-1182.

[38]Haftka, R.T., and Kao, P., "The use of Optimization for Sharpening Differences Between Models," *ASME Winter Annual Meeting*, Dallas, TX, November 1990.

[39]Ben-Haim, Y., and Elishakoff, I., *Convex Models of Uncertainty in Applied Mechanics*, Elsevier Science Publishers B.V., 1990.

[40]Wamelen, A. A. Van, "Optimal Design and Testing of Laminated Specimens to Evaluate Competing Composite Failure Criteria," *M.S. Thesis*, Virginia Polytechnic Institute and State University, July 1993.

[41]Ponslet, E., "Analytical and Experimental Comparison of Deterministic and Probabilistic Optimization," *Ph.D. Dissertation*, Virginia Polytechnic Institute and State University, October 1994.

[42]Juneja, V., Haftka, R.T., and Cudney, H.H.,"Locaion of Damage in a Space Structure by Contrast Maximization," *Proceedings of 35th AIAA/ASME/AHS/ASC Structures, Structural Dynamics and Materials Conference*, Hilton Head, SC, April 1994, pp. 296-306.

[43]Haftka, R. T., and Gürdal, Z,"Elements of Structural Optimization," Kluwer Academic Publishers, 1992.

Appendix A
Laboratory Determination of Optimum Excitation

In Chapter 2, we showed that if the response measure is chosen as the square of measured displacement amplitudes, then constructing A_d matrix requires measuring the receptance matrix, C_d. In this section we will show how to construct the matrix A when strain energy is chosen as the response measure.

The matrix A can be computed easily if the stiffness matrix K and the mass matrix M are known. Hence, A_O is determined analytically from the known model of the structure. If such a model is not available, this matrix can be measured in the same way described below for the damaged structure. We will show the derivation of the matrix A, when the structure is instrumented with active members or with collocated shakers/sensors.

A.1 *Structure with active members*

If the structure is instrumented with *m* active members, to construct *A* from the sensor measurements, we note that from Eqs. (2.3), (2.9) and (2.10),

$$K_a^T \, \mathbf{y} = \quad q, \qquad\qquad\qquad (A.1)$$

where

$$= K_a^T \, \tilde{B}^T \, [K - \quad {}^2M]^{-1} \, \tilde{B} \, K_a. \qquad\qquad (A.2)$$

Using the matrix identity,

$$\frac{\partial \, P}{\partial \, (\alpha)} = - \, P^{-1} \frac{\partial \, P}{\partial \, (\alpha)} P^{-1}, \qquad\qquad (A.3)$$

we get,

$$\frac{\partial \, A^{*}}{\partial \, (\omega^{2})} = K_a^T \, \tilde{B}^{T} \, [K - \quad {}^2M]^{-1} \, M \, [K - \quad {}^2M]^{-1} \, \tilde{B} \, K_a$$

$$= - \frac{1}{2} \, K_a^T \, \tilde{B}^{T} \, [K - \quad {}^2M]^{-1} \, [(K - \quad {}^2M) - K] \, [K - \quad {}^2M]^{-1} \, \tilde{B} \, K_a$$

$$= \frac{1}{2} (A - \quad). \tag{A.4}$$

Rearranging we get,

$$A = \quad + \quad 2 \frac{A^*}{2} \tag{A.5}$$

From Eq. (A.1), we see that the ith column of A^* is constructed by applying a unit elongation by the ith actuator and multiplying the measurement vector y by K_a. The matrix $\frac{\partial A^*}{\partial (\omega^2)}$ can be constructed from measurement of A^* at a series of adjacent frequencies.

Once the matrix A is constructed for both the damaged truss and the undamaged truss, the optimal excitation vector can be obtained from Eq. (2.19).

A.2 *Structure with Collocated Shakers/Sensors*

If the structure is instrumented with *m* collocated shakers/sensors, to construct *A* from the sensor measurements, we note that from Eqs. (2.3) and (4.1),

$$\mathbf{y} = C_d\, q, \tag{A.6}$$

where

$$C_d = B^T [K - \quad ^2M]^{-1}\ B \tag{A.7}$$

Using the matrix identity,

$$\frac{\partial P}{\partial (\alpha)} = - P^{-1} \frac{\partial P}{\partial (\alpha)} P^{-1}, \tag{A.8}$$

we get,

$$\frac{\partial C_d}{\partial (\omega^2)} = B^T [K - \ ^2M]^{-1}\ M\ [K - \ ^2M]^{-1}\ B$$
$$= - \frac{1}{2} B^T [K - \ ^2M]^{-1}\ [(K - \ ^2M) - K]\ [K - \ ^2M]^{-1}\ B$$
$$= \frac{1}{2} (A - C_d). \tag{A.9}$$

Rearranging we get,

$$A = C_d + 2 \frac{\partial C_d}{\partial (\omega^2)} \tag{A.10}$$

From Eq. (A.6), we see that the ith column of C_d is constructed by applying a unit force by the ith shaker and measuring the displacement vector y. The matrix $\frac{\partial C_d}{\partial (\omega^2)}$ can be constructed from measurement of C_d at a series of adjacent frequencies. Once the matrix A is constructed for both the damaged truss and the undamaged truss, the optimal excitation vector can be obtained from Eq. (2.14).

Appendix B
Identifying Boundary Conditions

Most model updating methods use some optimization scheme to determine the changes which should be made to the nominal model so that the analytical results matches with the experimental data. There is a danger that the analytical results fit well with the measurements but the model does not have a predictive value when different measurements are taken. This danger is particularly large when number of parameters is equal to the number of measurements to be matched. So we test the predictive capability of the model by checking it for a condition that was not used in fitting the data.

In this section, we assume that the mass and stiffness properties of the short and diagonal members of the truss are known to us accurately. The boundary conditions of the cantilevered truss have to be identified such that a good agreement between the experimental data and the analytical response is obtained. We will first show that by assuming the truss is perfectly cantilevered from the wall, errors as high as 8% were observed between the analytical and experimental natural frequencies. We try to obtain a good FEM model by connecting the wall nodes to the ground by massless springs of finite stiffness. An objective function which represents the difference between the analytical and experimental data is minimized to identify the wall stiffness. The resulting FEM model was used to predict changes in the natural frequencies of the truss. Three different objective functions were used to estimate the wall stiffness.

It is shown that a better agreement between the FEM model and experiments is obtained by considering the mass of the wall springs. This introduced three more design parameters into the identification problem. Two different approaches were tried to consider the mass of the wall nodes. The resulting FEM model was initially used for damage identification tests. For the damage identification tests, we needed a good match between the analytical and experimental receptance matrices. We modified the objective function to include the elements of the receptance matrix. First, we will describe the prediction test for the models obtained by minimizing the difference between the FEM model and the experiments.

B.1 *Prediction Test*

A net mass of 203 grams is attached to each of the nodes 7, 8,11 and 12. The change in the natural frequencies of the truss due to this change in the truss is measured to be

$$\omega_i^{exp} = \{-4.91, -5.99, -9.17\} \text{ Hz} \tag{B.1}$$

The changes in the natural frequencies obtained from an FEM model should match the experimental data.

B.2 *Results with Clamped Boundary Conditions*

It would be erroneous to assume that the nodes 1, 2 and 3 are rigidly clamped to the wall and the displacements of these wall nodes are zero. The theoretical cantilevered condition gives the natural frequencies of the structure as

$$_1=107.25 \text{ Hz}, \qquad _2=137.08 \text{ Hz}, \qquad _3=196.03 \text{ Hz}.$$

The measured natural frequencies of the truss are

$$_1=100.05 \text{ Hz}, \qquad _2=128.56 \text{ Hz}, \qquad _3=193.19 \text{ Hz}$$

The theoretical cantilevered truss was subjected to the prediction test and the changes in natural frequencies by adding the mass were

$$\omega_i^{FEM} = \{-5.77, -6.98, -10.47\} \text{ Hz} \tag{B.2}$$

The experimental natural frequencies of the truss are lower than the analytical natural frequencies obtained by imposing rigidly clamped boundary condition on the truss. This can possibly imply that the displacement of the wall nodes is non-zero and some potential energy is being stored by the mounting plate at the wall.
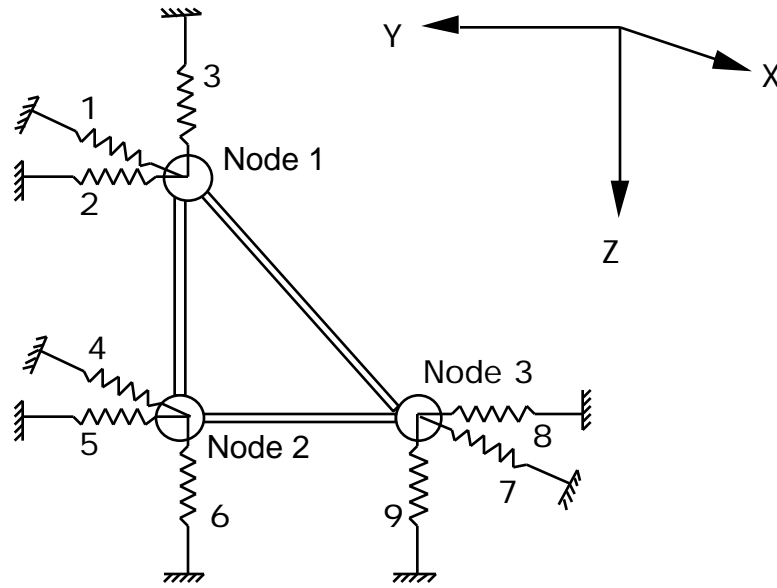
Figure B.1. Wall springs included in the FEM model.

B.3 *Boundary Conditions Modeled as Massless Springs:*

The finite element of the truss includes 3 springs for each node [Fig. 1] at the wall that account for the receptance of the plate and the wall. We assume that the 3 springs aligned in the x direction have equal stiffness, k_x. Similarly the 3 springs along the y direction have equal stiffness, k_y and the 3 springs along the z direction have equal stiffness, k_z. The stiffness properties of these springs are adjusted to match the experimental data. The natural frequencies and the mode shapes of the undamaged structure were measured at all the degrees of freedom away from the wall.

The model identifying problem is formulated as a least square error minimization. The error between the experimental data and the corresponding data obtained from the FEM model is minimized to identify the wall stiffness. Three different objective functions were used and the optimal wall stiffness for each objective function were computed. It was observed that there are numerous local minima of the objective function in the design space and the probability of achieving a global optima will increase if the objective function is minimized a number of times with different initial values for the design variables. Each objective function is minimized by using 200 different initial values of the design variables and the optimal value of the objective function is chosen as the least value of the resulting

optimal minima. The optimization was performed by the UMINF subroutine in the IMSL MATH/LIBRARY. This subroutine minimizes a function of N variables using a quasi-Newton method and a finite difference gradient.

i) The objective function, f_1 is based on the difference between the analytical and measured natural frequencies of the truss and is defined as

$$f_1 = \sum_{i=1}^{3} W_i (\omega_i^{FEM} - \omega_i^{exp})^2 \qquad \text{(B.3)}$$

where W_i are the appropriate weights to adjust the relative importance of the mode. The weights were chosen as 2.0, 1.5, and 1.0 respectively for the first 3 modes. The resulting minimum value of the objective function and the corresponding design variables was

$$(f_1)_{min} = 0.13$$

and

$$(\mathbf{k_{wall}})_1 = \{k_x, k_y, k_z\} = \{1.77 \times 10^8, 0.55 \times 10^8, 0.68 \times 10^8\} \text{N/m}.$$

The difference between the analytical natural frequencies and the measured natural frequencies of the truss was -0.11, +0.20 and -0.23 Hz respectively for the first three modes. The FEM model was subjected to a prediction test and the analytical change in natural frequencies was

$$\Delta\omega_i^{FEM} = \{-5.29, -6.64, -10.03\} \text{ Hz} \qquad \text{(B.4)}$$

The prediction errors in natural frequency for the first three modes are approximately 8%, 11% and 9%.

The displacement amplitudes at all the degrees of freedom away from the wall were measured. We measured the displacement amplitudes at 27 degrees of freedom. The displacement amplitudes at any degree of freedom at the wall will be relatively small with respect to displacement amplitudes near the free end and we believe that the measurements at such places will be corrupted with noise. The displacements at these degrees of freedom were ignored in both the FEM and measured mode shapes.

To further check the validity of the FEM model, the Modal Assurance Criterion (MAC) was computed to be at least 0.99 for all the 3 modes. This represents a good correlation between the experimental and analytical mode shapes. We also checked the orthogonality of the analytical mass matrix with respect to the measured mode shapes. The off-diagonal terms of the symmetric orthogonalized mass matrix were -0.1%, 0.6% and -0.3%. This represents a good correlation between the measured mode shapes and the analytical mass matrix.

ii) The objective function for model updating was modified as,

$$f_2 = \sum_{i=1}^{3} W_i (\omega_i^{FEM} - \omega_i^{exp})^2 + \sum_{j=1}^{3} \sum_{i=10}^{36} [\phi^{FEM}(i, j) - \phi^{exp}(i, j)]^2 \qquad (B.5)$$

The minimum value of the objective function and the optimal wall stiffness was obtained to be

$$f_2 = 0.38$$

and

$$(\mathbf{k_{wall}})_2 = \{1.66 \times 10^8, 0.61 \times 10^8, 0.64 \times 10^8\} \text{N/m}.$$

The difference between the measured natural frequencies and the analytical natural frequencies of the truss was -0.07, -0.10 and -0.38 Hz respectively for the first three modes. The FEM model was subjected to a prediction test and the analytical change in natural frequencies was

$$_i^{FEM} = \{-5.30, -6.63, -10.00\} \text{ Hz} \qquad (B.6)$$

The prediction error in natural frequencies are 8%, 11% and 9%. The MAC for the 3 modes was again calculated to be greater than 0.99 for the 3 modes.

From Eqs. B.3 and B.6, we see that the two FEM models obtained so far have the same predictive value. In other words, there is no visible improvement in the predictive value of the model by including the mode shapes in the objective function. Including the mode

shapes in the objective function increased the computation time and did not prove fruitful for predicting the natural frequency of the truss with additional mass.

Further, the high prediction error in the natural frequency of mode 3 leads us to believe that the two FEM models obtained are not a true representation of the structure. The high value of MAC for all the 3 modes could erroneously suggest that the models validate the actual structure. The MAC may not be a good predictor of the goodness of the model.

iii) We define an objective function as

$$f_3 = \sum_{i=1}^{3} W_i (\omega_i^{FEM} - \omega_i^{exp})^2 + \sum_{i=1}^{3} W_i^* (\omega_i^{FEM} - \omega_i^{exp})^2 \qquad (B.7)$$

where ω_i^{FEM} are the changes in the natural frequencies obtained from the FEM model when extra mass is added to the undamaged truss and ω_i^{exp} are the changes in the measured natural frequencies when extra mass is added to the truss. W_i and W_i^* are the appropriate weights to adjust the relative importance of the different components of the error function. They were taken as 2.0, 1.5, and 1.0 respectively, for the first three modes. The additional mass 29.75 grams each was placed at nodes 7,11 and 12. The best model obtained from the process of minimizing the objective function by using a number of different initial guesses was obtained as

$$(\mathbf{k_{wall}})_3 = \{1.29 \times 10^8, 0.71 \times 10^8, 0.78 \times 10^8\} \text{N/m}.$$

The difference between the measured natural frequencies and the analytical natural frequencies of the truss was -0.02, +0.03 and +0.01 Hz respectively for the first three modes. The FEM model was subjected to a prediction test and the analytical change in natural frequencies were

$$\omega_i^{FEM} = \{-5.28, -6.57, -10.09\} \text{ Hz} \qquad (B.8)$$

The prediction errors for the three modes are 8%, 10% and 10% respectively.

A comparison of the FEM models resulting from the three different objective functions is shown in Table B.1. It is seen that a good match between the measured and analytical natural frequencies of the truss without any extra mass is obtained of f_3 is used as the objective function. Adding the mode shapes to the frequencies (objective function f_2) was a step in the right direction because it increased the quantities to be matched, but possibly the modes do not reflect much the influence of the wall. Adding the effect of mass also went in the same direction as adding the mode shapes. The fact that f_3 gave better fit for frequencies indicates that the optimization for f_1 and f_2 was not good in spite of all the different initial guesses. The optimization scheme does not guarantee a global minima and taking more number of initial guesses increases the confidence in the optimality of the results.

Table B.1. Comparison of FEM models resulting from 3 different objective functions

Objective function	$(\omega_i^{FEM} - \omega_i^{exp})$			$(\omega_i^{FEM} - \omega_i^{exp})$		
	Mode 1	Mode 2	Mode 3	Mode 1	Mode 2	Mode 3
f_1	-0.11	0.20	-0.23	-0.38	-0.65	-0.86
f_2	-0.07	-0.10	-0.38	-0.39	-0.64	-0.83
f_3	0.08	0.03	0.13	-0.37	-0.58	-0.92

The three models could not accurately predict the changes in mode 3 when extra mass is added to the truss. It was observed that $|\omega_i^{FEM}|$ is higher than $|\omega_i^{exp}|$. This can possibly be due to model parameter errors or model order errors. The model parameter errors should include application of inaccurate boundary conditions. So far, we have considered massless springs to represent the plate on which the truss is mounted. If we associate inertia properties with the plate by assuming that the wall nodes are connected to ground by springs having some mass, then these springs will have certain kinetic energy associated with them. This should decrease the Rayleigh quotient and make ω_i^{FEM} closer to ω_i^{exp}. In the next section, we model the boundary conditions with springs having some mass associated with them.

B.4 *Boundary Conditions Modeled as Springs with Mass*

The model tuning problem is formulated as a least square error minimization problem in two different ways. For comparison, the boundary conditions are again modeled as massless springs and this corresponds to the third approach.

1) The support springs have some inertia associated to them and the 3 springs along the same direction have equal mass. This results in 6 parameters, namely, k_x, k_y, k_z, m_x, m_y and m_z.

2) The three springs at a given node have equal mass and this results in 3 mass parameters, m_1, m_2 and m_3 besides the 3 stiffness parameters.

3) The support springs are massless and only the stiffness properties needs to be adjusted. This assumption yields three parameters for the optimization problem, namely, k_x, k_y and k_z.

The objective function used for all the 3 approaches was to minimize an error function,

$$F = \sum_{i=1}^{3} W_i (\omega_i^{FEM} - \omega_i^{exp})^2 + \sum_{i=1}^{3} W_i^* (\omega_i^{FEM} - \omega_i^{exp})^2 \qquad (B.9)$$

W_i and W_i^* are the appropriate weights to adjust the relative importance of the different components of the error function. An extra mass of 29.75 grams each was added to nodes 7, 11 and 12. The three approaches were applied to obtain an FEM model that minimizes the error function and the results are summarized in Table B.2.

Table B.2. Experimental results and FEM results obtained by the 3 approaches.

Approach	Natural Frequencies of Undamaged Truss (Hz)			Change in Natural Frequencies due to adding mass (Hz)		
	1	2	3	1	2	3
Experimental	100.05	128.56	193.19	-4.91	-5.99	-9.17
Approach-1	100.05	128.56	193.09	-5.22	-6.45	-10.28
Approach-2	100.07	128.69	193.11	-5.27	-6.42	-9.86
Approach-3	100.13	128.59	193.32	-5.28	-6.57	-10.09

The 2nd approach produced the best match between the experiment and the FEM model. The optimal wall parameters were:

$\mathbf{k}^*=\{k_x, k_y, k_z\} = \{1.43995 \times 10^8, 0.48203 \times 10^8, 2.79512 \times 10^8\}$N/m and
$\mathbf{m}^*=\{m_1, m_2, m_3\}= \{0.0, 0.0, 61.0\}$ kg $\qquad (B.10)$

Initially, we used this FEM model was used for damage detection tests. For lower damage detectability measure, we needed a better match between the analytical and experimental receptance matrices, C_O for all the three modes of interest. The receptance matrix, C_O of the undamaged truss is measured by applying a force at a shaker location, and the response is measured at all the sensor locations. The receptance matrix is symmetric and for 3 collocated shakers/sensors, we have 6 independent elements for each vibration mode. We chose the 12 independent entries of C_O corresponding to modes 1 and 3 for shaker/sensor location 6Z, 7Z and 12Z and 18 independent entries of C_O for the three modes for shaker/sensor location of 7Y, 8Y and 10Y. We calculated,

$$g = \sum_{\substack{\text{Shaker} \\ \text{location}}} \sum_{\text{Modes}} \sum_{l=1}^{3} \sum_{k=1}^{3} \frac{(C_o(k,l)^{\text{exp}} - C_o(k,l)^{\text{FEM}})^2}{(C_o(k,l)^{\text{FEM}})^2}$$

from the FEM model using Eq. B.10 and obtained the value of g to be 3.15. To decrease the damage detectability measure, one possibility was decreasing the effect of measurement noise and modeling errors. The amount of noise was being quantified as the difference between C_O^{exp} and C_O^{FEM}, that is, the magnitude of g. In other words, getting a lower value of g would decrease the damage detectability measure and help us in the process of damage identification. We therefore modified the objective function to include the receptance matrices, C_O^{exp} and C_O^{FEM}.

B.5 *Modifying the Objective Function*

The FEM model should produce a close match with the measured natural frequencies of the undamaged truss and the truss with the measured receptance matrices. It should also be able to predict the changes in the natural frequencies by adding mass to the truss. The objective function is modified as

$$f_{\text{modified}} = \sum_{i=1}^{3} (\omega_i^{\text{FEM}} - \omega_i^{\text{exp}})^2 + \sum_{\substack{\text{Shaker} \\ \text{location}}} \sum_{\text{Modes}} \sum_{l=1}^{3} \sum_{k=1}^{3} \frac{(C_o(k,l)^{\text{exp}} - C_o(k,l)^{\text{FEM}})^2}{(C_o(k,l)^{\text{FEM}})^2} \quad \text{(B.11)}$$

The 6 design variables are the stiffness, k_x, k_y, k_z and the mass, m_1, m_2, m_3 of the wall springs. The optimal parameters were obtained as

$$\mathbf{k}^{**}=\{k_x, k_y, k_z\} = \{1.30\times 10^8, 0.61\times 10^8, 3.26\times 10^8\}\text{N/m} \quad \text{and}$$
$$\mathbf{m}^{**}=\{m_1, m_2, m_3\}= \{24.96, 0.0, 56.09\} \text{ kg} \tag{B.12}$$

The minimum value of the objective function was obtained to be

$$f_{min} = 0.76$$

To check the prediction value of this FEM model the natural frequencies of the truss with the additional mass and ω_i^{exp} was computed and compared to ω_i^{FEM} :

$$\omega_i^{exp} = \{4.91, 5.99, 9.17\} \text{ Hz;}$$

and

$$\omega_i^{FEM} = \{5.11, 6.24, 9.88\} \text{ Hz.}$$

The FEM model has a good prediction value for any changes made to the structure and it also produces the analytical $[C_o]$ which matches well with the corresponding elements of $[C_o]$ obtained experimentally. The value of g decreased from 3.15 to 0.53 and we expect that by using this model, we can lower the damage detectability measure and this would help us in successfully locating the damage. This FEM model will be used for damage identification.

To conclude, the boundary conditions need to be modeled as springs with mass. A good agreement between the FEM model and the experimental data is obtained when we assume that all the springs at a node have equal mass. Initially we used the FEM model given by Eq. (B.6) for damage identification tests. We needed a better match between the analytical and measured receptance matrix and we used the FEM model given by Eq. (B.7). We observed that the check of predicting the natural frequencies of a truss with additional mass seems to be a viable tool for having a high level of confidence in the updated model.

Appendix C
Signal Processing: Glossary of Terms

FFT: Fast Fourier Transform (FFT) computes the discrete Fourier transform pair:

$$Z(k) = \sum_{i=0}^{N-1} z(i)W^{ik}, \quad k=0,...,(N-1)$$

and

$$z(i) = \sum_{k=0}^{N-1} Z(k)W^{ik}, \quad i=0,...,(N-1)$$

where

$$W = e^{-j2\pi/N}$$

z(i) is a complex time history

Z(k) is a complex frequency function of the same number (N) of data values

N is the number of data points in a time history segment

Frame is defined as the block of sampled data values acquired for processing.

Frame Size is defined as the number of samples in the frame. For our analyzer, the selections are 64, 128, 256, 1024, 2048 and 4096. The number of frequency lines is the frame size divided by 2.56. Varying the frame size allows the user to trade off between frequency resolution and measurement time.

Baseband Mode: In baseband mode, the analysis is performed from 0 Hz to the bandwidth.

Zoom Mode: The analysis band is the center frequency plus and minus the bandwidth

Zoom Processing: It is an important capability for signal analysis. It allows the analysis to be focused over a specified frequency region. It provides an increase in resolution at the expense of increased measurement time.

Appendix D
Optimal Location of Shakers/Sensors

Optimal locations of collocated sensors/shakers will enhance the capability of the technique in locating the damage. The location should give different analytical optimal excitation vectors for varying damage locations and for all the modes of interest. In our experiments, we found that the excitation force at a node can be oriented 5 to 10 degrees away from the desired direction. This can lead to erroneous results. The location of shakers/sensors should also give least amount of error for the deviation of the excitation force from the desired direction.

We define a set of possible locations for collocated sensors/shakers. For any one set of m collocated sensor/shaker location, we perform contrast maximization to get the normalized optimal vectors $\mathbf{q}(i,j)$, for each damage scenario where i represents the damage scenario and j represents the mode number. We define the average optimal vector for each mode as,

$$\mathbf{q}_{av}(j) = \frac{\sum_{i=1}^{n_{ds}} \mathbf{q}(i,j)}{n_{ds}} \; ; \quad i=1,...,n_{ds} \; ; \quad j=1,...,n \tag{D.1}$$

The difference between $\mathbf{q}_{av}(j)$ and $\mathbf{q}(i,j)$ represents how different the contrast maximization vector is from the average contrast maximization vector of that mode. We define,

$$(i,j) = \|\mathbf{q}_{av}(j) - \mathbf{q}(i,j)\| \; ; \qquad\qquad i=1,...,n_{ds} \; ; \qquad j=1,...,n \tag{D.2}$$

and

$$= \sum_{i=1}^{n_{ds}} \sum_{j=1}^{n_\omega} (i, j) \tag{D.3}$$

where   is a function of the location of sensors/shakers. Our objective is to find the location of sensors/shakers which will maximize . It is also desired that the error in measured response due to error in the direction along which the force is applied should be decreased. For each set of possible sensor/shaker location and for each mode, we define

the percent error in measured response for mode j when the shaker is at location k and sensor is at location l as,

$$\varepsilon(k,l,j) = \left| \frac{y_{ideal} - y_{error}}{y_{ideal}} \right| ; \quad k = 1,...,m; \quad l = 1,...,m ; \quad j = 1,...,n$$

where y_{ideal} is the response when there is no error in the direction of the applied force and y_{error} is the response when there is 5 degrees of error in the direction of the applied force. The applied force can be arbitrary oriented in the 3 dimensional space. To decrease the computational time, we make an assumption regarding the direction of the error in the applied force. The error in the applied force can be along either of the two directions which are perpendicular to the desired direction of the applied force. That is, if the force is desired to be along Z axis, the error in the force is assumed to be along either X axis or Y axis. We have assumed that there are only two directions in which the force can be applied. This assumption is valid since the linearity in the structure implies that the principle of superposition is valid. The direction which gives the maximum y_{ideal} is chosen as the direction of the applied force. The average error for this set of sensors/shakers over all the modes is,

$$\bar{\varepsilon} = \frac{\sum\limits_{j=1}^{n} \sum\limits_{k=1}^{m} \sum\limits_{l=1}^{m} \varepsilon(k,l,j)}{m^2 n} \tag{D.4}$$

The average error, $\bar{\varepsilon}$ should be less than some desired value, $\bar{\varepsilon}_{desired}$. The problem statement of finding the optimal set of sensors/shakers from the set of all possible locations of sensors/shakers is

$$\text{Max} \quad \text{such that} \quad \bar{\varepsilon} < \bar{\varepsilon}_{desired}$$

The resulting set of sensors/sensors should benefit the process of damage identification. The algorithm is applied to generate good shaker/sensor locations for the 36 degree of freedom, cantilevered truss. The problem is formulated as a two step process:

i) Compute locations which give $\bar{\varepsilon} < \bar{\varepsilon}_{desired}$.

110

ii) Find   for the chosen locations and find the location which maximizes .

The wall nodes have small displacements and were thought to be unfit for a shaker/sensor location. There are 2925 independent combinations of the sensor/shaker locations which span the remaining 27 degrees of freedom of the truss. The average error,   was computed for all these locations and Fig. D.1 shows a histogram of the number of locations in a 25.0 range of average error. The statistics of the distribution are obtained to be

$$\mu = 86.67; \qquad = 94.25; \qquad _{max} = 1041.4; \qquad _{min} = 20.97$$

The value of   desired was chosen to be 25.0 and this process reduced the number of good locations from 2925 to 42. It is to be noted that for a given location of shaker/sensor, computing   is a relatively easy task as compared to computing .

For the 42 selected locations of shaker/sensor, we computed the value of . Figure D.2 shows a histogram of the number of locations of the shaker/sensor which are in 5.0 range of . The statistics of the distribution are obtained to be

$$\mu = 33.93; \qquad = 15.67; \qquad _{max} = 76.61; \qquad _{min} = 11.3$$

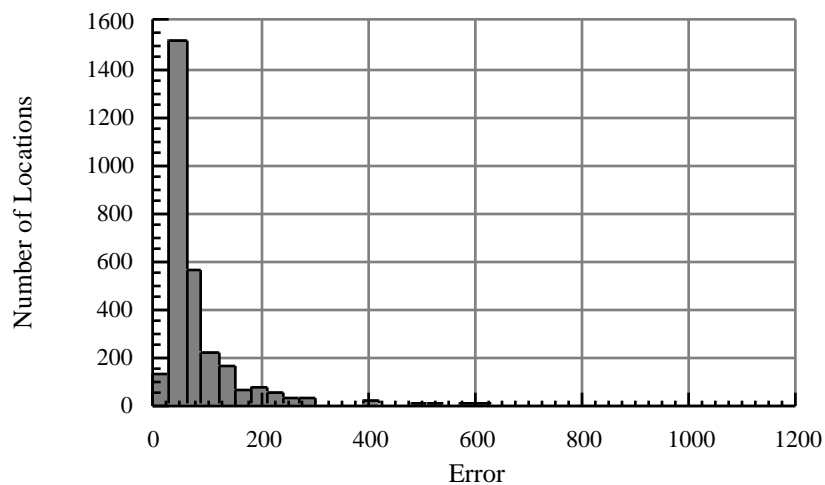The best location of shaker/sensor is at degrees of freedom 7Y, 8Y and 10Y.

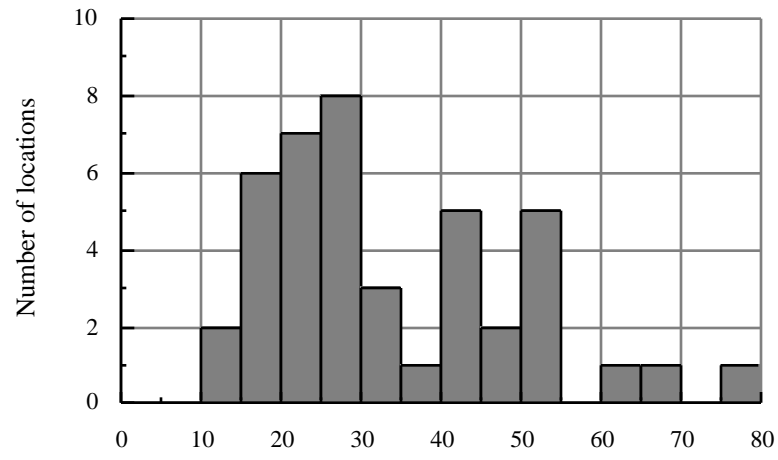**Figure D.1. Histogram of the distribution of Average Error.**

111

Figure D.2. Histogram of the distribution of γ **.**

Vita

Vikas Juneja was born in Agra, India, on the 25th of October, 1967. He graduated in May 1989 with a degree of Bachelor of Technology (B. Tech.) in Mechanical Engineering from the Indian Institute of Technology, Kanpur. His senior year project was devoted to the design and fabrication of a soiled currency bill cleansing machine.

He worked in Maruti Udyog Limited, a leading automobile manufacturer in India during summer 1989. In September, 1989, he enrolled in the M.S. program in Auburn University, Alabama. He worked under the guidance of Dr. S. C. Sinha and got his degree in Mechanical Engineering in August, 1991. In August, 1991, he enrolled in the Ph.D. program in the Department of Engineering Science and Mechanics at Virginia Tech.